Silica Aerogel, an Alternative to Micromachined Air Gap for Thermal Insulation of Microheaters

A Dissertation

Presented to the

Graduate Faculty of the

University of Louisiana at Lafayette

In Partial Fulfillment of the

Requirements for the Degree

Doctor of Philosophy

Seyed Mohammad Seyed Jalali Aghdam

Spring 2015

Silica Aerogel, an Alternative to Micromachined Air Gap
for Thermal Insulation of Microheaters

Seyed Mohammad Seyed Jalali Aghdam

APPROVED:

Mohammad Madani, Chair Associate Professor of Electrical and Computer Engineering	Nian-Feng Tzeng, Co-Chair Professor of Computer Engineering The Center for Advanced Computer Studies
Magdy Bayoumi Professor of Computer Engineering The Center for Advanced Computer Studies	Danella Zhao Professor of Computer Engineering The Center for Advanced Computer Studies
Afef Fekih Associate Professor of Electrical and Computer Engineering	Mary Farmer-Kaiser Dean of the Graduate School

DEDICATION

To my wife and children:
this is our dissertation

ACKNOWLEDGMENTS

"All praise is to Allah, who guided us to this; we would not have attained the right path had Allah not guided us" (The Holy Quran, 7:43).

It is extremely difficult for me to express my gratitude to the many people who have helped me to accomplish this dissertation. First and foremost, I owe my deepest gratitude to my chair advisor, Dr. Mohammad Madani, for his continued guidance that has always been incredibly motivating and helpful in every single stage of my research. I would also like to thank the other members of my dissertation committee, Dr. Nian-Feng Tzeng, Dr. Magdy Bayoumi, Dr. Danella Zhao, and Dr. Afef Fekih, for their valuable insights and comments.

It is my pleasure to thank my friends Koutilya, Sanjay, and Anderson for their help and useful comments and ideas that have always been constructive for this work. I am also very thankful to Mr. Shelby for his continuous assistance in providing the required software and many other laboratory tools.

I wish to extend my heartfelt appreciation to my dear wife, Saeideh Amrollahi, for her unconditional patience, support, and encouragement. I also owe a special thank you to my children, Seyed Ali and Fatemeh Sadat, for brightening up our life at hard times.

Last but not least, I consider it an honor to thank my parents, my wife's parents, and my brother for their continuous support, motivation, and inspiration to complete my study.

TABLE OF CONTENTS

LIST OF TABLES

LIST OF FIGURES

LIST OF ABBREVIATIONS

AFM	Atomic Force Microscopy
CMOS	Complementary Metal Oxide Semiconductor
DI water	Deionized water
FEA	Finite Element Analysis
FTIR	Fourier Transform Infrared
HCPCF	Hollow-core Photonic Crystal Fiber
HF	Hydrofluoric Acid
IR detector	Infrared detector
LLNL	Lawrence Livermore National Laboratory
LSI	Large Scale Integration
MEMS	Micro-Electro-Mechanical System
μHP	Microhotplate
MOX	Metal Oxide
NASA	National Astronautics and Space Administration
NiCr	Nickel Chromium
P_c	Critical Pressure
$P_{cap.}$	Capillary Pressure
PEDS	Polyethoxydisiloxane
PEG	Polyethylene Glycol
R_a	Average Roughness
RICH detector	Ring Imaging Cherenkov detector

RPM	Revolutions Per Minute
SEM	Scanning Electron Microscopy
T_c	Critical Temperature
TCR	Temperature Coefficient of Resistivity
TEOS	Tetraethoxysilane
TEM	ThermoElectroMechanical
TIR	Total Internal Reflection
TMAH	Tetra Methyl Ammonium Hydroxide
TMCS	Trimethylchlorosilane
TMOS	Tetramethoxysilane
ULSI	Ultra Large Scale Integration
VLSI	Very Large Scale Integration

1. INTRODUCTION AND OBJECTIVE

1.1 Introduction

In the recent years, there has been an increasing interest in deployment of olfactory sensors or electronic noses in different fields of industry. They have many applications in sensing minute outgas of materials such as detecting flammable/hazardous substances in factories, exploring environment, detecting narcotics and explosives in borders security, monitoring pollution, assessing the freshness of food [1-5], etc.

Among different practices available for gas sensor fabrication, metal oxide semiconductor (MOX) transducers are one of the most widely used in electronic nose applications, due to their high sensitivity and low cost [6]. Figure 1.1 depicts some examples of typical MOX gas sensors commercially available in the market. As observed, they are tiny in the size of not more than a couple of millimeters on a side and therefore suitable for portability purposes.

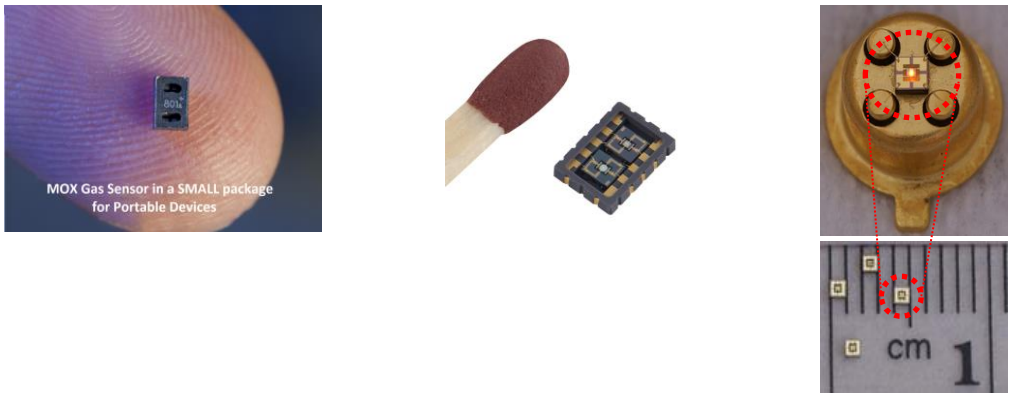

Figure 1.1 Examples of commercially available MOX gas sensors [7-9].

The principle operation of the MOX sensors is based on the ability of the sensing material changes in its resistivity while being exposed to gaseous species. However, the actual operational temperature of the sensing material is between 300ºC to 500ºC [10]. Hence, the microhotplates (μHPs) are formed using micromachining of silicon wafer to suspend the plates in air, which acts as a thermal insulator. Then the sensor element is fabricated on top of the μHP. Passing over the sensing layer, different gases increase or decrease the resistance of sensing material depending on the type of gas and the sensing material.

Table 1.1 presents a concise overview on sensing behavior of different metal oxides to various gaseous species, reported by Errana et al. [11]. It can be inferred from the table that an array of sensors including only a few metal oxides is capable of sensing a wide range of different gases reported in the table. For instance, tin oxide (SnO_2) shows the most promising sensing capability by detecting all the reported gases in the table except ethane, which can be detected by zinc oxide (ZnO_2). Therefore, by having a sensor including SnO_2 and ZnO_2 all the above mentioned gases are able to be detected. It is noticeable that the range of operating temperature and the range of detection limits is different for different metal oxides in response to different gases [11].

Table 1.1 Sensing behavior of different metal oxides to various gaseous species, repoeted by Errana et al. [11].

	Metal oxides																			
Gas	Al	Bi	Cd	Ce	Cr	Co	Cu	Ga	In	Fe	Mn	Mo	Ni	Nb	Ta	Sn	Ti	W	Zn	Zr	Mx
Acetone (CH_3·CO·CH_3)			X							X				X		X			X		
Acetaldehyde (CH_3CHO)																X					
Ammonia (NH_3)					X	X		X	X			X	X	X		X	X	X	X		X
Arsine (AsH_3)																X					
Automobile exhaust gases								X								X					X
Benzene (C_6H_6)																X					
Butane (C_4H_{10})	X							X	X	X						X			X		
Butanol									X					X		X			X		
Carbon dioxide (CO_2)	X	X	X	X	X	X	X			X			X			X	X		X	X	X
Carbon monoxide (CO)		X				X	X	X	X	X		X	X	X		X	X	X	X	X	X
Chlorine (Cl)									X							X					
Dimethyl disulfide																X			X		
Dimethylamine (DMA)									X					X		X	X	X	X		
Ethane (C_2H_6)																			X		
Ethanol (C_2H_5OH)	X			X			X	X	X	X		X		X		X	X	X	X	X	X
Humidity (H_2O)	X									X	X				X	X		X	X		X
Hydrocarbons (HC)																X				X	X
Hydrogen (H_2)	X	X	X	X	X		X		X	X			X			X	X	X	X		X
Hydrogen sulfide (H_2S)				X			X									X		X	X		X
Inflammable Gases																X					
Liq Petroleum Gas (LPG)								X		X						X			X		X
Methane (CH_4)					X	X		X		X			X			X	X		X		X
Methanol (CH_3OH)	X			X												X	X				
Methyl mercaptan (CH_3SH)																X					
NO, NO_2, NO_x					X	X		X	X	X		X	X			X	X	X	X	X	X
Oxygen (O_2)	X	X	X	X	X	X	X	X		X		X	X			X	X	X	X	X	X
o-xylene																X					
Ozone (O_3)									X	X		X				X	X	X	X		X
Petrol/Gasoline																X		X	X		
Phosphine (PH_3)																X					
Propane (C_3H_8)						X		X	X	X						X			X		
Propanol (C_3H_7OH)									X					X		X	X		X		
Smoke		X														X					
Sulfur dioxide (SO_2)													X			X					X
Trimethylamine (TMA)									X					X		X	X	X	X		

1.2 MOX gas sensors features

As mentioned earlier, MOX sensors need to operate at relatively high temperatures to be able to sense gases. In fact, the resistance of the sensing element changes only at high temperatures by exposure to the gas. The most important component of a MOX sensor is a small hot plate that is called microhotplate (μHP), since it is typically in micron size. The small size of the μHP helps providing fast temperature rises (quick response time) as well as low power consumption. The conventional method to fabricate the microhotplates (μHPs) is to micromachine the silicon wafer to suspend the plates in air.

There are two types of micromachining: front side micromachining and back side bulk micromachining. In the former, after all the layers of heaters, insulators, sensing electrodes, and sensing elements are deposited and fabricated, the silicon substrate under these layers is masked through a photolithography procedure and etched to leave a suspended bridge with all other components on it. Usually, this membrane is made of Si_3N_4 due to its high mechanical stability and good electrical insulation. In the latter, micromachining is performed from the back side of the silicon substrate all the way to reach the membrane. In both cases, micromachining is a post-processing procedure as it is done after all the layers are deposited and fabricated. Figure 1.2 demonstrates examples of two types of micromachining. In the case of front side micromachining, four opening windows are observed which are for the purpose of etching the silicon substrate under the μHP to create a cavity filled with air to thermally insulate the heat sink to the substrate.

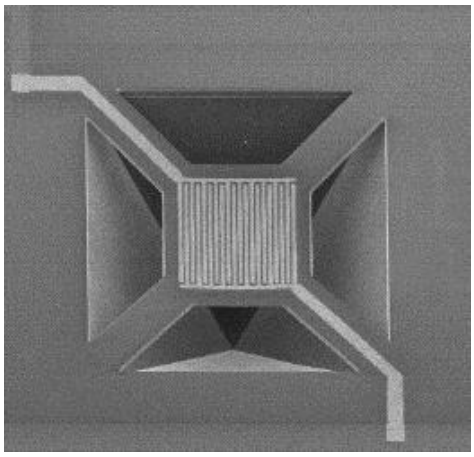

(a)

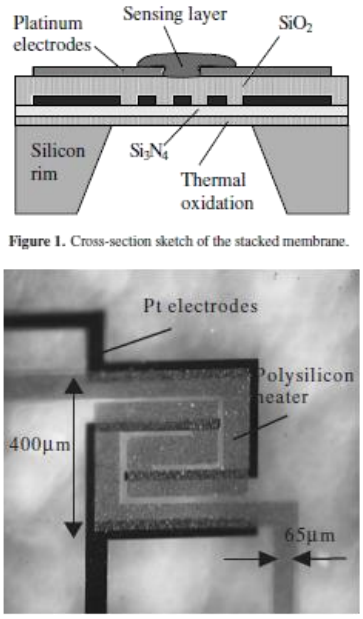

Figure 1. Cross-section sketch of the stacked membrane.

(b)

Figure 1.2 Examples of micromachining; (a) front side [12], (b) back side [13].

To elaborate more on the design parameters and operational factors of MOX gas sensors, Table 1.2 is prepared as a comparative study on some recently reported publications on microhotplates. As shown in the table, the operating temperature is ranging from 200°C to 550°C and power consumption is in the range of 15 to 250 mW. It is very important to consider the heated area for the consumed power at a given temperature to evaluate the performance of the µHP. In other words, low power consumption by itself does not represent the power efficiency of the µHP.

Table 1.2 Microhotplate features according to some recently repoeted publications.

Operating Temperature (°C)	Power Consumption (mW)	µHeater Area (μm^2)	Power per Heated Area ($\mu W/\mu m^2$)	Sacrificed Chip Area (μm^2)	Micromachining	Ref. / Year
430	15	1,200	12.5	202,500	Back-side	[14]/2015
200	140	585,000	0.24	1,610,000	Back-side	[15]/2012
500	170	90,000	0.78	640,000	Back-side	[16]/2012
550	25	6,400	3.9	40,000	Front-side	[17]/2011
400	18	14,700	1.2	122,500	Front-side	[18]/2011
250	250	1,000,000	0.25	2,250,000	Back-side	[19]/2011
300	16	17,670	0.90	246,300	Back-side	[20]/2009
300	23	36,100	0.64	90,000	Front-side	[21]/2009
500	58	108,900	0.53	3,062,500	Back-side	[22]/2008
325	66	562,500	0.12	2,250,000	Back-side	[23]/2008

1.3 Disadvantages of micromachining

As mentioned in the last section, the air cavity that is formed for thermal insulation purpose has to be done by micromachining. There are a few disadvantages to this approach. The first issue is the high fragility and low mechanical stability of the thin (a few microns or less) membranes during processing and operation [24]. Particularly, micromachining is implemented in a post processing stage after all other layers are fabricated, either for front side or back side micromachining. This will bring up the breakage of the suspended membrane during wet etching [25]. Figure 1.3 shows a couple of examples of breakage of the straps while wet etching the silicon substrate.

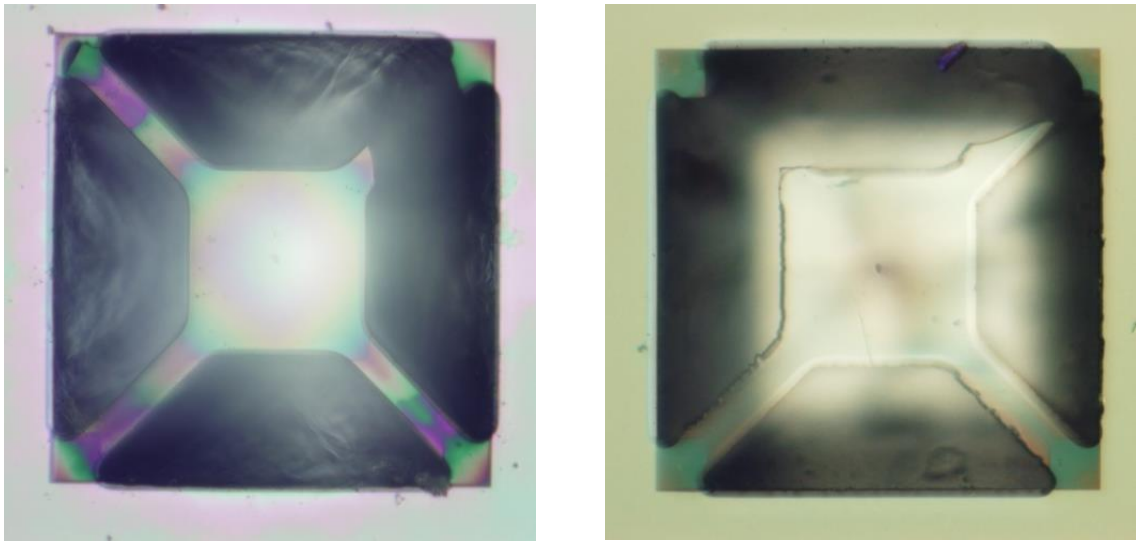

Figure 1.3 Optical images of the broken straps while micromachining, taken in our Microelectronics and Sensors Research Lab at UL Lafayette.

Second, the lithographic processing of metal oxide sensing on top of the suspended layers becomes impossible due to the fact that the front side micromachined structures contain etch troughs and therefore the surface is not flat [26], hence the micromachining must be done as a post process after the sensor electrodes are processed, which lowers the yield drastically.

The other drawback to the micromachining is the large chip area that is sacrificed to create the necessary air pit for a single μHP. Accordingly, the sensor array density will decrease remarkably. Table 1.3 provides the sacrificed chip area of the microhotplates presented in Table 1.2.

Table 1.3 Sacrificed chip area and heater area for different microhotplate designs.

Ref. / Year	μHeater Area (μm^2)	Sacrificed Chip Area (μm^2)	μHA/SCA (%)
[14]/2015	1,200	202,500	**0.6**
[15]/2012	585,000	1,610,000	**36.3**
[16]/2012	90,000	640,000	**14.1**
[17]/2011	6,400	40,000	**16.0**
[18]/2011	14,700	122,500	**12.0**
[19]/2011	1,000,000	2,250,000	**44.4**
[20]/2009	17,670	246,300	**7.2**
[21]/2009	36,100	90,000	**40.1**
[22]/2008	108,900	3,062,500	**3.6**
[23]/2008	562,500	2,250,000	**25.0**

1.4 Proposed idea

To overcome the limitations of the current MOX sensors technology to prepare heat insulation for the microhotplates and to reduce the processing cost, in this dissertation we investigate and demonstrate a novel approach of using silica aerogel as heat insulator rather than creating air pits, which involves time consuming and costly micromachining. Aerogels are one of the most amazing synthetic materials, due to their versatile, wide range, and unique properties. Due to their incredible characteristics and flexibility of synthetic choices which allows desired properties to be obtained, there has been a wide research area on potential applications and more efficient production procedures of aerogels in the last two decades. We have surveyed the number of scientific publications on silica aerogel using ScienceDirect database from 1940 to present (January, 2015). We have graphed the number of publications per decade as shown in Figure 1.4.

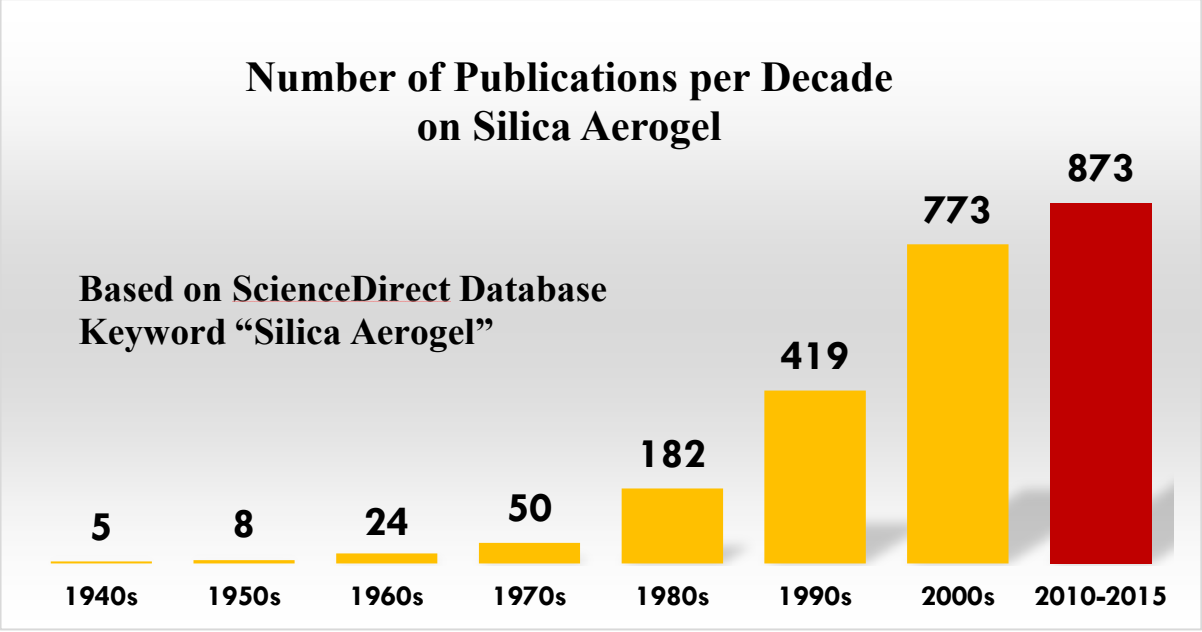

Figure 1.4 Growth in publications on Silica Aerogel.

The steady increase in the number of publications per decade and in particular the very large number of publication from 2010 to 2015, which exceeds the last decade, indicates the incredible interests of the scientific community in silica aerogel and challenges and benefits.

Aerogel is basically a highly porous gel filled mostly with air, thus called "frozen smoke." This fascinating material is produced by the so-called "sol-gel process" in which organic compounds containing a metal undergo a chemical reaction producing a metal oxide. The solution is liquid at first and, as the reaction proceeds, a network is then created with metal and oxygen bounds, making it more viscous until it becomes a three-dimensional network gel filled with the solvent. After a drying stage (commonly supercritical drying), the solvent is extracted from the gel to make a porous network largely filled with air, creating "aerogel."

Aerogels can be produced from metals, inorganic-organic sources, and whole organic precursors. Metals used in making aerogel include silicon, titanium, aluminum, zinc, etc., among which, silica is the most promising due to its thermal stability and tunability of porosity [27]. Therefore, in this work we have concentrated on silica aerogels. They have such novel properties as low thermal conductivity, low density, small refractive index, high porosity, high thermal stability, large surface area, etc., making them suitable for various science and industry applications including but not limited to thermal insulators, sound insulators, electronic sensors, low dielectric materials, Cherenkov detectors, optical fibers, drug delivery systems, catalysts, and nano-composites [28-31].

1.5 Research organization

In this dissertation, for the very first time we demonstrate the application of silica aerogel thin and thick film as thermal insulator replacing the conventional micromachining.

The low power consumption and the high area efficiency are among the many advantages of this approach. Chapter 2 delivers the background of silica aerogel and the idea to make it. Later, it explains the most common procedures to synthesize aerogel. The unique properties of aerogels are also presented in this chapter, followed by their applications in various fields of industry.

Chapters 3 and 4 elaborate on the simulation study of recessed silica aerogel into the silicon substrate and the multilayer thin film, respectively. The area efficiency and the low power consumption of such design is investigated in detail and the advantages of filling the air cavity with silica aerogel is discussed as well as the multilayer film without the cavity.

In Chapters 5 and 6, we demonstrate the experimental procedure of making single layer silica aerogel via ambient drying and supercritical drying, respectively. Physical and electrical characteristics of the thin film such as refractive index, porosity, and dielectric constant are investigated.

In Chapter 7, we present our novel technique (patent pending) for sol-gel processing that resolves the limitations of thin/thick films manufacturing by avoiding any further steps including solvent exchange and/or supercritical drying. The impregnation of ethanol with functional colloidal alcogel particles is introduced as a distinctive and different approach from the conventional methods where tiny aerogel particles are formed on the wafer networked together just by exposure to air during spin coating. Chapter 8 covers the feasibility study of use of our new method to produce thick film aerogels for thermal insulation of microhotplates, both by experiment and simulation. Finally, we will have conclusion and future work in Chapter 9.

2. SILICA AEROGEL: PREPARATION, PROPERTIES, AND APPLICATIONS

2.1 Silica Aerogel Background

In 1931, Kistler introduced a new method to obtain a gel filled with air. The idea was to remove the liquid from the gel and replace it with air. Before Kistler's idea, the liquid was replaced with another liquid, for example alcohol, for microscopy purposes in biology [29]. However, the problem was the considerable shrinkage while drying the gel in air. The reason was the large surface tension resulted by liquid-vapor interfaces within the gel network, leading to the collapse of the network.

Kistler claimed that: "If one wishes to produce an aerogel, he must replace the liquid with air by some means in which the surface of the liquid is never permitted to recede within the gel. If a liquid is held under the pressure always greater than the vapor pressure, and the temperature is raised, it will be transformed at the critical temperature into a gas without two phases having been present at any time" [32]. This was, therefore, the beginning of supercritical drying method to achieve a non-collapsed, highly porous gel.

Kistler performed the first set of experiments to obtain aerogel, with sodium silicate (water glass) that is an inorganic salt, as silica source, however, in the late 1960s, organic precursors were introduced which provided a shorter method for obtaining aerogel. The advantage of applying such precursor stemmed from using a tetra-functional siliconalkoxide ($Si(OR)_4$) to eliminate the laborious solvent exchange steps involved in Kistler's method. It was that time when tetramethoxysilane (TMOS) introduced to aerogel production. After two decades, the toxic TMOS was replaced with tetraethoxysilane (TEOS). In the mid 1980's, an ultralow density silica aerogel was prepared by Hrubesh at Lawrence Livermore National Laboratory (LLNL) by applying the two-step sol-gel method first presented by Brinker in

1982. Currently, this silica aerogel is used in National Aeronautics and Space Administration (NASA) as interstellar dust collector to capture tiny particles without damaging them [30].

2.2 Synthesis of silica aerogel

2.2.1 Sol-Gel processing

Aerogels are prepared by a process called Sol-Gel processing. First, a suspension of solid particles is formed by polymerization of metal oxide (M-O) or metal hydroxide (M-OH) groups to form interlinked bridges of M-O-M or M-OH-M between metallic atoms. This is very similar to polymerization process taking place in organic chemistry, where carbon atoms are the repeating agent. Here, there are metal atoms acting as repeating unit. At first, the size of the independent colloidal particles dispersed in the liquid solution is in the range of 1-1000 nm. This colloidal suspension is called “Sol.” As time passes, the individual particles make connections with each other to build a three-dimensional network that is filled with a liquid, resulting in “Gel.” The obtained gel is then aged – usually in a solvent – to strengthen the network. Aging and drying processes will be discussed in detail in the following sections in this chapter. The process parameters such as type of precursors, solvent, acid or base catalyst, temperature, and pressure control the desired properties of the final aerogel. Figure 2.1 illustrates the schematic procedure steps of aerogel preparation.

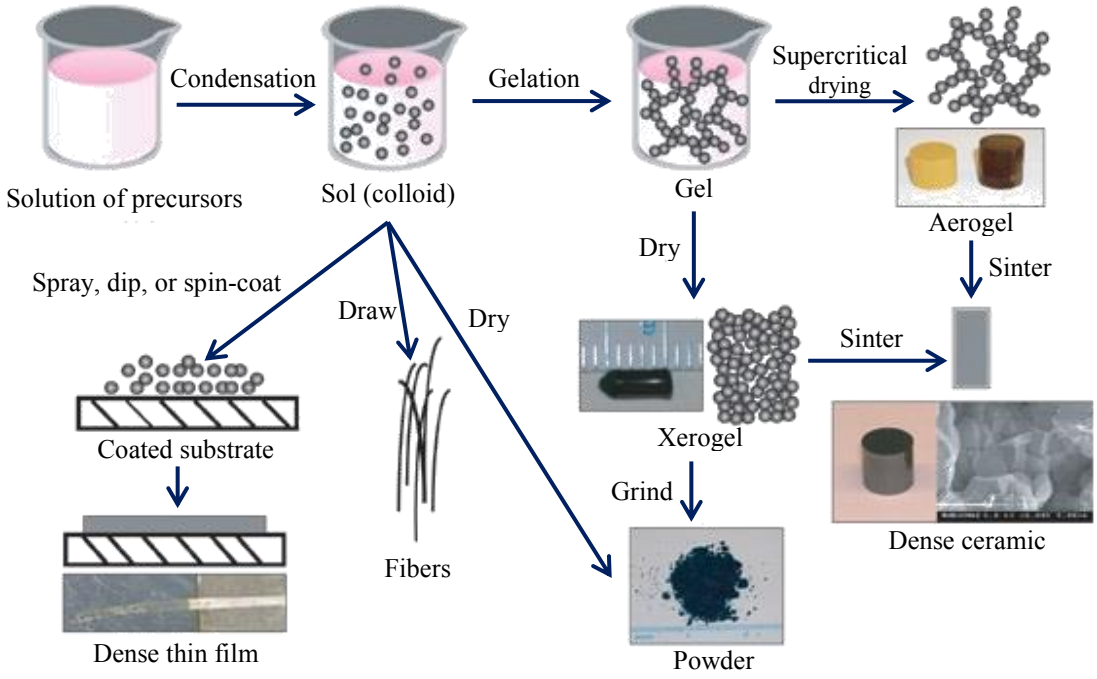

Figure 2.1 Procedure steps of aerogel preparation [33].

The synthesis of aerogels involves three main steps: preparation of the gel, aging, and drying.

2.2.2 Preparation of the gel

Silica aerogels can be made of different silicon sources as starting material out of which sodium silicate (water glass) and tetraalkoxysilane (TMOS or TEOS) are mostly used in industry. We have, therefore focused on these two types of precursors.

i. Sodium silicate as precursor

Kistler, as the very first man, created silica aerogel by reacting aqueous sodium silicate with hydrochloric acid under the following reaction:

$$Na_2SiO_3 + 2\,HCl + (x\text{-}1)\,H_2O \rightarrow SiO_2 \bullet x\,H_2O + 2\,NaCl \qquad (2.1)$$

After obtaining the wet gel, he had to remove the water inside the gel by converting it to a supercritical fluid. However, the pressure and temperature were so high (P_c=22.1 MPa, T_c=374°C) that the super critical water dissolved the silica itself. Therefore, he washed the gels again with water to remove the excess ions and then replaced the water with ethanol that had much lower critical conditions (P_c=6.3 MPa, T_c=243°C). Finally, he could vent the supercritical ethanol to end up with silica aerogel.

ii. Tetraalkoxysilane as precursor

Tetraalkoxysilane is a four-branched alkoxide all branches of which are connected to a silicon element at the center. The most well-known examples are tetramethoxysilane (TMOS) and tetraethoxysilane (TEOS) (Figure 2.2).

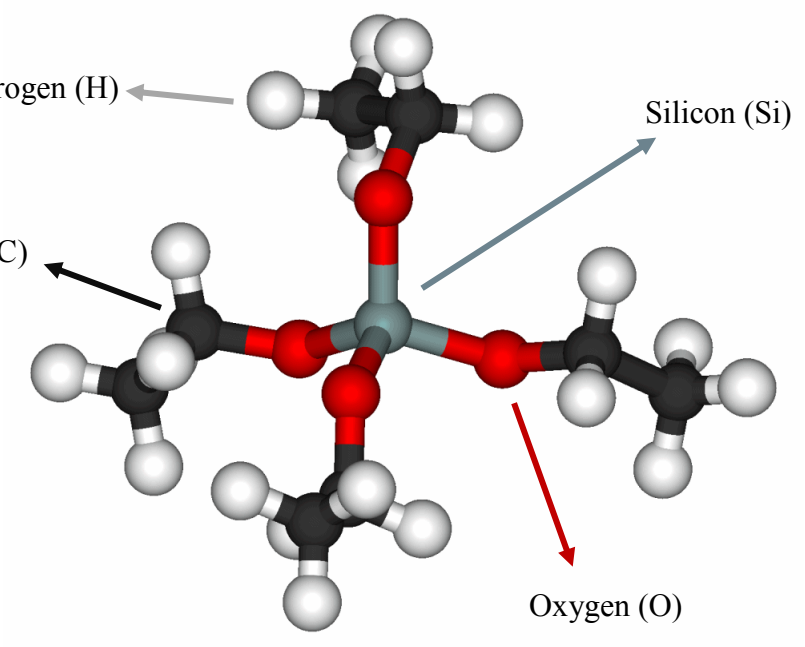

Figure 2.2 3D schematic of TEOS [34].

Three major reactions take place during sol-gel processing of alkoxysilanes [28]:

$$\equiv Si - OR + H_2O \longrightarrow \equiv Si - OH + ROH \quad (2.2)$$

$$\equiv Si - OR + HO - Si \equiv \longrightarrow Si - O - Si + ROH \quad (2.3)$$

$$\equiv Si - OH + HO - Si \equiv \longrightarrow Si - O - Si + H_2O \quad (2.4)$$

The first reaction (2.2) is hydrolysis of the alkoxide that results in silicon hydroxide and alcohol. The second and the third reactions that occur simultaneously with the first one are alcohol condensation and water condensation, respectively. The products of the last two reactions create the networks of the final desired silica gel (Si–O–Si). The remarkable point here is that the first reaction does not proceed by itself, because alkoxysilanes and water are not miscible. So an amount of a solvent is added to the mixture to homogenize it. The solvent is usually an alcohol (e.g. ethanol) that is absolutely miscible in water. Figure 2.3 provides a better understanding of the miscibility of the alkoxysilanes-water-alcohol system.

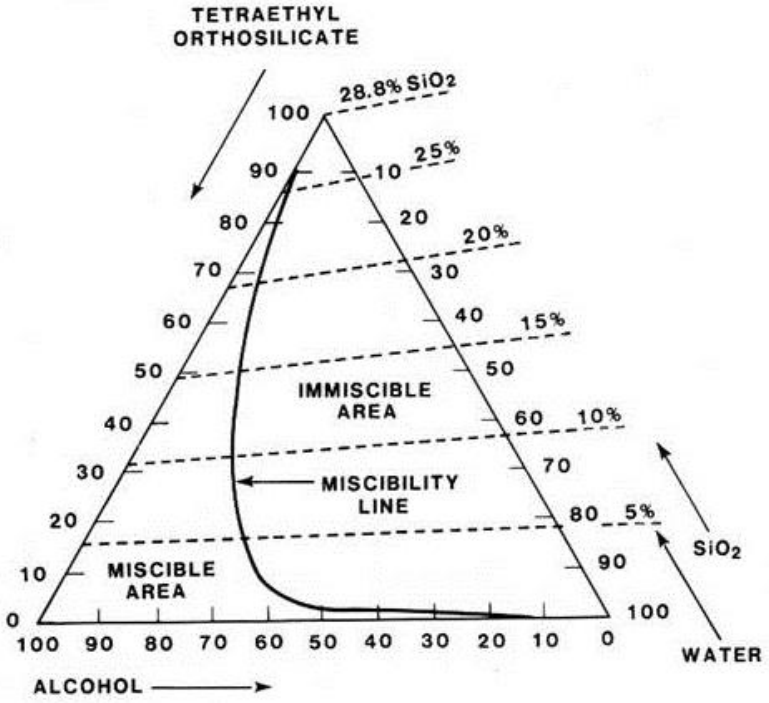

Figure 2.3 Ternary phase diagram of TEOS-Ethanol-Water [28].

At the beginning, the rate of the first reaction dominates the process. While the silicate hydroxyl increases as the product of reaction 2.2 the rate of the second and third reactions raises up and overcomes the hydrolysis reaction, creating monomers, dimers, and higher order rings of siloxane links (Si–O–Si). The most considerable advantage of using alkoxysilane as a precursor is that there will be no impurities such as salts as byproducts of the reactions, hence eliminating the washing step needed in Kistler's method that was laborious and time-consuming. Sol-gel processing of alkoxysilanes has been improved over the time and can be divided into three main methods:

a. One-step method

In this method, the alkoxide is hydrolyzed with water at the presence of a solvent (e.g. ethanol) and a catalyst (acid or base), all in a single step. Three abovementioned reactions

take place, promoting the creation of Si–O–Si grid networks. Meanwhile, alcohol and water are produced as byproducts, encouraging the reverse reactions of esterification in reactions 2.3 and 2.4. However, the rate of these reactions slows down as more networks of gel are created. The properties of the final aerogel are drastically dependent on the variations in process conditions, including but not limited to the molar ratio of the starting chemicals, the catalyst type (acid or base) and its concentration, the solvent, temperature, and pressure.

b. Two-step method

This method is basically an alteration to the one-step process that was first done by Brinker et al. [35]. At the first step of the procedure, silica precursor is reacted with a lower amount of water than is needed to complete the hydrolysis reaction, under acidic conditions. This way all the water is consumed in the reaction completely, leading to the formation of a cluster of partially condensed silica. In the second step, the partially condensed silica is allowed to react with an additional amount of water under basic or acidic conditions, resulting in larger bridges of cross-linked Si–O–Si to form even more condensed networks of silicon oxide polymers that are essentially pure SiO_2.

c. Modified two-step method

The alcohol product of the first step reaction tends to force the equilibrium towards the left side (reaction 2.2), reproducing alkoxysilane groups. This phenomenon is also known as reesterification. It causes not only the long gelation time, but also the loss of transparency of the final aerogel. To avoid this drawback the alcohol generated in the first step is removed by a distillation process and replaced with an aprotic solvent that does not display hydrogen bonding and also can stabilize the ions [36]. In the second step, the hydrolysis reaction is

completed under basic conditions with an excess amount of non-alcohol solvent. However, the disadvantage of this method is the time-consuming and tedious distillation of alcohol.

iii. Effect of process parameters

There are so many parameters through synthesis and preparation of silica aerogels that can affect the properties of final product including but not limited to silica precursor, solvents, water content, catalysts, molar ratios of components, timing (aging), and drying conditions. In the following sections we discuss some of the most significant parameters.

a. Effect of silica precursor

The first effect of the precursor nature can be said to be on the hydrolysis and condensation rates. It was shown that using larger volume precursors with longer chains would result in decreasing the hydrolysis rate and, inversely, increasing the condensation rate [37]. Although the initial condensation rate is high, further condensation happens only by cross-linking of already created short chains that requires diffusion and collision between chains. Therefore, precursors with longer chains and larger volumes show longer gelation times.

The other influence of the precursor type is on the properties of the aerogel. It was shown that aerogels made of TMOS and polyethoxydisiloxane (PEDS) had a narrow and uniform pore size distribution [38]. The particles were also smaller than those of TEOS aerogels that resulted in higher optical transmission. It was also found that surface area was more in the case of TMOS and PEDS than that of TEOS aerogels which was due to the smaller size of silica particles.

b. Effect of solvent

Solvents are usually added to avoid phase separation during the hydrolysis reaction and also to control the concentrations of silicate and water. Solvents can be categorized as polar or non-polar and as protic or aprotic. The polarity determines the solvating ability of polar or non-polar species. More polar solvents such as water and ethanol are normally used to solvate polar tetra-functional silicates used in sol-gel processing. However, less polar or non-polar solvents such as hexane and dioxane can be used in incompletely hydrolyzed systems.

By protic solvent we mean a solvent that has removable or labile proton which determines whether anions or cations are solved more through hydrogen bonding [28]. It also influences the extent of the reverse reactions of 2.2, 2.3, and 2.4. Specifically, aprotic solvents do not participate in aforementioned reverse reactions because they lack electrophilic protons and thus are unable to donate protons to nucleophiles, e.g. OH^-, that is necessary for those reactions. Therefore compared to alcohol or water, aprotic solvents do not take part in sol-gel processing reactions. A list of classified solvents is given in Table 2.1 [29].

Table 2.1 Classified solvents [29].

Protic polar solvent	Aprotic polar solvent	Nonpolar solvent
Water	Acetone	Hexane
Ethanol	Acetonitrile	Benzene
Methanol	Dimethylformamide	Dioxane

c. Effect of water content

Water participates in both hydrolysis and condensation reactions. Specifically, water takes part in the hydrolysis reaction so its amount determines the number of hydrolyzed monomers formed. Considering reaction 2.2, the most obvious effect of the increase in the molar ratio of water to silica precursor (r_{ws}) is the acceleration of the hydrolysis reaction. The higher value of "r_{ws}" causes more complete hydrolysis of the monomers before significant condensation occurs [39]. From reactions 2.3 and 2.4 it is clear that different amounts of monomer hydrolysis would affect the relative rates of the alcohol or water producing condensation reactions. Usually with lower amounts of water than stoichiometric level ($r_{ws} << 2$), the alcohol producing reaction is favored, while the water producing reaction is favored with $r_{ws} \geq 2$ [40].

Although increasing "r_{ws}" promotes hydrolysis, when the ratio of solvent to silicate is kept constant, the silicate concentration is reduced. Therefore, the rates of hydrolysis and

condensation reduce, causing an increase in the gel time. Figure 2.4 shows gelation times for different values of "r_{ws}" at three ratios of Ethanol (solvent) to TEOS (silicate precursor) [41].

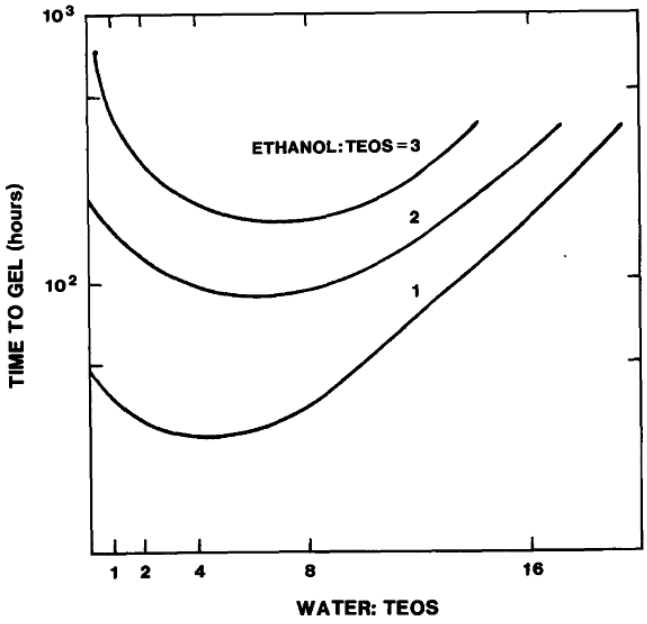

Figure 2.4 Gel times versus "r_{ws}" for three ratios of ethanol to TEOS [41].

d. Effect of catalyst

Generally, acid catalysts accelerate the hydrolysis and base catalysts promote the condensation reaction. Using acid postpones the condensation reaction farther, whereas base catalysts result in an earlier start of condensation. Since acid-catalyzed hydrolysis is an electrophilic reaction, the rate is governed by the concentration of H^+ in the solution. In the case of lower pH, the reaction occurs more rapidly [42]. So in the first stages of the reaction the monomers are hydrolyzed faster than chains that result in the formation of short linear chains [43]. On the other hand, in the case of base catalyzed hydrolysis, the reaction is nucleophilic. In fact, the rate of the reaction is a function of the hydroxyl concentration in

solution [42]. This type of reaction favors the formation of long chains or colloidal particles [43].

The pH is not the only factor that affects the reactions and thus, the properties of silica gels. The other factor is the nature of the catalysts. The best example is F^- agent in HF or NH_4F. In an investigation by Pope [44] six different catalysts were used to monitor the rates of hydrolysis and condensation reactions as far as the gelation time (Table 2.2 [44]). As can be seen in the table, although the gelation time is the lowest for HF, its pH level is intermediate. The reason lies in the fact that fluorine anion is smaller than hydroxyl and hence, is much more effective in catalyzing the condensation by nucleophilic attack.

Table 2.2 Gel times and solution pH for TEOS systems employing different catalysts [44].

Catalyst	Consentration (Mol.: TEOS)	Initial pH of solution	Gelation time (h)
HF	0.05	1.90	12
HCl	0.05	0.05*	92
HNO_3	0.05	0.05*	100
H_2SO_4	0.05	0.05*	106
CH_3COOH	0.05	3.70	72
NH_4OH	0.05	9.95	107
No catalyst	-	5.00	1000

* Between 0.01 and 0.05

2.2.3 Aging

After the preparation step the gel is aged usually in its mother solvent. It means that if they are produced by ethanol as the solvent, they will be aged in ethanol. The purpose of aging is to strengthen the gel network so that it encounters the minimum possible shrinkage

during drying. The point is that after the gel is created, the reactions are still taking place inside the gel despite the fact that the solution restrains the flow of the liquid. Actually, the gel point represents the moment when the last link is formed in the chain of bonds that constitutes the spanning cluster. Aging the gel promotes the hydrolysis and condensation reactions to stiffen the gel. Therefore, controlling the aging parameters especially the choice of solvent has a very significant effect on the final properties of aerogel. The stiffer and stronger the gel network becomes, the better it can withstand the capillary pressure and thus, aged gels crack much less than non-aged ones. For instance, Einarsrud et al. [45] showed that the stiffness of the gels prepared by polyethoxydisiloxane can be increased by dipping the gel in polyethoxydisiloxane solution. Dai et al. [46] also reported the use of ionic liquids with extremely low vapor pressure that eliminated the shrinkage caused by solvent evaporation during the aging process. The gels synthesized by this method were so stable that even conventional drying caused just a little shrinkage.

2.2.4 Drying

Since the wet gel is a porous network filled with fluid, capillary forces should be considered for removal of the liquid from the structure. According to Brinker [28] a layer of liquid on a solid surface has two interfaces, solid-liquid (with specific energy of γ_{SL}) and liquid-vapor (with specific energy of γ_{LV}). The difference in the specific energy of the solid-vapor interface (γ_{SV}) and the solid-liquid interface (γ_{SL}) causes liquids to spread out onto a solid surface. So the change in energy produced by spreading of the liquid film is:

$$\Delta E = \gamma_{SL} + \gamma_{LV} - \gamma_{SV} \qquad (2.5)$$

If $\Delta E < 0$, the liquid will spread spontaneously, otherwise a contact angle (θ) will be created at the solid-liquid-vapor interface. The balance of tensions at the intersection point results in a relationship between the surface tensions known as Young's equation:

$$\gamma_{SV} = \gamma_{SL} + \gamma_{LV} \cos(\theta) \quad (2.6)$$

In the case of cylindrical capillary, the liquid climbs up the wall and replaces the solid-vapor interface with a solid-liquid interface, gaining energy equal to:

$$\Delta E_{cap.} = 2\pi rh\,(\gamma_{SV} - \gamma_{SL}) \quad (2.7)$$

Where "r" is the radius of the tube and "h" is the height the liquid rises up to. The work done by the liquid to overcome gravity equals to the product of the capillary pressure ($P_{cap.}$) and the volume of the moved liquid ($\Delta V = \pi r^2 h$). So the capillary pressure can be determined by equating the energy gained and the work done as:

$$P_{cap.} = -2\,\frac{\gamma_{SV} - \gamma_{SL}}{r} = -2\,\frac{\gamma_{LV}\cos(\theta)}{r} \quad (2.8)$$

The negative sign implies that the liquid is in tension. When the radius of the tube or capillary is very small the pressure is very high and this high stress affects the solid phase during the drying step. There are two common solutions to eliminate or alleviate the high capillary stress during drying: supercritical drying and surface modification of the gel.

i. Supercritical drying

Kistler [47] suggested that the problems of shrinkage and cracking that are due to capillary forces could be avoided by removing the liquid from the pores above the critical temperature (T_c) and critical pressure (P_c) of the liquid. As it can be seen in the Figure 2.5, above T_c and P_c there is no phase distinction between the liquid and the vapor and therefore

no capillary pressure exists. In the supercritical drying method the gel is placed in an autoclave and the temperature and pressure are increased above the supercritical point of the liquid inside the gel (Figure 2.5, path A-B). Then solvent venting is performed at a constant temperature (Figure 2.5, path B-D). Finally, the autoclave is cooled down to room temperature (Figure 2.5, path D-A) resulting in a gel free of the liquid, avoiding the phase boundary between liquid and gas (point E in Figure 2.5).

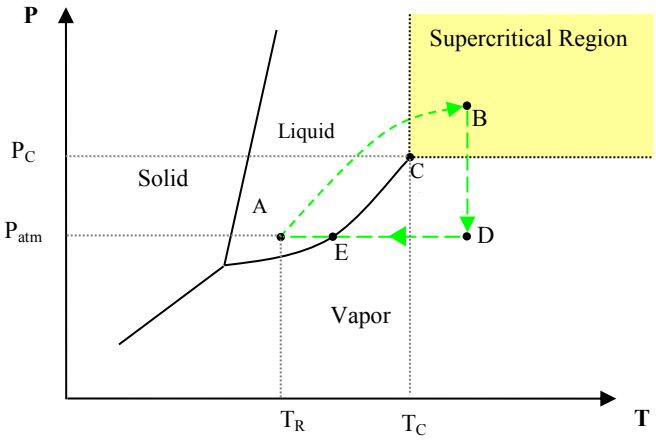

Figure 2.5 Super critical drying demonstration.

Critical points of some of the solvents are presented in Table 2.3. Since achieving high pressure and temperature is both time consuming and expensive, it is preferable to process by a solvent with lower T_c and P_c. In that case a solvent replacement with the liquid inside the gel is required. Supercritical CO_2 can be one the best choices for this purpose as it has a very close to room temperature T_c (31.1°C) and it is also conveniently available.

Table 2.3 Critical points of solvents [30].

Solvent	T_c *(°C)*	P_c *(MPa)*
CO_2	31.0	7.37
Methanol	239.4	8.09
Ethanol	243.0	6.30
Water	374.1	22.04

ii. Surface modification

The other method of drying for the preparation of aerogels involves surface modification of the gel to both lower the capillary pressure and strengthen the gel network [29]. Basically, the inner surface of the gel is modified by silylation that means the OH groups of silanols (Si-OH) are replaced with methyl groups (CH_3) of trimethylchlorosilane (TMCS) resulting in hydrophobic surface. During ambient drying, the modified gel begins to shrink due to capillary forces, however, the silyl groups near the surface allow the gel body to expand back and suffer less shrinkage. It has been also reported that TMCS is mixed with a low surface tension solvent (e.g. hexane, cyclohexane, and heptane) before surface modification [48] and actually the replacement of the solvent with the liquid inside the gel would lower the capillary stress for easier drying.

2.3 Silica aerogel applications

There are vast amounts of different applications of aerogels in various fields of industries mentioned in the literature [28, 49-50] such as thermal insulation, catalysts, adsorbents, fiber optics, acoustic insulation, low dielectric materials, transducers, Cherenkov detectors, etc. Different applications of aerogels can be categorized based on their form or

shape of creation. They can be made in the forms of pads, fibers, powders, thin films, etc. [28]. In the following sections we describe some of the applications of silica aerogels in different formats.

2.3.1 Applications as optical fiber

Grogan et al. [51] demonstrated the application of silica aerogel as the core of hollow-core photonic crystal fiber (HCPCF). The core of the fiber was filled with silica aerogel and the transmission spectrum of the filled fiber exhibited the expected shift in the wavelengths of band gap guidance, and guidance by total internal reflection (TIR) at other wavelengths. The other optical application of silica aerogel was studied by Hrubesh et al. [52]. They fabricated thick aerogel films for use as cover slips on solar cells. The low refractive index aerogel caused less reflective Fresnel loss for incident light at its outer surface, allowing more light to reach the active surface. Therefore, the solar cell efficiency increased.

2.3.2 Applications as low dielectric material

Porous silica aerogels are very good choices to be used as low dielectric materials. Kawakami et al. [53] reported preparing silica aerogel thin film with high porosity and super low dielectric constant of 1.1 for ULSI applications. They showed that their process was compatible for inter-metal dielectrics of LSI processing. Joshi et al. [54] presented a spin-coating technique to prepare porous SiO_2 films to lower the dielectric constant which improved the suitability of the film to be used as an interlayer dielectric for ULSI applications. Li et al. [55] also were successful to deposit thick porous SiO_2 films with dielectric constant of 1.79 to be used as thermal-insulation layer of thin film IR detector.

2.3.3 Applications as Cherenkov counters

A very low refractive index medium is required for the detection of fast pions, kaons or protons in Cherenkov counters. Ishii et al. [56] confirmed that the silica aerogel with refractive index in the range of $1.08 < n < 1.25$ satisfied the condition needed as Cherenkov radiator. Silica aerogel was also applied in Ring Imaging Cherenkov detector (RICH detector) by Barnyakov et al. [57]. They used blocks of aerogel with dimensions of 200 × 200 × 50 mm^3 and refractive index of 1.03 for the hadron identification between 2 and 10 GeV/c.

2.3.4 Application as dust capture

Silica aerogels have the capability of capturing extraterrestrial grain traveling at hyper-velocities of more than 3 km/s [55] because of their porous structure that makes them capable of dissipating the kinetic energy of the cosmic particles and catching them. NASA is using STARDUST, a spacecraft equipped with aerogel, to encapsulate comet dust samples and return them to earth for laboratory analysis [58].

2.3.5 Applications as catalyst

The activity of heterogeneous catalysts strongly depends on the surface area of the catalyst [29]. Since aerogels have extremely high surface area they can be used as catalyst materials. Dunn et al. [59] demonstrated loading cobalt on silica aerogel to analyze synthesis activity. Their results showed that the large surface area, mesoporosity, and large pore volume characteristic of silica aerogels were maintained when loaded with cobalt and also good selectivity for the heavy hydrocarbons (C_{10+}) was observed.

2.3.6 Applications as thermal insulator

Low thermal conductivity of silica aerogels (0.005~0.014) [60-61] has made them very good insulators for different purposes such as window insulation, clothes, pipe insulation [31], and interlayer insulation in microelectromechanical systems (MEMS) [52]. Particularly, we focus on the huge number of studies that have been recently conducted in the field of electronics to introduce silica aerogel as a super insulator material.

Li et al. [55] reported preparing a film of 3 μm thickness with 59% porosity that was uniform, crack-free, and smooth for using as a thermal insulation layer to block the diffusion of heat flow from the pyroelectric layer to the silicon substrate in multilayer pyroelectric thin film IR detector. Liu et al. [62] also introduced providing a thick layer of 22 μm thickness with 48% porosity by multi-coating silica aerogel particles onto the silicon wafers for the application in large-scale uncooled IR detectors as a thermal insulating layer.

As mentioned before, the other possible application of aerogel can be defined as thermal insulator and low dielectric interlayer material in microhotplates to avoid the expensive process of micromachining commonly used in VLSI fabrication to produce air gap [63]. In the following chapters we will experimentally investigate the development of silica aerogel in the bulk and thin film formats and also the possibility of utilizing thin film aerogel as a low-dielectric interlayer.

3. RECESSED SILICA AEROGEL FOR HEAT INSULATION

In the operation of air pitted gaseous sensor, the microhotplate (μHP) consumes almost all the power used by the sensor. The required area to micromachine the air pit for the μHP of a single sensor is several times more than the actual area required by the sensor itself. The feasibility of implementing low power and ultra-dense gaseous sensor array is investigated by developing a new μHP structure using recessed silica aerogel. In comparison with the conventional μHP structure, the recessed aerogel not only has decreased the used area of the chip almost ten folds (181×181 μm^2 vs. 573×573 μm^2) to maintain a temperature of 360°C but also has decreased the power consumed by each μHP more than two folds (1 mW vs. 2.1 mW). As the number of sensors increases in a sensor array, the saved area of the chip increases quadratic by using the new structure. Moreover, the power consumed by the new designed structure reduces drastically.

3.1 Introduction

Silica aerogel has gained attention both in research and industrial communities due to its unique properties of ultra-low thermal conductivity, high thermal stability, high specific surface area, etc. [64-65]. Recently there have been several studies on aerogel applications in the various fields including but not limited to capacitive deionization of water [66], aero capacitor due to high surface area of aerogel [67-68], and sound absorption in ultrasonic devices [69-70]. More recently, aerogels have been successfully synthesized in different forms of microspheres [71], thin films [72], and flexible sheets [73-74] among which thin films have received more interest in applications such as ideal dielectrics for ultrafast integrated circuits [75] and heat insulator in gaseous sensors [63] due to the low thermal conductivity of aerogel. Combining it with microelectromechanical systems (MEMS)

expands the applications of aerogel even more in devices requiring a steady high temperature.

The MOX gas sensors should operate at temperature range of 200°C to 500°C [22] for maximum sensitivity. The sensing material is deposited on a plate called microhotplate (μHP). The high operating temperature of metal oxide (MOX) gas sensor demands an efficient design to consume low power in order to raise the temperature of μHP to desired level as quickly as possible. Various designs and materials have been considered for microhotplate fabrication [76-78]. Specifically, a micro hotplate fabricated with an active surface area of 50x60 μm^2 was reported to consume 30 mw power when operating at 350°C [78]. In another article, a circular active surface area of 80 μm^2 in diameter was developed to operate at higher temperature of 400°C consuming some 8.9 mW only [76-77]. The latter achieves significant improvement in power efficiency by increasing its pit height to 400 μm based on front side bulk micromachining [77]. However, this power efficiency is at a significant expense of chip area taken by each sensor. By simple calculation one can quickly realize that minimum chip area needed to micromachine such a deep pit would be in order of 566×566 μm^2, which is 64 times the size of microhotplate itself. As a result, microsensor arrays obtained using such microhotplate design will undoubtedly suffer from a very low sensor density. Briand et al. [79] have reported to make microhotplate gas sensor on a polyimide layer (as insulating layer) to avoid tedious front micromachining involved in processing air pit microhotplate gas sensors. However, they end up with a hotplate size of 1.5 mm wide and power consumption of 66 mW to reach the temperature of 325°C. Therefore, we are in urgent need of area efficient gaseous sensor design with low power consumption to present a cost-effective manufacturing of sensor arrays on the wafer.

To overcome the limitation of low density sensor arrays and high power consumption to reach high temperature on microhotplate, we proposed a novel approach of using aerogel as heat insulator rather than using air. The conventional method to insulate the micro hotplate from the silicon substrate is to micromachine the Si substrate to form an air pit. Wet micromachining is a post processing step, where over etching may occur while masking the sensor and its circuitry due to improper etching time control or pinholes in the masking material. This can reduce the yield and compromise the mechanical stability of the μHP. During the fabrication process of μHP, Laconte et al. [25] reported broken membranes due to backside micromachining with Tetra Methyl Ammonium Hydroxide (TMAH) etchant, which also damaged aluminum interconnections when masking layers failed. Furthermore, many of those surviving membranes were broken during subsequent deposition of the sensing layer material, photolithography processes, and selective wet etching. Dicing is another cause of the yield loss, since conventional dicing uses high water pressure to remove debris from the chip surface [80].

Madani et al. [63] reported that using relatively thick (40-100 μm) aerogel material instead of air as heat insulator yields the following advantages: (1) ultra-low power consumption, (2) area-efficient design to support high sensor density, (3) excellent temperature uniformity across the microhotplate surface, (4) low manufacturing costs (due to high yields), (5) high mechanical stability, and (6) fast fabrication. However, processing a thick layer of aerogel of 5 μm or more is extremely difficult using multilayer processing since the spin coating of aerogel is limited to 0.6 to 3 μm per layer [62, 81-82]. In view of the fact that a relatively thick layer of aerogel is required for ultra-low power MOX sensors, the step coverage problem for the metal interconnection lines between the sensor array and the

CMOS chip circuitry will pose significant yield problem. However, we have demonstrated in this chapter that the recessing of the thick aerogel in a selected area of the chip not only resolves the step coverage problem but also avoids tedious and difficult multilayer processing of thick aerogel film. Furthermore, the recessed aerogel processing will not adversely lower the yield caused by post processing of the sensor array.

3.2 Design considerations

The whole structure of the air pit is made of 3 layers as shown in Figure 3.1 (a). At the bottom there is a p-type silicon substrate in which an air pit is created to provide thermal insulation. The first layer is a dense 2 μm thick thermally grown SiO_2 or Si_3N_4 serving as micromachining mask shaped into four suspended bridges for mechanical support of the sensor shown in Figure 3.1 (a). But in case of aerogel, this layer is a complete layer of SiO_2 on top of the aerogel and the thickness can be as low as 0.2 μm (Figure 3.1 (b)). The second layer is the NiCr (Ni80/Cr20) on top of SiO_2 which is also 0.2 μm. This layer can be highly doped polysilicon for CMOS process compatibility. Finally, the third layer is an SiO_2 layer of 0.6 μm thickness to provide electrical insulation of heater from the micro hotplate. It also yields better temperature uniformity across the microhotplate since SiO_2 is relatively a good temperature conductive material. As reported in our previous study for the non-recessed spin coated thin aerogel, micromachining of the silicon is completely eliminated. Although the thicker aerogel reduces the power drastically, high step coverage decreases the yield severely. In this section we have investigated the recessed aerogel with micromachining a large area of silicon for sensor arrays prior to the fabrication of the sensor. Then we fill the anisotropically etched cavity with aerogel.

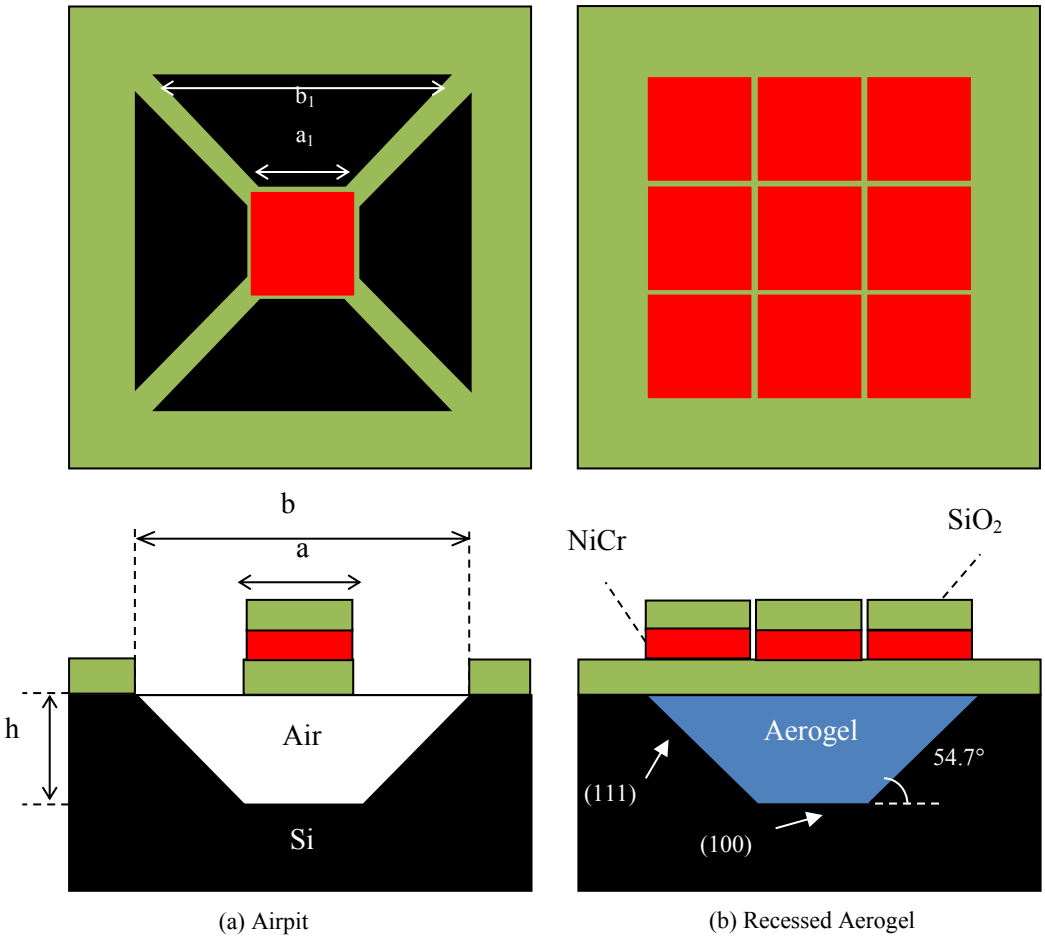

Figure 3.1 Design schematic of (a) single µHP on air pit and (b) array of µHP on recessed aerogel.

Anisotropic etching is used to form the cavity underneath the hotplate of the gas sensor. The etching is called anisotropic since the etching rate is high in the (100) direction and low in the (111) direction. Etch rate in the two direction can be different as 600 to 1 [83]. In the silicon crystal lattice structure, the (111) planes are oriented at 54.7º relative to the (100) plane (Figure 3.1(b)). A square mask opening on the surface of the wafer will yield an etched feature in the shape of inverted pyramid at the depth determined by the intersection of (111) plane. To suspend the micro hotplate in the air a mask is made with four trapezoids (with dimension: a_1=short base, b_1=long base, and h_T=altitude) placed close together from

their short bases "a_1" to form an area of square of "a×a" where $a=a_1+2\Delta w$ for the hotplate (Figure 3.1 (a)). The area considered for the hotplate is 181×181 μm^2 (a=181). The four long bases of the trapezoids "b_1" will form the mask opening area of "b×b" where $b= b_1+2\Delta w$. The four straps that hold the micro hotplate suspended in the air after micromachining have the width $w=(\sqrt{2}).\Delta w$ and the length of straps $L=((\sqrt{2}).(b-a))/2$.

The thermo-electrical analysis of our designed structures is performed by utilizing a MEMS simulation software, IntelliSuite. The software is equipped with different modules of: IntelliMask to design the mask; 3D Builder to create the meshed solid blocks and differentiate their entities on different layers; TEM (ThermoElectroMechanical) to assign the properties of each entity, load the initial conditions, and simulate the temperature gain by applying voltage to one end of the heater, keeping the other end at zero potential; the IntelliEtch will figure out the final shape of micro machined structure by using an etchant like KOH buffer. The temperature at the bottom of the silicon substrate is set to room temperature of 27°C to resemble the reference temperature. Input power can then be calculated by knowing the applied voltage and reading the current density passed through the heater.

3.3 Results and discussion

3.3.1 Area efficiency

To etch out the silicon from underneath of an "a×a" hotplate "h" deep, a square size opening of

$$b = a + 2h / (\tan(54.7°)) \quad (3.1)$$

is required. The etchant will etch the silicon through the opening area of the trapezoid to make the air pit as shown in Figure 3.1 (a). On the other hand, in order to make the pit filled with aerogel there is no need of a trapezoid mask, but a simple square mask would create the pit as illustrated in Figure 3.1 (b). According to equation 3.1 the area of the mask opening or the total area used increases as a square function of the height of the pit. Hence, one can calculate the percentage of saved area as:

$$\text{Saved Area} = (b_2 - a_2) / a_2 \times 100 \tag{3.2}$$

which implies that the micromachined air pit for each individual sensor in a sensor array uses much more area of the chip than using aerogel on the wafer for the same array. Figure 3.2 demonstrates the percentage of the saved area for different depths of the micromachined pit.

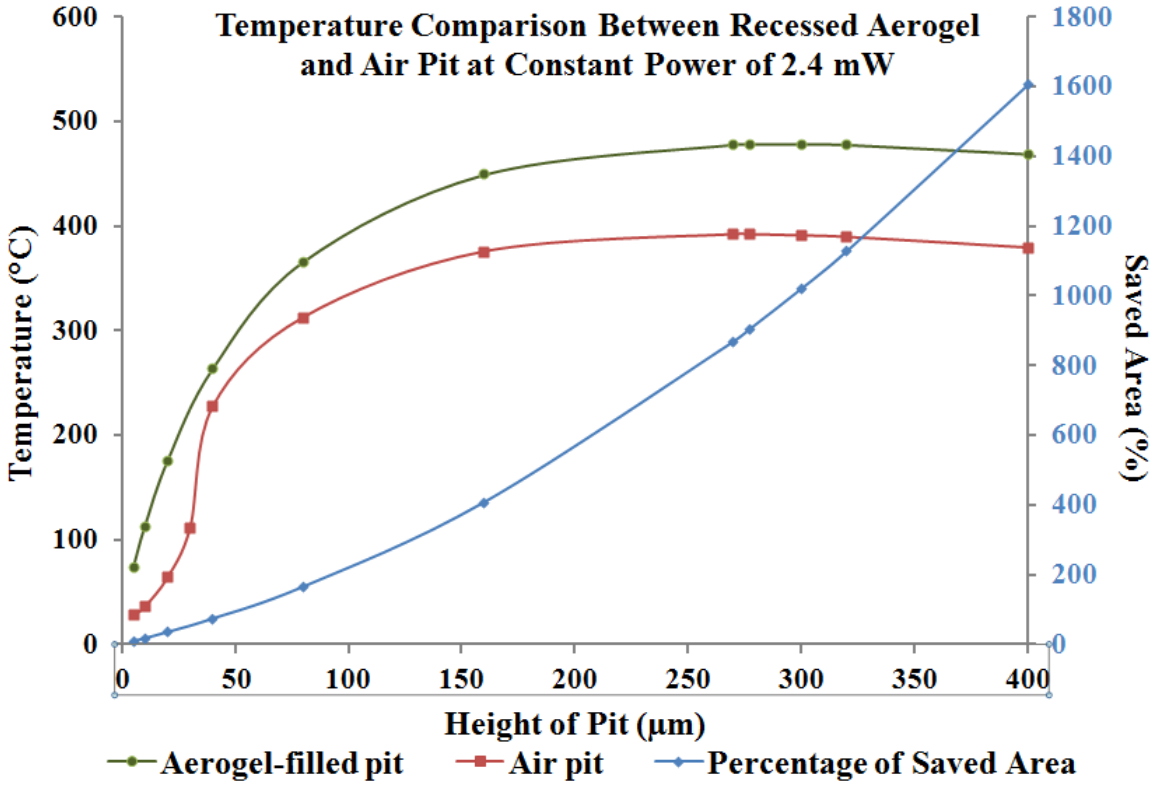

Figure 3.2 Temperature and saved area for different heights of pit.

For instance, by having a depth of only 160 µm pit filled with aerogel, we can significantly save four times less area than that of air pit. In another word, for every sensor processed with air pit we can have 5 sensors using aerogel. As the height of the aerogel increases more space would be saved by a parabolic factor. Hence, a denser sensor array can be fabricated quite easily by using aerogel as compared to micromachined air pit.

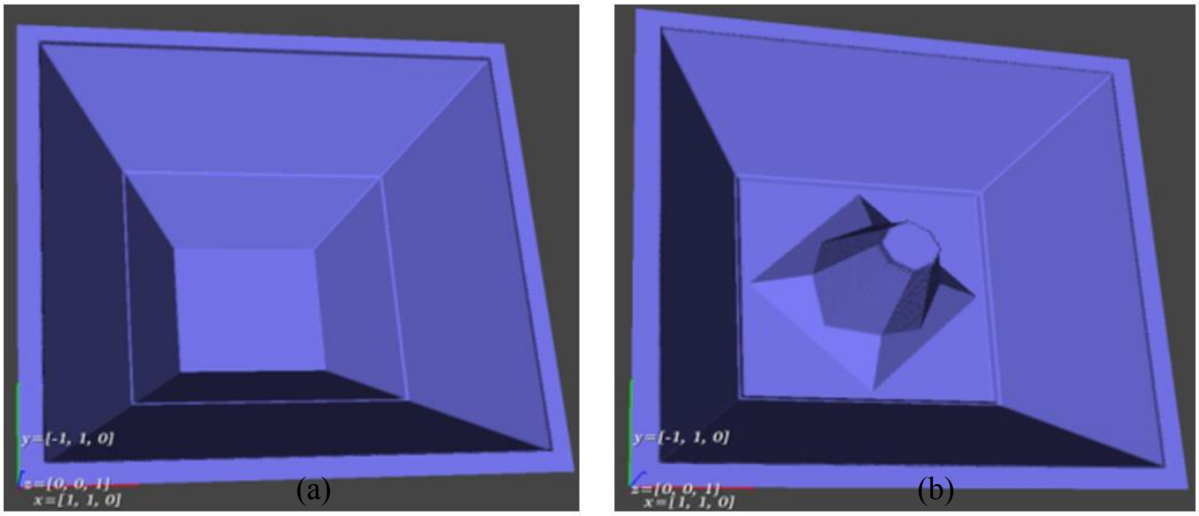

Figure 3.3 A column of silicon will remain as a heat sink for a shallow pit; (a) Completely etched (b) partially etched structure.

3.3.2 Micromachining limitation

In order to build the air pit we are limited by the trapezoid openings in micromachining. For instance, up to a certain height "h", a column of silicon will remain unetched as shown in Figure 3.3. The unetched silicon column will act as a heat sink between the μHP and the substrate preventing the temperature to reach to the desired value. However, for the recessed aerogel any desirable size of the pit height is achievable with a simple Manhattan mask opening. Once the pit is filled with aerogel an array of μHPs is processed on top of the recessed aerogel.

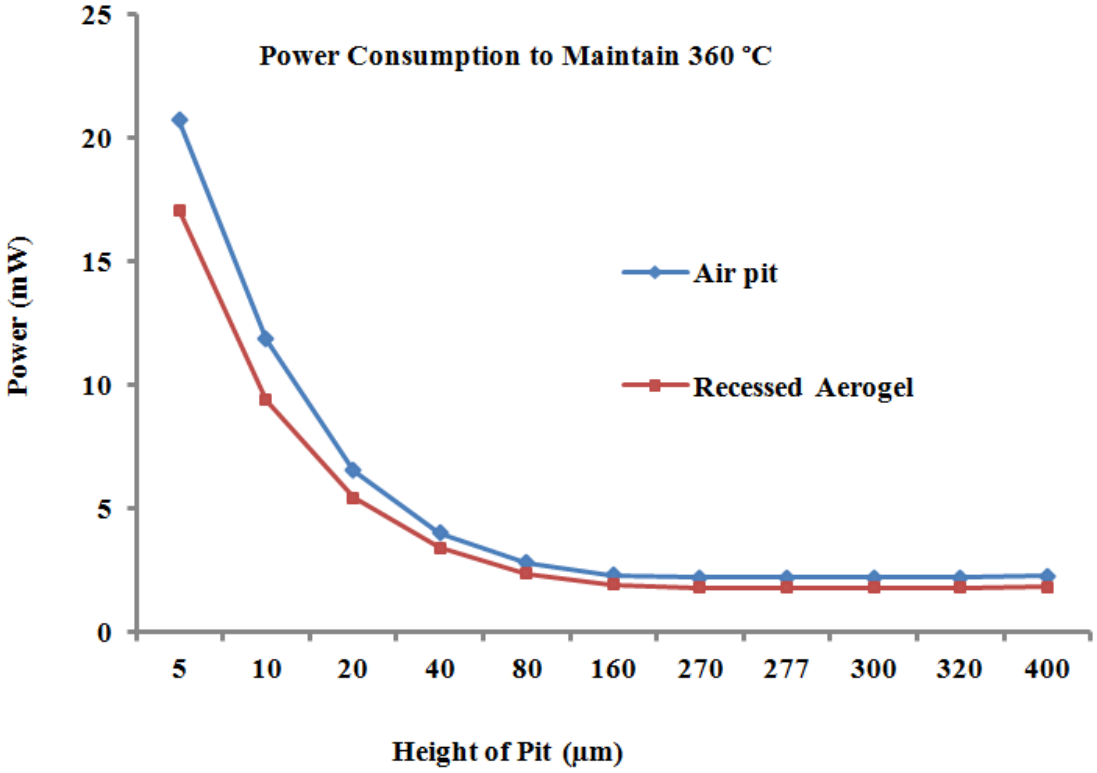

Figure 3.4 Power consumption versus height of the pit to maintain 360°C.

3.3.3 Effect of air pit height

As shown in Figure 3.4, to maintain 360°C the power consumption by µHP array reduces exponentially as the height of the recessed aerogel increases. For the height equal and greater than 160 µm the power consumed by sensor array will reach to a minimum value of 2.0 mW.

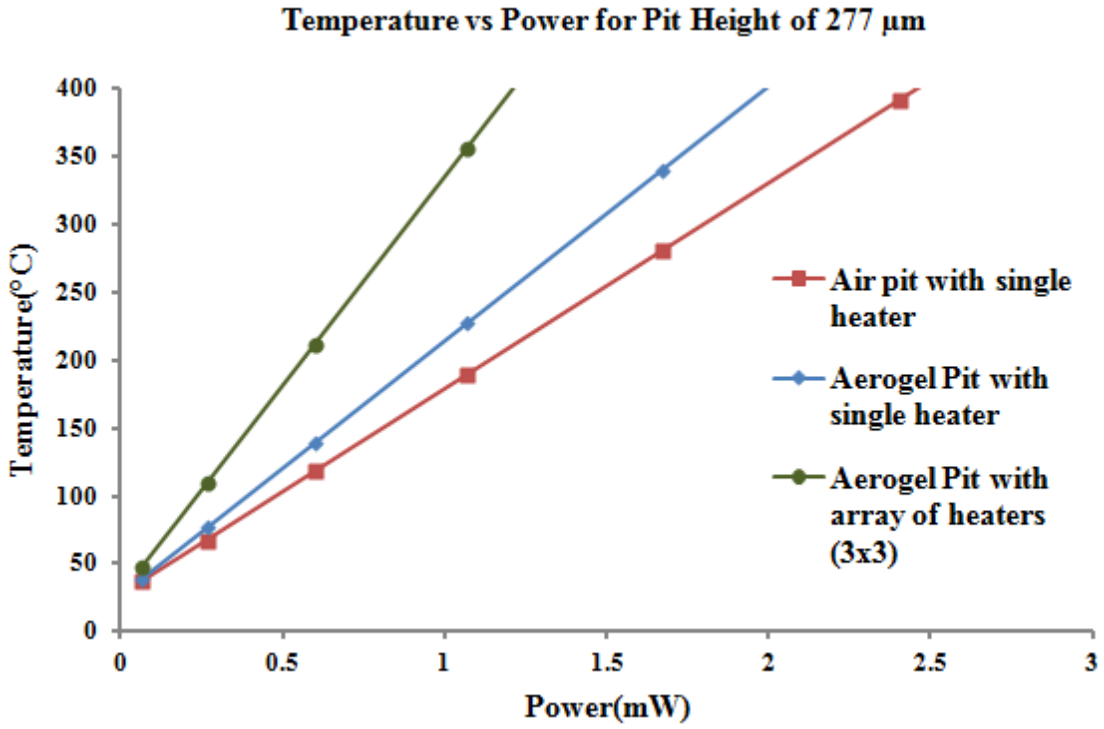

Figure 3.5 Temperature versus power for the given height of 277 µm.

3.3.4 Power efficiency

In Figure 3.5 temperature versus the consumed power per µHP is plotted for an air pitted recessed aerogel, and 3×3 array (573×573 μm^2) of µHP on recessed aerogel. The height of the pit is 277 µm. The power consumed by a µHP of an array made on the recessed aerogel gave the best result. In Figure 3.5 for applied power of 2.4 mW to an individual heater for air pitted and recessed aerogel shows superior heat insulation of recessed aerogel. However, for the air pitted µHP that the height is not sufficient to have a large "b" for a given "a" according to equation 3.1, the temperature would stay low because of the heat sink path through the unetched column.

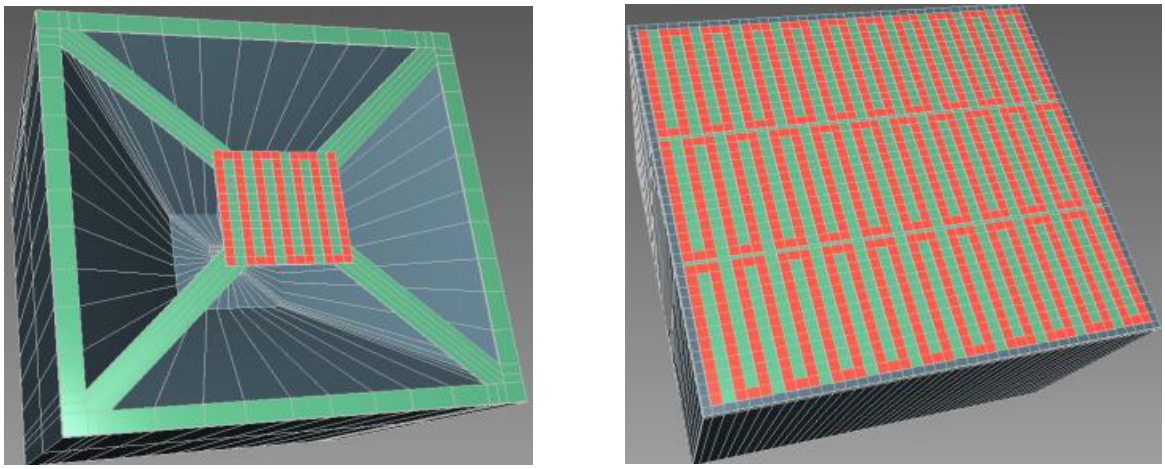

(a) (b)

Figure 3.6 3D view of (a) air pit with single heater (b) recessed aerogel with array of heaters (3×3).

3.3.5 High density array

The two structures depicted in Figure 3.6 demonstrate the air pit with single heater and recessed aerogel with array of heaters. The high density of heaters for the same occupied area of the chip is remarkably observed in case of utilizing the recessed aerogel in the pit.

3.4 Conclusion

We have reported a remarkably efficient structure for ultra-dense gaseous sensor arrays by defining a new design which uses recessed aerogel in the micro machined pit to provide an ultra-low power consuming μHP at a little expense of only 1 mW. Recessing aerogel eliminates the problem of step coverage that can severely reduce the yield of micro sensors. In addition, by recessing aerogel the problem of multilayer processing of aerogel to obtain a thick layer is removed. Also, the recessed aerogel has the advantage of micromachining the desired cavity of any size and height prior to fabrication of the sensor arrays. To demonstrate the power and area efficiency of our design we have shown that by using power as low as 1 mW, not only we can maintain the temperature of 360°C on the μHP of size 181×181 μm^2 but also we can save on area as large as ten times (2.95×105 μm^2) compared to conventional μHP structure.

4. SIMULATION STUDY OF MULTILAYER SILICA AEROGEL

In this chapter, we investigate the feasibility of multilayer silica aerogel interleaved with thin layers of SiO_2, to replace the micromachined air pit used in fabrication of metal oxide (MOX) gas sensors. Microhotplate is the most important structure of MOX gas sensors since it provides the desired uniform temperatures ranging from 200ºC to 500ºC for the sensing material. As discussed in the previous chapter, in order to achieve this operating temperature we must have a thick layer of 5 to 20 μm aerogel. However, in the literature we cannot find reports that indicate multilayer spin-coated aerogel is possible. In our laboratory, we have successfully spin coated two layers of aerogel with high porosity of 85% and low refractive index of 1.05. We have investigated the formation of thicker multilayer aerogel by having sputtered SiO_2 as interlayer. The heat insulation capability of multilayer is reported in both steady state and transient mode.

4.1 Introduction

In the previous chapter, we explained that the thickness of a single spin-coated layer of aerogel does not exceed a few microns, demanding multilayer spin-coating which is extremely difficult due to the porosity of the underneath aerogel layers, leading to penetration of the above layers before well spreading which results in a non-uniform surface. In this chapter, we propose the multilayer processing of silica aerogel interleaved with 200 nm sputtered SiO_2 as depicted schematically in Figure 4.1. The heat insulation capability of the proposed multilayer and the equivalent single layer is studied in both steady state and transient mode.

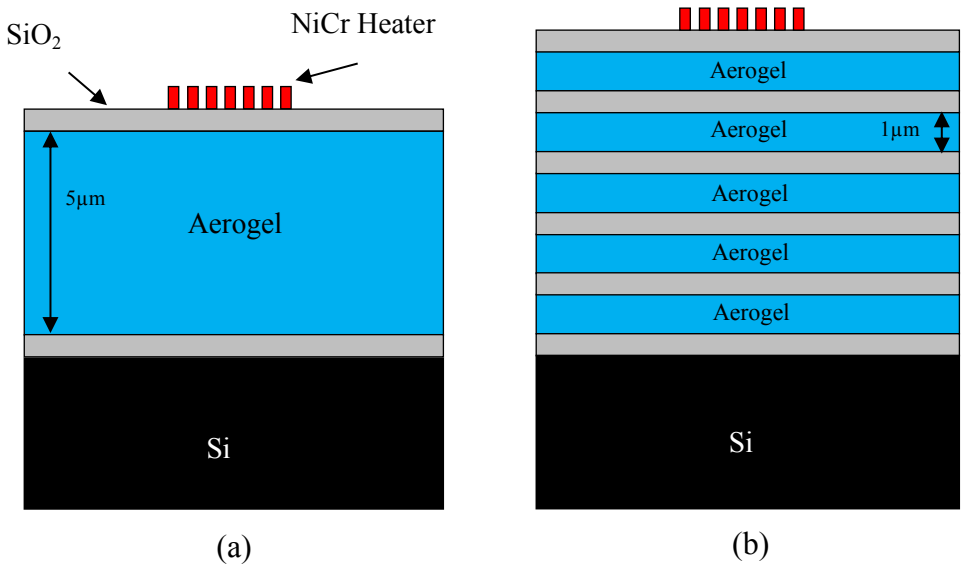

Figure 4.1 Schematic of (a) single thick layer aerogel and (b) proposed multilayer aerogel interleaved with sputtered SiO2.

4.2 Experimental procedure

The thin film aerogel was prepared using the following procedure; at first a solution was prepared implementing a two-step sol-gel method by mixing TEOS, ethanol, water, and HCl with the molar ratio of $1:4:4.2:4\times10^{-4}$, respectively. After an hour of stirring, 0.86 ml of NH_4OH 0.06 M was added and stirred for 5 more minutes. The sol-gel was deposited on the wafer after 60% of gelation time (20 minutes), followed by spin coating at 2000 RPM for 15 seconds. Next, an ethanol exchange was carried out for a period of 24 hours to strengthen the gel network. Finally, the aerogel thin film was obtained by supercritical drying the wafer with CO_2 followed by annealing at 450°C for an hour.

The thickness obtained was around 0.8 µm which was not sufficient to provide required thermal insulation to achieve high temperature with low power consumption as explained previously. To increase the thickness of the aerogel film another layer was spin-coated on the first layer. However, due to the porous nature of the first aerogel thin film, the second layer penetrated down while spin-coating, resulting in non-uniform surface. Moreover, the penetrated solution fills the pores of the first layer, making it a non-porous dense film.

To avoid the abovementioned limitations, an interlayer thin film SiO_2 (200 nm) was sputtered, before processing the next aerogel layer. The sputtered SiO_2 covers the porous surface of the aerogel thin film, enabling multilayer aerogel processing as shown schematically in Figure 4.1 (b).

4.3 Results and discussion

4.3.1 Thin Film Characterization

The obtained thin film aerogel was characterized with atomic force microscope (AFM) and spectroscopic reflectometer (SR300) to study the surface topology and measure the thickness of the thin film, respectively. AFM image shown in Figure 4.2 demonstrates the smooth surface topology of the thin film aerogel as well as its porosity. The porous structure can be clearly observed in the image. The root mean square roughness on the surface was determined as low as 1.33 nm which represents the smooth surface of the aerogel thin film. The extremely low roughness of the thin film enables high quality photolithography and masking.

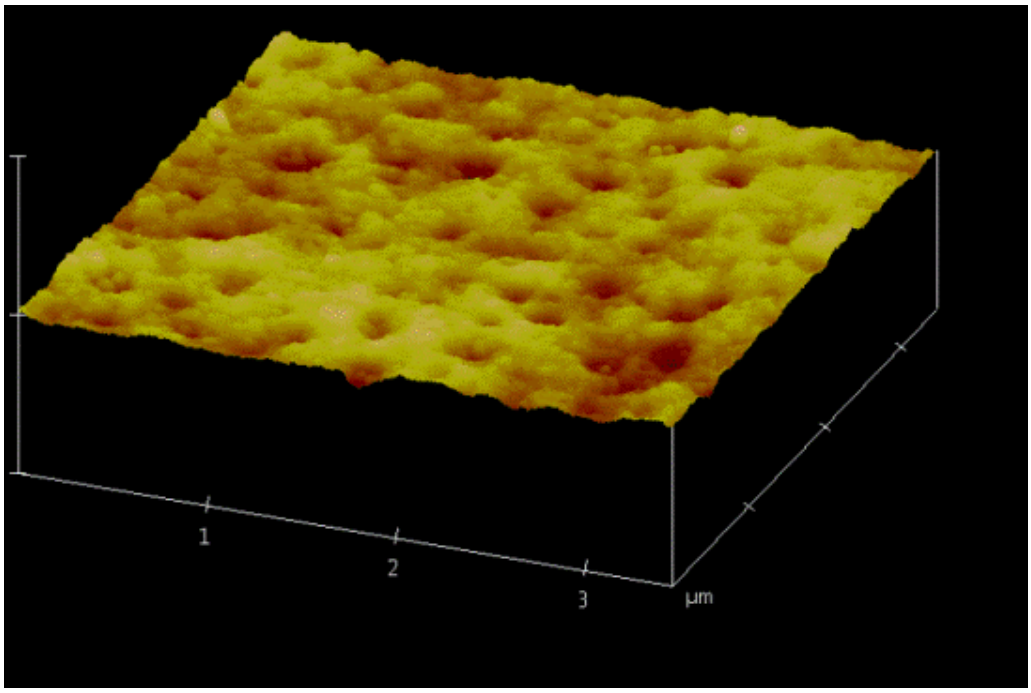

Figure 4.2 AFM image of the spin coated thin film aerogel.

The thickness of each thin film aerogel layer was measured as 800 nm. The refractive index was also determined by spectroscopic reflectometer as low as 1.053 at wavelength 633 nm as shown in Figure 4.3. The porosity of a thin film is related to its refractive index according to the following equation [21]:

$$\pi = 1 - \left(\frac{n_{film}-1}{0.209\rho_s}\right) \tag{4.1}$$

where π is the thin film porosity, n_{film} is the refractive index of the film, and ρ_s is the density of thermal oxide SiO_2 (2.19 g/cm^3). The corresponding porosity was determined as 85%. This high porosity ensures excellent thermal insulation.

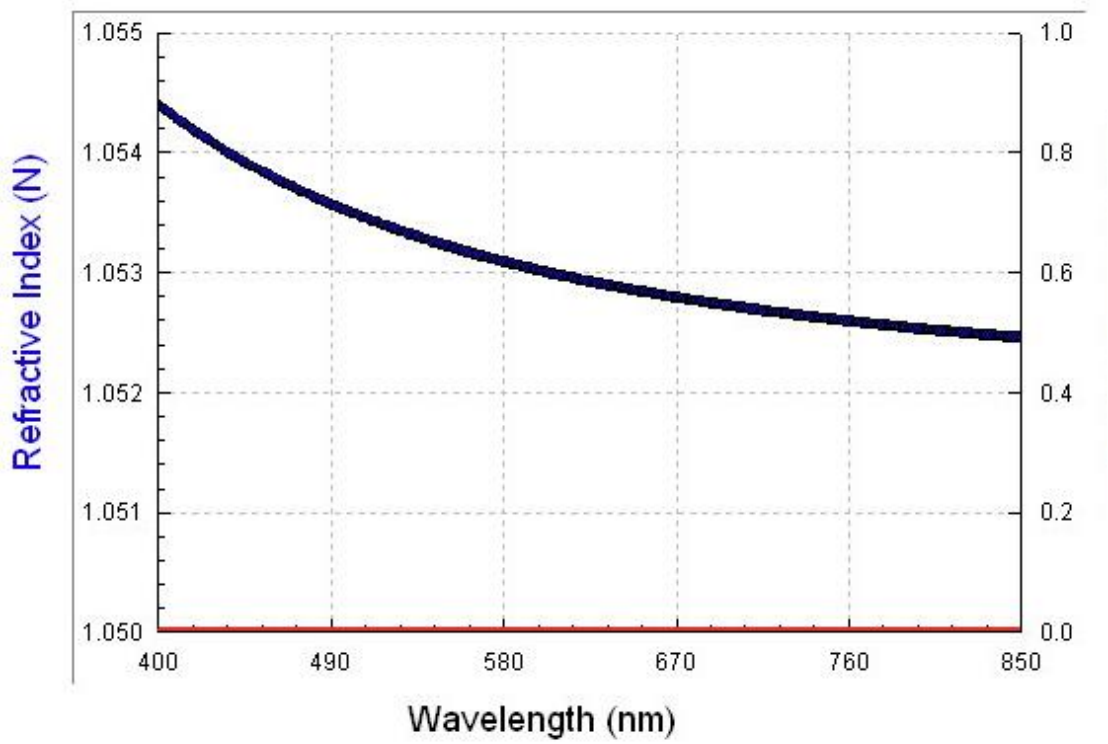

Figure 4.3 Refractive index of the thin film aerogel measured by spectroscopic reflectometer at different wavelengths.

4.3.2 Simulation

The performance of the multilayer aerogel (five layers of 1 μm each, interleaved with sputtered SiO_2) and the thick single layer aerogel (5 μm) was investigated by thermo-electrical module of IntelliSuite software. The software is equipped with different modules of: Intelli Mask to design the mask; 3D Builder to create the meshed solid blocks and differentiate their entities on different layers; TEM (Thermo Electro Mechanical) to assign the properties of each entity, load the initial conditions, and simulate the temperature gain by applying voltage to one end of the heater, keeping the other end at zero potential. The temperature at the bottom of the silicon substrate is set to room temperature of 27°C to resemble the reference temperature.

A steady state analysis was performed for both single and multilayer aerogel to investigate the temperature gain versus consumed power. As demonstrated in Figure 4.4, both structures achieved same temperature at any given power. For instance, applying 15 mW power corresponds to the temperature of 320°C. This promises multilayer processing with the advantage of having SiO_2 to cap the bottom aerogel layer avoiding the penetration of the above aerogel, and meanwhile no temperature loss due to utilizing the SiO_2 interlayer which itself is a very good heat conductor.

Transient analysis was also conducted over a period of 1 second to investigate the required amount of time to reach the steady state temperature. As demonstrated in Figure 4.5, it took 70 ms for both structures to reach steady state temperature of 360°C, which again verifies the capability of the interleaved multilayer aerogel to reach high temperature as fast as the thick single layer aerogel.

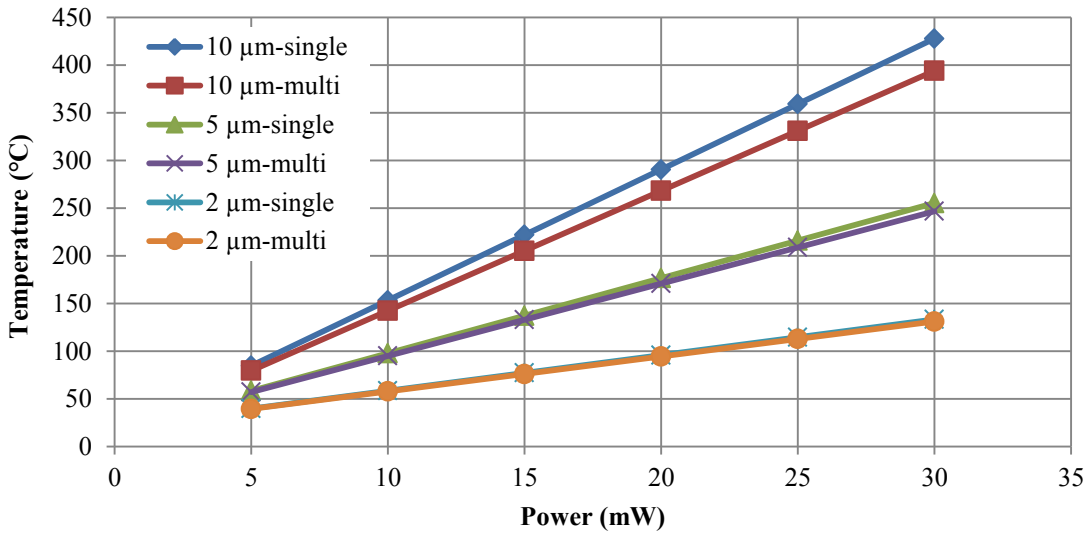

Figure 4.4 Comparing obtained temperature for single and multilayer aerogel in steady state mode.

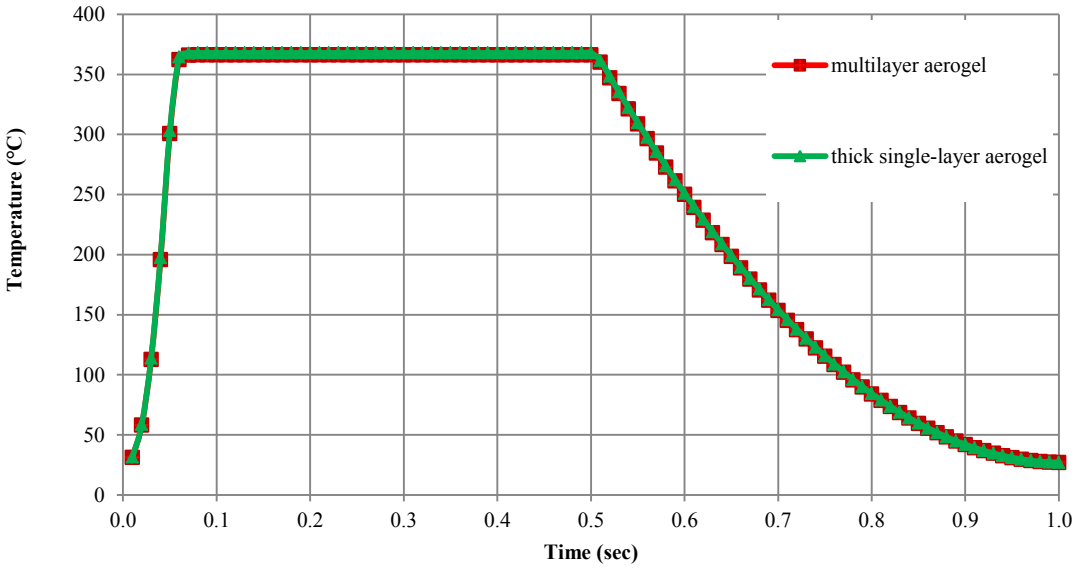

Figure 4.5 Transient analysis of single and multilayer (5-layer) aerogel.

4.4 Conclusion

In this chapter we presented a new approach to process multilayer aerogel thin film with interlayer sputtered SiO_2. A smooth two-layer aerogel with 85% porosity was successfully processed. The simulation was carried out to study the heat insulation capability of multilayer aerogel and thick single layer aerogel in both steady state and transient mode. It turned out the multilayer aerogel contributed same steady state temperature at any given power as the thick single layer aerogel. Moreover, it took same amount of time for both cases to reach the steady state temperature.

5. SINGLE LAYER SILICA AEROGEL VIA AMBIENT DRYING

A silica aerogel thin film with high porosity and excellent uniformity has been developed on silicon wafers, using Tetraethylorthosilicate (TEOS) as the silica precursor at ambient pressure via 1-step sol-gel method, avoiding super critical drying commonly used in aerogel processing. With its surface modification performed by Trimethylchlorosilane (TMCS) solution in Cyclohexane, the thin film developed has an extremely low dielectric constant of 1.49 without any crack. Film thickness and the refractive index were measured by Spectroscopic Reflectometer as 1250 nm and 1.133, respectively. Porosity calculated from the refractive index equals 71.1%, closely matching 70.8% obtained using the reflectometer. FTIR peaks confirm the presence of Si-CH_3 bonds, interpreting the hydrophobicity of the aerogel thin film.

5.1 Introduction

As mentioned previously, there has been research into potential applications of silica aerogel, which possesses such unique properties as low thermal conductivity, ultra-low dielectric constant (k), and high thermal stability. Among those applications, thin film processing received considerable attention in micro electromechanical systems (MEMS) processing as interlayer dielectrics for ULSI systems. A variety of materials and methods has been pursued for processing silica aerogel thin films. While Tetramethoxysilane (TMOS) and polyethylene glycol (PEG) were deemed preferred for creating thin film aerogel as a low-dielectric material in ULSI applications [53] their involved process required super critical drying at high pressure of 16 MPa.

Separately, tetraethoxysilane (TEOS) along with HF as the catalyst was applied to develop a porous SiO_2 thin film for use as an interlayer dielectric [54]. Although the FTIR

(Fourier Transform Infra-Red) spectroscopy showed the presence of SiO_2 on the thin film so developed, its porosity did not exceed 27.4% and its dielectric constant did not go below 3.1.

Meanwhile, silica aerogel has been employed as a matching layer for efficient operations of air-coupled piezoelectric transducers [85]. However, such a silica aerogel layer failed to be uniform, crack-free, and well-adhesive to the substrate (i.e., polyimide). The thickness of the aerogel thin film developed for such a matching layer never exceeded 0.5 μm [53-54, 85].

In another effort to provide aerogel thin films, TEOS was processed with HCl and NH_4OH through a laborious 2-step method, and the solution was spun on the silicon wafers coated with 100 nm thermal oxide layer [86]. However, in this work we report our successful development of high quality hydrophobic silica aerogel thin films which are crack-free with high porosity and good adhesion to the bare silicon substrate, without thermal oxide layer, via a 1-step procedure, using HF as acid catalyst. Developed at ambient pressure to avoid super critical drying, such a thin film has an extremely low dielectric constant of 1.49 that can be used as interlayer insulator in ULSI fabrication.

5.2 Experimental

The materials used in our work include TEOS (Sigma-Aldrich, as silica precursor), ethanol (Sigma-Aldrich 200 proof, as solvent), deionized (DI) water, and HF (as the catalyst). Using HF as acid catalyst is more preferable than HCl because the weak acidity of HF and alkaline of F ion control the rate of the hydrolysis and condensation reactions, leading to more uniform microstructure of the gel [87]. According to our experimental findings, the best molar ratios of TEOS, ethanol, water, and HF equal 1: 3: 20: 0.1, when mixed together. After mixing the chemicals, the solution was aged till 80% of its gelation

time in order to promote the hydrolysis and condensation reactions. The viscous solution was then spun onto the p-type silicon wafer (100) at 3000 RPM for 15 seconds to yield a uniform thin film layer. The spin-coated film was aged for 10 minutes to ensure complete gelation. Next, the wafer was dipped into ethanol and then placed in a furnace at 70°C for 1 hour to strengthen the gel network and extract the remaining unreacted water inside the gel.

1. TEOS + ethanol + water + HF (1 : 3 : 20 : 0.1 molar ratio)
2. Age till 80% of gelation time
3. Pour the solution on the p-type silicon wafer
4. Spin-coat at 3000 RPM for 15 seconds
5. Age for 10 minutes at room temperature
6. Age in ethanol at 70°C for 1 hour
7. Surface modification by TMCS at 70°C for 2 hours
8. Dry at room temperature
9. Anneal at 450°C

Figure 5.1 Processing steps for ambient dried thin film silica aerogel.

The alcogel film was then aged in a solution of TMCS/Cyclohexane (4.5 vol. %) at 70°C for 2 hours to extract the ethanol from the alcogel. Finally, the gel was annealed at 450°C after dried at room temperature, obtaining the thin film silica aerogel desired. Figure 5.1 demonstrates the overall procedure steps followed by our processing to yield quality hydrophobic silica aerogel thin films. Spectroscopic reflectometer (model: SR-300, by Angstrom Sun Technologies Inc.) was used to measure the thickness and the refractive index of the thin film developed. Next, FTIR (Spectrum 65, by Perkin Elmer) was employed to investigate the chemical species and bonding state. Scanning Electron Microscope (model:

JEOL-6300) and Atomic Force Microscope (by Digital Instruments) were then used to explore the surface morphology of the thin film.

5.3 Results and discussion

5.3.1 Molar ratio

We have experimentally determined the processing steps to achieve high quality thin film silica aerogel. Since the molar ratio of water to TEOS is critical to the sol-gel processing of silica aerogels9 and also to the characteristics of final aerogel, we varied the amount of water used in mixed solution while keeping the contents of TEOS, ethanol, and HF unchanged. Figure 5.2 shows the different gelation times for solutions with various molar ratios of water to TEOS (H_2O /TEOS), ranging from 7 to 25.

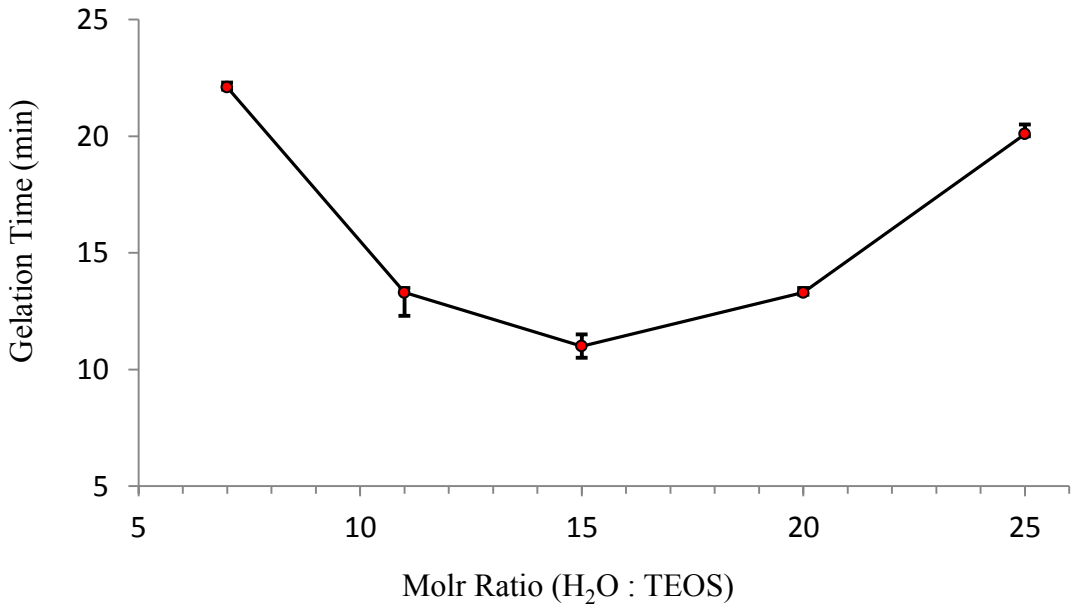

Figure 5.2 Gelation times for solutions with different water ratios.

5.3.2 Refractive index

Five different samples were made by using H_2O /TEOS molar ratios of 7, 11, 15, 20, and 25, according to our procedure steps listed in Figure 5.1. Figure 5.3 illustrates how the refractive index changes with varying molar ratios of water to TEOS. As shown in the figure, the refractive index of the film with the relative molar ratio of 20 is the lowest. The thickness and the refractive index of the thin films were measured by a spectroscopic reflectometer (Model: SR-300). The reflection spectrum of the sample is shown in Figure 5.4, where the model curve is seen to match the measured data curve very well (with an R-square of 0.99), revealing the confident measurement results.

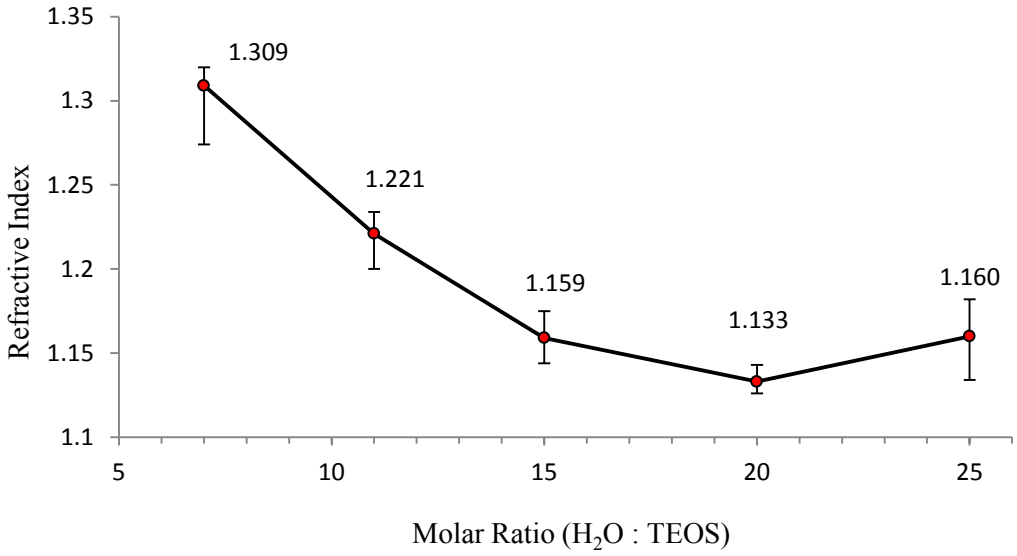

Figure 5.3 Refractive index versus molar ratio of water to TEOS.

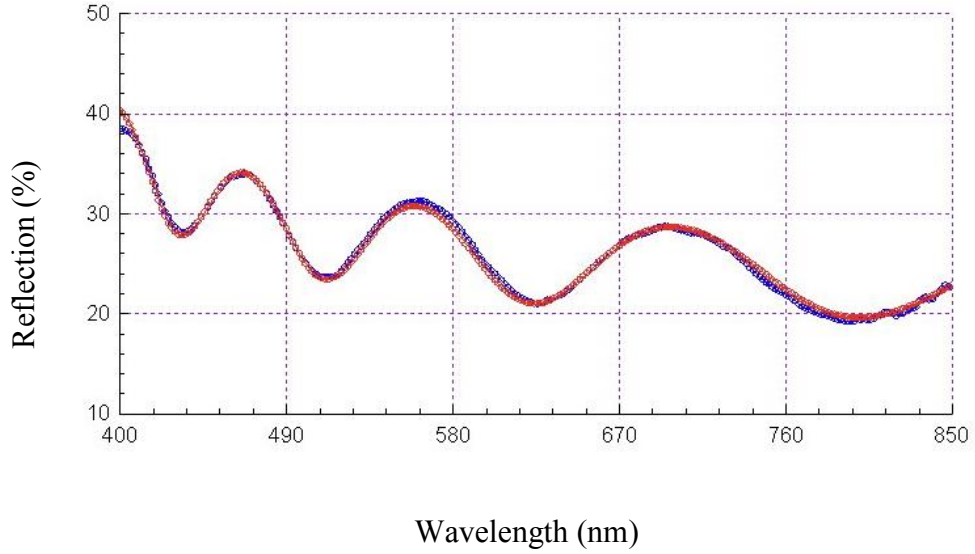

Figure 5.4 Reflection of thin film versus wavelength.

The film thickness was measured also by a surface profiler (model: Tencor-P10) to verify accuracy of the reflectometer thickness measurement. As can be observed in Table 5.1, both set of measurements give similar values, confirming accuracy of the reflectometer results.

Table 5.1 Thicknesses measured by reflectometer and surface profiler.

H_2O/TEOS Molar Ratio	Thickness measured by surface profiler (*nm*)	Thickness measured by Reflectometer (*nm*)	Deviation (%)
7	1517	1505	0.8
11	1414	1398	1.1
15	1237	1219	1.4
20	1241	1250	0.7
25	957	987	3.1

The refractive index of the thin film with the H_2O/TEOS molar ratio of 20 was measured as 1.133. Figure 5.5 demonstrates the influence of different annealing temperatures on the refractive index of the thin film. It is concluded that annealing up to 450°C could lower the refractive index. However, the structure of the thin film changes to become denser if annealing with a temperature above 450°C, resulting in a higher refractive index.

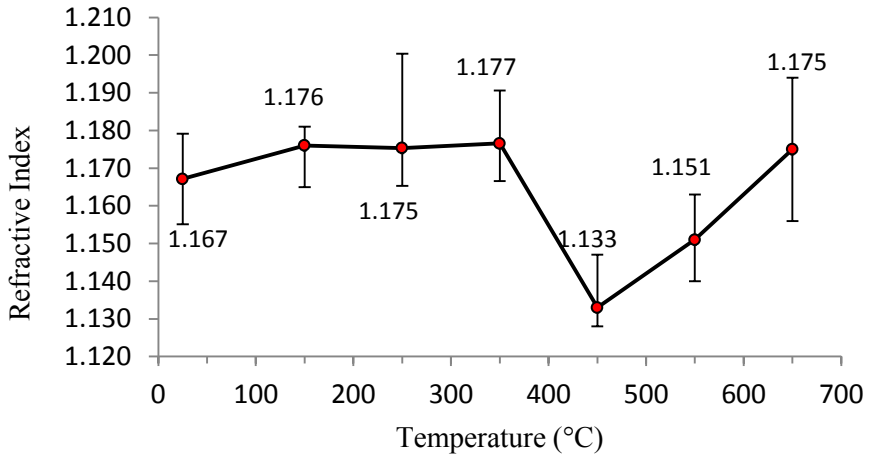

Figure 5.5 Effect of annealing temperature on the refractive index.

5.3.3 Porosity

The porosity (P) of a thin film can be obtained from the extended Lorentz-Lorenz equation [88] below:

$$P = \frac{\left(n_{f0}^2 - n_b^2\right)\left(n_a^2 + 2n_b^2\right)}{\left(n_{f0}^2 + 2n_b^2\right)\left(n_a^2 - n_b^2\right)} \qquad (5.1)$$

where n_{f0}, n_b, and n_a are the refractive indexes of the film without adsorbed water, of the dense film without pores (= 1.458), and of the air (= 1.0), respectively. The porosity of the thin film with a refractive index of 1.133 was calculated as high as 71.1%. The porosity was also inspected by our spectroscopic reflectometer on the composite layer module. In this module, the layer was defined as a composite of SiO_2 and air. The latter volume fraction

would represent the porosity, which was determined as 70.8% (which is fairly close to the theoretically calculated value of 71.1%).

5.3.4 FTIR spectroscopy

The FTIR spectrums of thin film silica aerogel with various annealing temperatures and of a non-processed thin film are demonstrated in Figure 5.6 (a), where no solvent extraction or surface modification by ethanol or TMCS was applied. All the peaks in the graph match well the findings of previous aerogel processing studies [48, 60-61, 82, 87, 89-92]. However, our work here is different in either the procedure or materials. The peaks at 1091, 811, and 457 cm^{-1} represent asymmetric stretching, symmetric stretching, and bending (rocking) vibrations of Si-O-Si bonds [61, 82, 89]. As shown by the curves, the silica aerogel thin film is remarkably thermally stable up to 450°C. However, a decrease in intensity of the Si-O-Si peaks can be observed at 550°C, particularly the peak diminishes at 457 cm^{-1}.

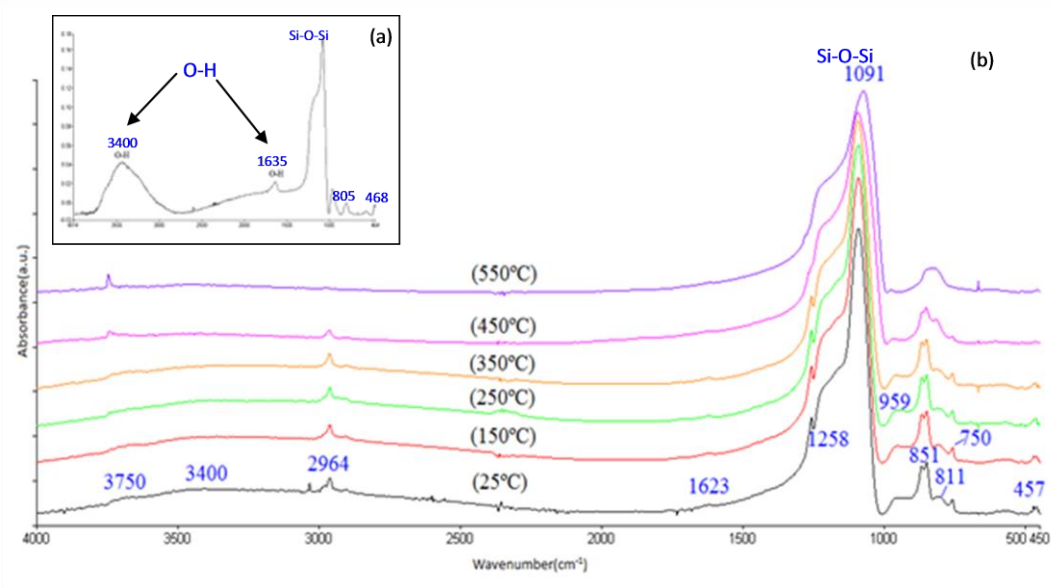

Figure 5.6 FTIR spectrum results of the silica aerogel thin film annealed at (a) room temperature, (b) 150°C, (c) 250°C, (d) 350°C, (e) 450°C, and (f) 550°C.

Comparing Figures 5.6 (a) and (b), one can find four different peaks introducing Si-CH_3 bonds at 2964, 1258, 851, and 760 cm^{-1} [48, 60, 90] with all of them confirming the effect of surface modification with TMCS, which makes the silica aerogel hydrophobic. Thin film hydrophobicity is seen stable up to 450°C, where the peaks at 1258 and 760 cm^{-1} start to fade away. All the -CH_3 peaks disappear completely at 550°C due to the fact that –CH_3 groups become oxidized and evaporate, encouraging the silica aerogel to become hydrophilic [48]. The stretching vibration of Si-OH bonds can be observed at 959 and 3750 cm^{-1}[87, 91-92] interpreting the incomplete hydrolysis of TEOS [92]. Two more peaks related to O-H asymmetric vibration and H-O-H bending vibration can be found at the wave numbers of 1623 and 3400 cm^{-1} [55, 91] The latter actually comprises a broad peak centered at 3400 cm^{-1}. From Figures 5.6 (a) and (b), one can observe how well unreacted water and hydroxyl groups are substituted by methyl (-CH_3) groups. The peak at 3750 cm^{-1} is hidden at low temperature annealing FTIRs. However, it reveals peaks above 450°C, with the flattening of 3400 cm-1 broad peak of H-O-H bond. Although the peaks of O-H bonds begin to vanish beyond 450°C, the silanol bond (Si-O) peak of 959 cm^{-1} still remains even at 550°C, suggesting that the hydroxyl groups decomposed and disappeared whereas Si-O bonds are still stable enough.

Since silica aerogel is a composition of SiO_2 particles and air, it can be viewed as a two-phase material. There are several mathematic models capturing the relationship between porosity and the dielectric constant of a two-phase medium, with Clausius-Mossotti being a simple equation as

$$\frac{\varepsilon_c - 1}{\varepsilon_c + 2} = (1 - p)\frac{\varepsilon_0 - 1}{\varepsilon_0 + 2} \tag{5.2}$$

where ε_c and ε_0 (=3.81) are dielectric constants of a porous and a dense SiO_2 films, respectively, and p is the porosity of the thin film [93]. Given our obtained porosity of 71.1% to the equation, we have the dielectric constant of as low as 1.49.

Figure 5.7 is the high magnification SEM micrograph of the thin film surface, which clearly shows the uniformity and crack-freeness of the film. The pore size of nano-scale can also be seen in the range of about 20 nm. Figure 5.8 depicts the AFM image of the thin film, reaffirming its high porosity. The root mean square roughness on the surface is as low as 1.33 nm, far smaller than the value of 7.25 nm reported previously [55] signifying the better smoothness of the layer.

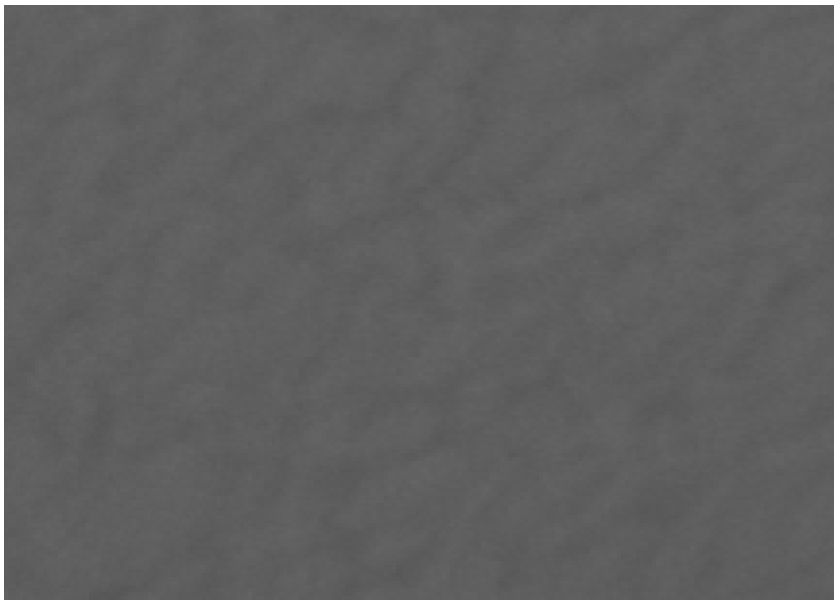

Figure 5.7 High magnification SEM image, with 20,000× of aerogel showing its high porosity and pore size of about 20 nm.

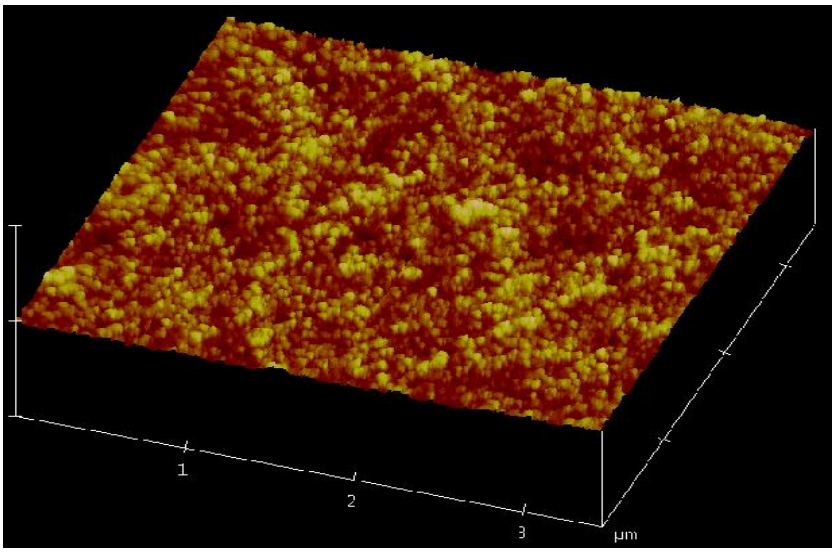

Figure 5.8 AFM 3D image of silica aerogel thin film.

5.4 Conclusion

A 1250 nm thin layer with low dielectric constant silica aerogel has been developed successfully on top of a silicon wafer at ambient pressure using TEOS, ethanol, water, and HF, through a 1-step sol-gel processing. The refractive index of 1.133 was obtained by annealing the film at 450°C, with a higher temperature raising the refractive index. The molar ratio of 20 for water and TEOS was found to result in the lowest refractive index, when annealing at a constant temperature of 450°C. The porosity was measured as 70.8%, in comparison to the calculated value of 71.1% under a refractive index of 1.133. The dielectric constant was determined to be as low as 1.49. The FTIR spectrum confirms the presence of Si-O-Si bonds and their thermal stability up to 450°C. It also reveals the film hydrophobicity with the presence of $-CH_3$ peaks, which all remain until the annealing temperature approaches 450°C. Our quality silica aerogel thin film developed has an extremely low dielectric constant and is also uniform, smooth, and crack-free, as confirmed by SEM and AFM results. It has potential applications to ULSI as an interlayer dielectric material and as a

microhotplate thermal insulator for replacing micromachined air gaps in metal oxide gas microsensors.

6. SINGLE LAYER SILICA AEROGEL VIA SUPERCRITICAL DRYING

A thin film of silica aerogel has been spin coated on silicon wafers to investigate its super thermal insulating capability. The temperature of the thin film heaters fabricated on the aerogel coated wafer is measured at different applied powers. Simulations are performed to compare the aerogel coated wafers with the micromachined wafers. Both experimental and simulation results show better heat insulation for aerogel coated wafers as compared with simulated micromachined wafers. The measurement and simulation results of aerogel coated wafers are in good agreement. The aerogel film can replace the air cavity created by conventional micromachining of wafers to save power and chip area in metal oxide gas sensor arrays.

6.1 Introduction

Metal oxide (MOX) sensors have significant domestic and industrial applications in gas detecting instruments. The main component of MOX gas sensors is a plate called a microhotplate (μHP), on which the gas-sensing elements are fabricated. The temperature of the sensing elements must be maintained in the range of 300°C to 500°C [22] for efficient gas detection. This demands a highly efficient heater with minimum power consumption, maximum density, and fast response time when used in a sensor array. The current approach to achieve the desired temperature is to micromachine the semiconductor substrate to have an air pit acting as a thermal insulator. However, a large area is sacrificed to micromachine the air cavity, leading to a low density sensor array. It also results in low reliability in detection because of a less available number of sensors in a given area. The other issue is to minimize power consumption, which is mainly caused by the μHPs. Previous studies have reported

power consumption per unit area of 0.12–10 $\mu W/\mu m^2$ to maintain the temperature in the range of 300°C to 400°C [78–79, 94].

We have previously simulated the operation of a μHP built on aerogel coated silicon wafers. The simulation result was found to be highly promising [95]. In this chapter, we experimentally verify the previous simulation results by implementing a single layer thin film silica aerogel as a heat insulator on silicon wafers through supercritical drying.

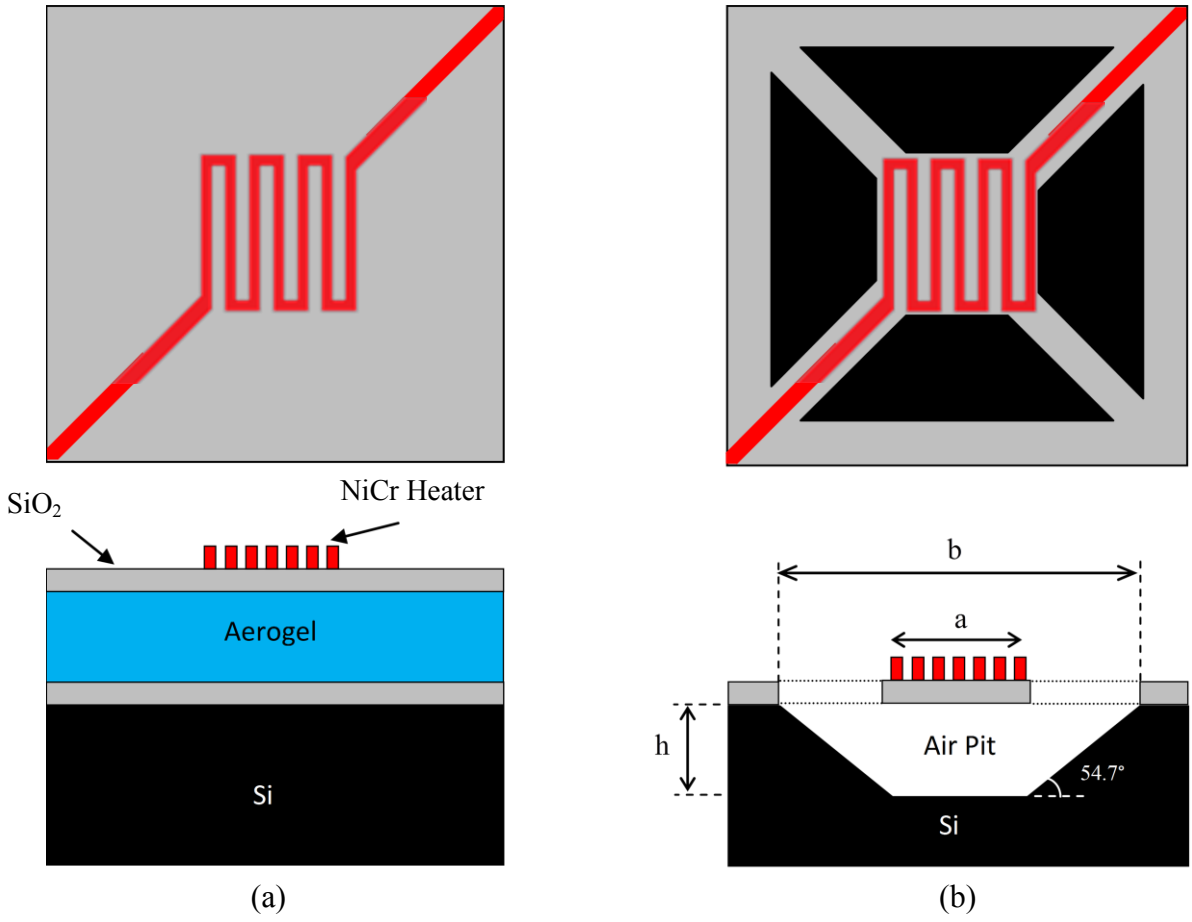

Figure 6.1 Schematic structures of heaters for experiment and simulation; (a) heater built on aerogel, (b) heater built on air pit.

6.2 Experimental

The thin film aerogel was prepared using the following procedure; at first, a solution was prepared implementing a two-step sol–gel method by mixing TEOS (Si precursor), ethanol (solvent), water and HCl (acid catalyst) with a molar ratio of $1:4:4.2:4 \times 10^{-4}$, respectively. After an hour of stirring the solution, 0.86 ml of NH_4OH 0.06 M (base catalyst) was added and stirred for five more minutes. The sol–gel was deposited on the wafer after 60% of gelation time (20 min), followed by spin coating at 2000 RPM for 15 s. Next, an ethanol exchange was performed for a period of 24 h to strengthen the gel network. Finally, aerogel thin film of 0.5 μm thickness was obtained by supercritically drying the wafer with CO_2 followed by annealing at 450°C for an hour. To create thin film nichrome heaters with good adhesion to aerogel, an interlayer of SiO_2 was sputtered before sputtering NiCr (Ni80/Cr20) on the wafer. For CMOS compatibility, polycrystalline silicon can be used as the heater element. Later, a photolithography procedure was carried out to obtain the desired heater structure shown in Figure 6.1. The schematic structure used in our experiment and simulation are shown in Figure 6.1 (a). The simulated air pit structure created by conventional micromachining is shown in Figure 6.1 (b).

The root-mean-square roughness on the surface is as low as 1.33 nm which represents the smooth surface of the aerogel thin film. The refractive index and the thickness of the thin film were studied using a spectroscopic reflectometer (SR300) which measured the reflecting light signal from the sample. The refractive index was measured as 1.053 at a wavelength of 633 nm. Finally, the thickness of the film was determined as 807 nm.

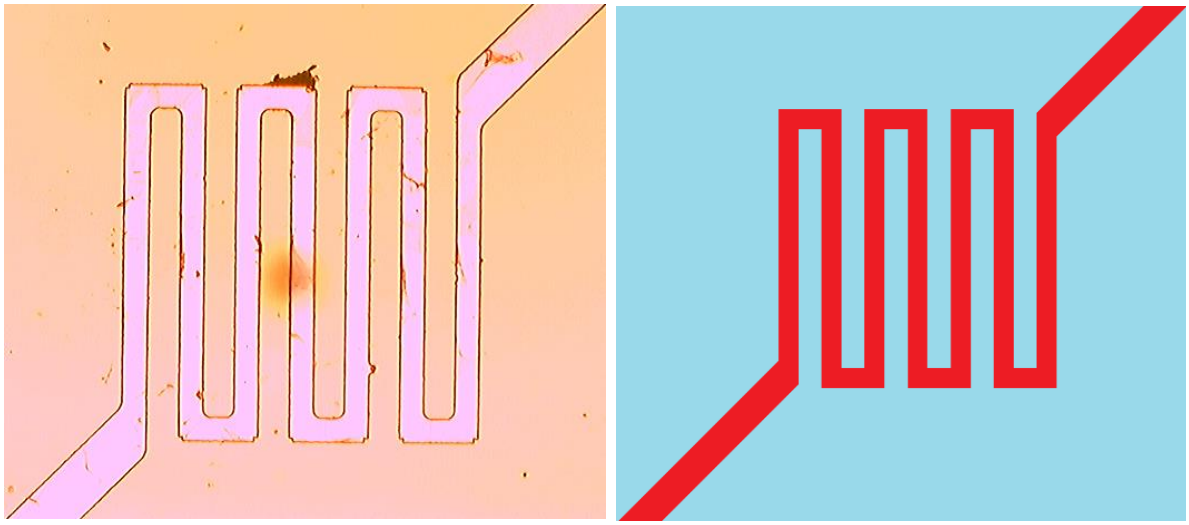

Figure 6.2 Photograph of the fabricated Nichrome heater on aerogel coated wafer (a) and the corresponding simulated scheme (b).

Figure 6.2 depicts the actual low magnification image of the fabricated Nichrome heater on aerogel coated wafer (Figure 6.2 (a)) as well as the corresponding simulated scheme (Figure 6.2 (b)).

6.3 Simulation

To verify the experimental results, a thermo-electrical analysis of our designed structures was performed using a MEMS simulation software, IntelliSuite. The software is equipped with the following modules: IntelliMask to design the mask; 3D Builder to create the meshed solid blocks and differentiate their entities on different layers; ThermoElectroMechanical to assign the properties of each entity, load the initial conditions and simulate the temperature gain by applying voltage to one end of the heater while keeping the other end at zero potential.

6.4 Results and discussion

The temperature of the heater was measured against the applied electrical power by measuring the change in heater resistance based on the following equation:

$$\frac{\Delta R}{R_0} = \alpha \cdot \Delta T \tag{6.1}$$

where α is the temperature coefficient of resistivity and R_0 is the initial resistance of the heater at the reference temperature (27°C). There are three major observations with regard to the obtained temperature at different applied powers per unit area, as noted in Figure 6.3. First one is the comparison of the experimentally measured temperature of heaters processed on aerogel and heaters processed on the silicon wafer without heat insulation (no aerogel and no air). The excellent ability of aerogel to insulate heat is pronouncedly seen where a good increase of temperature is detected in the case of aerogel coated wafers (0.8 μm), whereas almost no change in temperature is observed for the wafers without the aerogel, indicating the presence of a heat sink in the form of silicon substrate under the heater.

Second, we should notice the comparison between the simulation results of aerogel coated wafers and wafers with a micromachined air pit with the same aerogel thickness and air pit depth. Yet again, a better thermal insulation is observed for the aerogel compared with air due to ultra-low thermal conductivity of the aerogel. Although we have simulated an air pit of 0.8 μm depth, it is not possible to micromachine such a shallow pit using the usual trapezoidal-shaped mask. In fact, to etch out the silicon from underneath an $a \times a$ hotplate h deep, the required square size opening is

$$b = a + \frac{2h}{\tan(54.7°)} \tag{6.2}$$

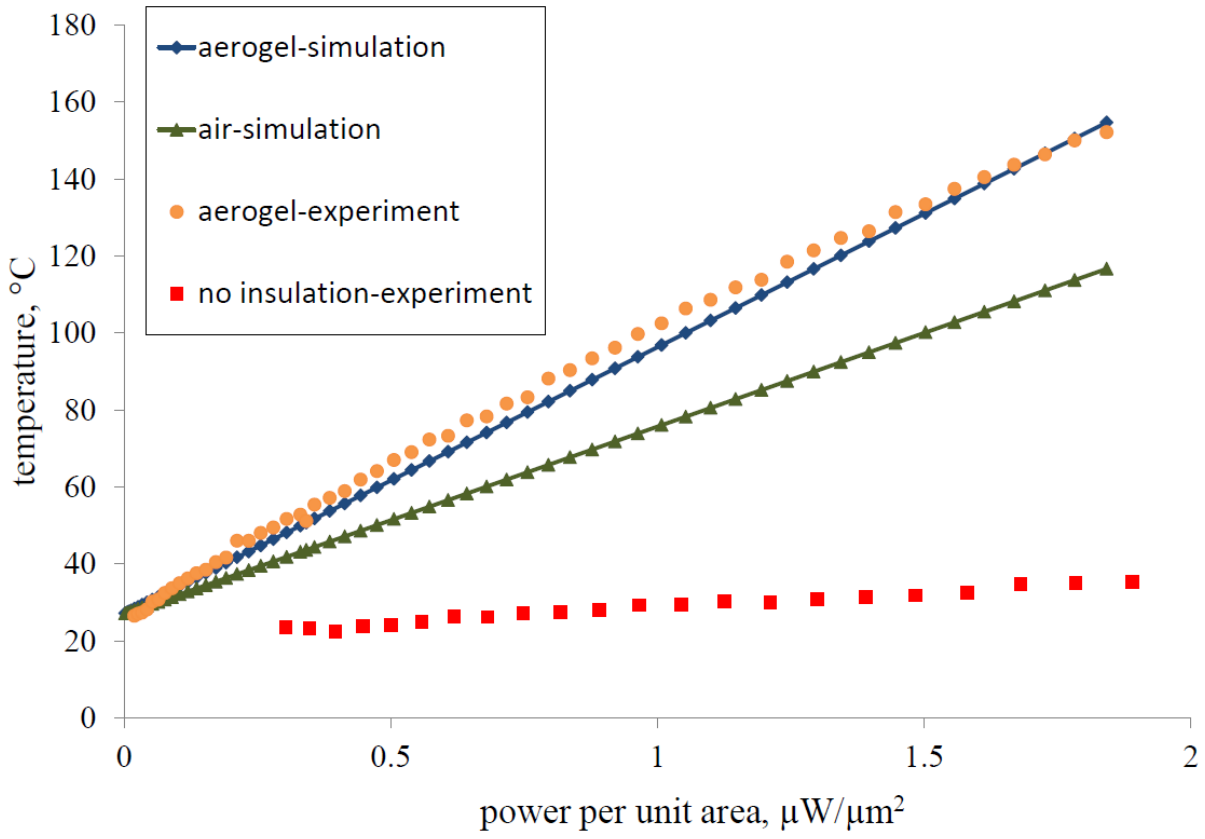

Figure 6.3 Obtained temperatures against power per unit area for 0.8 μm-thick aerogel insulation, 0.8 μm-deep air insulation, and no insulation.

The etchant will etch the silicon through the opening area of the trapezoid to make the air pit as shown in Figure 6.1 (b). However, to build the air pit, we are limited by the trapezoid openings in the micromachining. For instance, up to a certain height h, a column of silicon will remain unetched as demonstrated by the experiment and the simulation, as seen in Figure 6.4. The unetched silicon column will act as a heat sink between the μHP and the substrate, preventing the temperature from reaching the desired value.

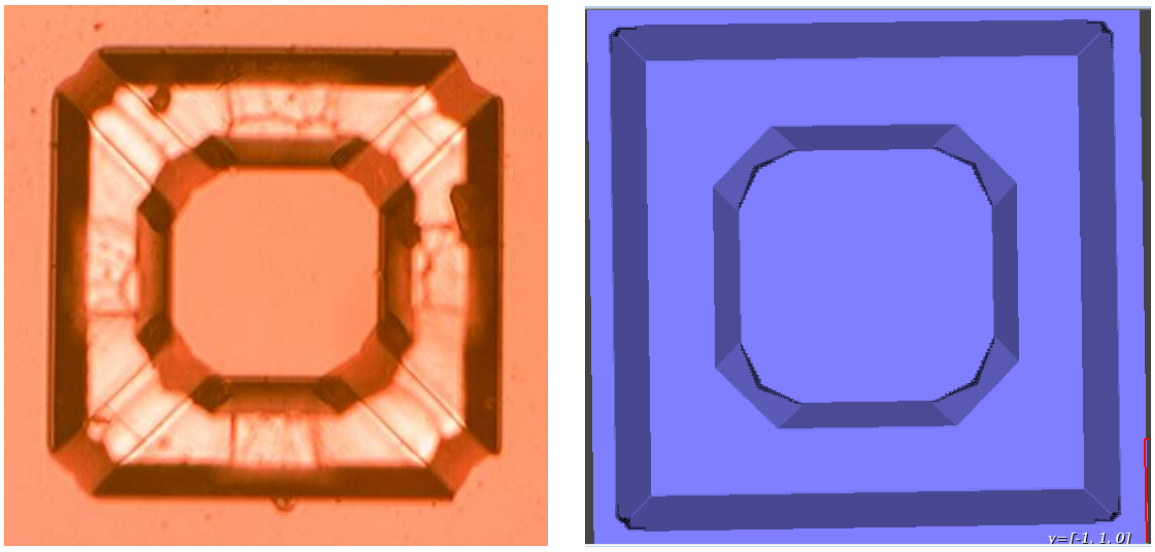

Figure 6.4 Trapezoid opening limitation on perfect etching; (a) fabricated unetched column, (b) simulated unetched column.

In addition, we have previously shown by simulation that for the applied power per unit area of 0.07 μW/μm^2 an air pit of 160 μm depth is needed to obtain 360°C compared with an 80 μm thick layer of aerogel. Moreover according to equation 6.2, the area of the mask opening or the total occupied area to suspend a single hotplate increases as a square function of the height of the pit. Hence, one can calculate the percentage of saved area as

$$S = \frac{b^2 - a^2}{a^2} \times 100 \tag{6.3}$$

which implies that the micromachined air pit for each individual sensor in a sensor array uses much more area of the chip than using aerogel on the wafer for the same array. Hence, a denser sensor array can be fabricated quite easily by using aerogel as compared with a micromachined air pit.

The last and most significant observation from Figure 6.3 is the remarkable match between experimental and simulation results for aerogel coated wafers considering temperature against applied power per unit area. For instance, for the applied power per unit area of 1.6 $\mu W/\mu m^2$, the measured temperature is 140°C compared with the simulated temperature of 133°C.

6.5 Conclusion

Using aerogel as a heat insulator yields the following advantages over the micromachined air pit conventionally created as a heat insulator in MOX gas sensors: (i) superior heat insulation capability hence lower consumed power, (ii) more mechanical stability of aerogel by not suspending the sensor structure by four thin straps, and (iii) a denser sensor array by avoiding micromachining. Most significantly, the measurement and simulation results of aerogel coated wafers were in very good agreement with each other.

7. OUR NOVEL SOL-GEL METHOD

In this chapter, we present the development of a novel technique for sol-gel processing that resolves the aforementioned limitations of thin/thick films manufacturing by avoiding any further steps including solvent exchange and/or supercritical drying. The impregnation of ethanol with functional colloidal alcogel particles is a distinctive and different approach from the conventional methods where tiny aerogel particles are formed on the wafer networked together just by exposure to air during spin coating. The novelty of this method is not limited to thin/thick film processing of silica aerogel but applies to many other sol-gel processes. The initial motivation of this development was to replace the high costing micromachined air gaps in silicon wafers with silica aerogel as a super heat insulating material for metal oxide sensors, but our developed "Special Sauce" can be applied for many other industrial applications.

7.1 Introduction

Even though some of the applications from bulk processing of aerogel are being used by industry, the attempts of fabricating aerogel as thin film or thick film are hampered due to low porosity, cracking, and roughness of aerogel and therefore the research has been limited only to academic publications. Today, the processing of thin/thick film aerogel is labeled as too complex and challenging by the experts in the field. The complexity of aerogel thin film processing comes from the induced high stress and shrinkage during drying. With supercritical drying and/or solvent extraction no more than a couple of microns thick film is yielded [96]. There has been no breakthrough to resolve the problems associated with thick film (4 -50 μm) aerogel processing nor any reports is cited in the existing literature regarding the roughness of the thick film. Roughness of the film is very important for microsensor

fabrication where planar technology is required for producing minimum feature size microstructure on the film. In this chapter, we reveal our patent pending state-of-the-art technique of sol-gel processing eliminating all the constraints involved in producing thick film aerogels. Although we have proposed our invention for the microheater applications, this technique can be applied to many other coating applications, including but not limited to insulation (such as heat insulating textile and heat and sound insulation coatings), nano-composites, adsorbents, optical devices, waveguides and fiber optics, inter-metal dielectrics, integrated circuit manufacturing and integrated circuit heat management, drug delivery systems, gas sensors, solar cells, fuel cells, gas storage, and Cherenkov detectors.

7.2 Experimental procedure

The process for producing thin and thick layer aerogels described herein comprises spraying the right solution into ethanol, aging the impregnated ethanol, and then depositing the enriched ethanol on the substrate multiple times to result in a thick layer of aerogel without further treatments. Specifically, supercritical drying and solvent exchange are not used in the process. By using the process described herein, very tiny sol particles are created which are functional and able to link with ethanol to prepare small gel particles with the capability of being dried while spin/spray coating, which makes it possible for thin film or thick film processing.

7.2.1 "Special Sauce" preparation

The "Special Sauce" was prepared using the following procedure. First, a solution was prepared implementing a 2-step sol-gel method by mixing tetraethyl orthosilicate (TEOS), which is a Si precursor, ethanol (a solvent), water, and HCl (the acid catalyst) with the molar ratio of 1:4:2:4.3 x 10^{-4}, respectively. After an hour of stirring the solution, 0.64 ml

of 0.066 M NH_4OH solution (the base catalyst) was added and stirred for 5 minutes. The resulting mixture was sprayed into a 2 foot long column of ethanol (25 ml) after approximately 15 % gelation time by an aspirator for 15 minutes. Any aspirator with a head opening size of 0.02 inches to 0.05 inches in diameter can be used. This results in the impregnation of ethanol with functional colloidal alcogel particles. After aging the impregnated ethanol at room temperature for approximately 24 hours, the solution was ultrasound for 8 minutes. Then the impregnated ethanol solution was filtered using a 0.2 micrometer filter. Any filter can be used as long as the filter can filter particles greater than 0.2 micron.

7.2.2 Thin and thick films

The filtered impregnated ethanol solution was then spin coated on a silicon wafer at approximately 1150 RPM for 40 seconds. In one embodiment, ambient spin coating is performed at between 300 to 400 RPM at the initial time of dispensing and approximately 1150 RPM for the final spinning speed, using an acceleration rate of approximately 110 RPM/sec. Any spin coater with the specified RPM and timing can be used. Additional layers are spin coated onto the wafer in succession to yield a smooth (less than 40 nm Ra roughness), thick, and highly porous multilayer without supercritical drying or solvent exchange.

7.3 Discussion on process parameters

7.3.1 Apparatus setup

The example diagram in Figure 7.1 shows the processing apparatus to make the impregnated ethanol liquid. However, any set up that accomplishes a similar impregnation of ethanol with functional colloidal alcogel particles can be used. In Figure 7.1, the nebulizer nebulization rate is approximately 0.2 ml/min. The nebulizer operating pressure is approximately 12-18 psig. The nebulizer orifice size is approximately 500 µm. The ethanol container's internal diameter is 1.2 cm. The internal diameter of the tubing is 0.5 cm. Additionally in Figure 7.1, the low pressure is located right after the nebulizer orifice and the high pressure is before the orifice opening.

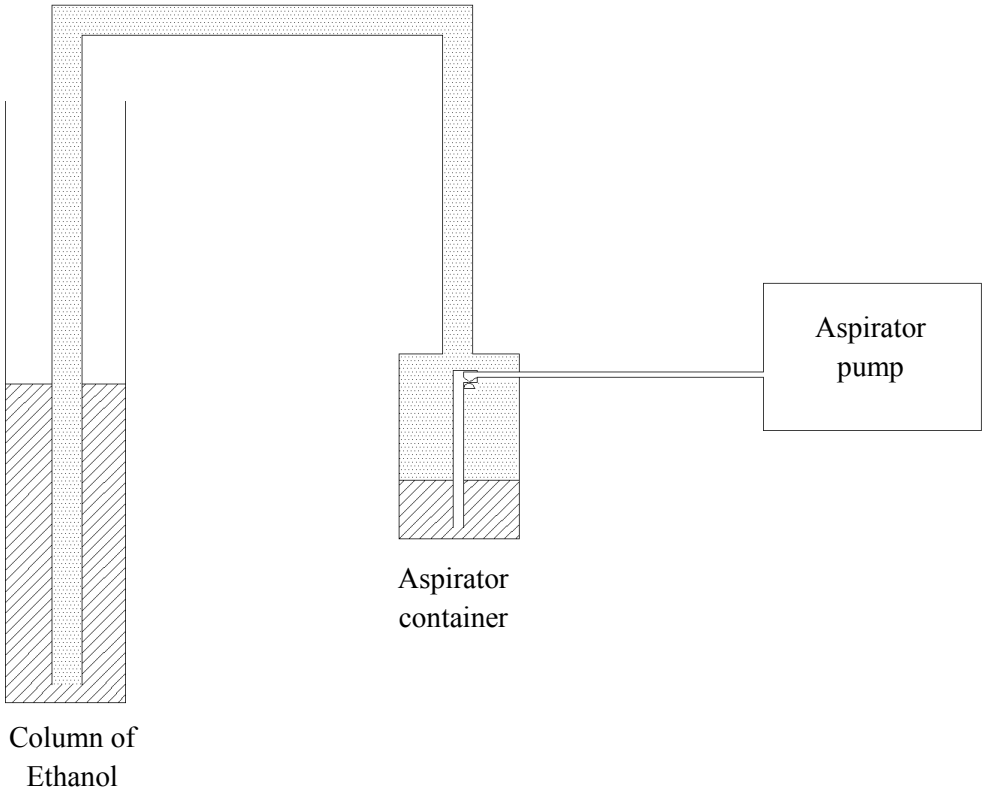

Figure 7.1 The schematic of the apparatus for the impregnation of ethanol.

7.3.2 Acid/base molar ratio

Figure 7.2 indicates the film produced by spin coating as the acid/base concentration is changed. The sol-gel described herein needs a specific range acid and base catalyst concentration with respect to solvents and precursors to function properly. In Figure 7.2, the molar ratio of acid and base in the initial mixed solution was increased as the texture of the film improved from (a) to (f). The film texture shown in Figure 7.2 (f) is the ideal ratio where the ratio is 7.7/42.03=0.183 µmole acid/µmole base.

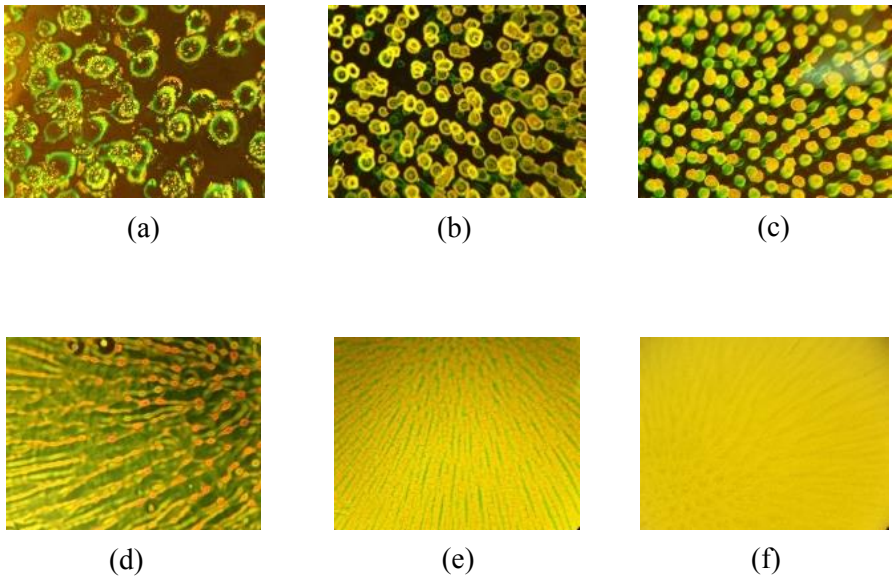

Figure 7.2 The ratio of µmole acid/µmole base: (a) 0.385/7.005=0.055, (b) 1.925/56.04=0.034, (c) 1.925/112.08=0.017, (d) 3.85/84.06=0.046, (e) 5.775/98.07=0.059, and (f) 7.7/42.03=0.183.

7.3.3 Aging time

The preparation of the initial sol liquid to be used for impregnation of the ethanol requires: 1) an acid and base catalyst with respect to solvents and precursors, and 2) starting impregnation before complete gelation. The sol-gel is formed after aging of the impregnated ethanol mixture. It has been found that the present sol-gel process can yield films with thermal conductivity as least as good as the prior art supercritical dried bulk aerogel if the spin coating is done in a time window of the liquefied maturity prepared by the disclosed method before gelation. Gelation is defined as the state of the solution when it doesn't flow anymore and becomes a complete gel. For this disclosed process, with parameters as previously noted, the window of maturity lasts about 2 hours. This time window is for a specific aging time of about 24 hours. It means that the impregnated ethanol should be aged for 24 hours before spin-coating begins and the preferred time window of using this solution is 2 hours. After this time, the ongoing reactions in the solution result in particles to aggregate too much and the quality of the film will degrade. In other words, during this 120 minutes, the sol-gel can yield uniform, crack free, smooth thin or thick films, dried upon spin coating at atmospheric condition with ultra-low thermal conductivity as low as 0.001 W/m/K, which is one order of magnitude lower than the reported thermal conductivity of prior art aerogels.

7.3.4 Other factors

In the coating process, the rate of evaporation of the solvent is controlled by the parameters affecting the evaporation rate. These parameters are the spin coating speed (in RPM), temperature, duration of spinning, and the partial pressure on top of the wafer. Using the disclosed sol-gel method for multi-spin coating of prepared solution yields an aerogel

with high porosity and eliminates any further post-processing, such as conventional processes of solvent exchange, supercritical drying, heat treatment, etc. In this process, there is no need to use any additives to reduce the capillary stress in the deposited film during drying. One of the fundamental differences between our sol-gel method and other reported aerogel film processes is that in the other reported aerogel film processes, first an alcogel is made and then the aerogel is obtained by further drying processes while the sol-gel described herein, the deposition and inherent drying occur at the same time. By alcogel we mean the gelled solution filled with the solvent and water.

7.4 Conclusion

A state-of-the-art sol-gel processing (patent pending) for the preparation of silica aerogel was revealed that avoided the conventional supercritical drying and/or solvent exchange processes involved in producing aerogels. The invention introduced impregnation of ethanol with functional colloidal alcogel particles linking together over an appropriate aging period to get mature enough to provide crack-free, uniform, smooth, and porous films by spin-coating the solution on the silicon substrate. Different parameters were investigated to get the highest quality films, among which molar ratio of acid to base was found to be crucial. Our novel sol-gel processing can be specifically applied for many coating applications where thermal insulation is an issue.

8. SILICA AEROGEL THICK FILM VIA THE NOVEL METHOD

Uniform, smooth, and crack-free multilayer silica aerogel film as thick as 5 μm is successfully coated on top of silicon wafer. The multilayer spin coated aerogel film was made possible by using our recently developed novel state-of-the-art aerogel processing technique. The use of the thick aerogel film for thermal insulation of microhotplate (μHP) is studied. The super heat insulator aerogel can replace the micromachined air cavity conventionally created under μHPs for fabrication of metal oxide (MOX) gas sensors. The thermal insulation capability of our unique aerogel film was investigated by measuring the temperature of the nichrome heaters built on the aerogel coated silicon wafers at different applied powers. The temperature coefficient of resistivity of the heaters was measured by monitoring the change in resistance of the heaters at different temperatures. Simulations were also performed by COMSOL multiphysics software for verification of the experimental results, showing good agreement.

8.1 Introduction

General metal oxide (MOX) gas sensors use a thin membrane suspended in the air cavity created by micromachining the silicon to thermally insulate the heated components from the substrate [15-16, 18]. A drawback of this approach is the high fragility and low mechanical stability of the thin (a few microns or less) membranes during processing and operation [24]. In addition, the lithographic processing of metal oxide sensing on top of the suspended layers becomes impossible due to the fact that the front side micromachined structures contain etch troughs and therefore the surface is not flat [26], hence the micromachining must be done as a post process after the sensor electrodes are processed, which lowers the yield drastically.

We have previously explained [97] the thermal insulating capability of a monolayer thin film silica aerogel of less than 1 μm thickness, processed on silicon wafer through supercritical drying, for developing ultra-dense and ultra-low power microhotplates, to replace the air cavity conventionally created by micromachining of wafers. However, uniform crack-free silica aerogel films of more than a few microns have not been reported yet, to the best of our knowledge. He et al. [96] deposited highly transparent silica aerogel films of less than 3.6 μm on fluorine doped tin oxide glass via doctor-blade method, for applications in intermetal dielectrics. However, they stated that films were uniform only up to the thickness of 2.9 μm and that they could not prepare good aerogel films by spin- or dip-coating due to the high surface tension of the aqueous water glass precursor. Bauer et al. [81] developed silica aerogel films of only 0.25-1.28 μm thickness via several laborious solvent exchange steps, and measured the thermal conductivity as 0.024 W/m/K to ensure insulation capability of aerogel films. Wang et al. [82] evaluated the electrical sensing properties of silica aerogel thin films to humidity, fabricated on alumina substrate by dip-coating silica colloid followed by supercritical drying, resulting in a thickness of less than 0.2 μm. Yokokawa et al. [98] and Fan et al. [64] both reported multiple spin-coating of silica aerogel for investigation of mechanical properties, which concluded to not more than 2 μm thickness.

In all previous works reported so far, none has successfully demonstrated the fabrication of microheaters on top of the aerogel. In this chapter, for the very first time, we are presenting the utilization of high quality thick silica aerogel films (5 μm) processed through our novel multilayer technique (patent pending) avoiding supercritical drying and solvent exchange which are common in sol-gel processing of aerogels.

8.2 Thick film preparation

A solution was first prepared by mixing TEOS, ethanol, water, and HCl (acid catalyst) with a molar ratio of $1:4:2:4.3\times10^{-4}$, respectively. The solution was stirred for one hour followed by addition of 0.64 ml of NH_4OH 0.066 M (base catalyst) and stirring for 5 more minutes, resulting in a sol-gel with the gelation time of about 3 hours. The solution was then undergone a specific aging process (patent pending) to yield the final liquid suitable for spin-coating. Right before spin-coating, the liquid was ultrasound for 8 minutes and filtered by a 0.2 μm filter. The filtered liquid was spin-coated on silicon wafer at 1150 RPM for 40 seconds. 70 layers, one after the other, were spin coated to yield a smooth (less than 40 nm roughness), crack-free, thick (5 μm), and uniform multilayer aerogel film avoiding supercritical drying or any solvent exchange. The thick silica aerogel was then covered with an interlayer of SiO_2 (0.5 μm) by RF magnetron sputtering at 125 W. Next, nichrome micro-heaters were fabricated after photolithography processing of sputtered NiCr (Ni80/Cr20) on the wafer. The interlayer SiO_2 provides good adhesion of sputtered NiCr to aerogel film. Figure 8.1 depicts the fabricated micro-heaters on the thick film aerogel. The roughness of the film was measured by a surface profiler (Tencor P-10) as low as 37 nm, verifying the smoothness of the aerogel film. The thickness of the film was also measured with the surface profiler as 5.0 μm.

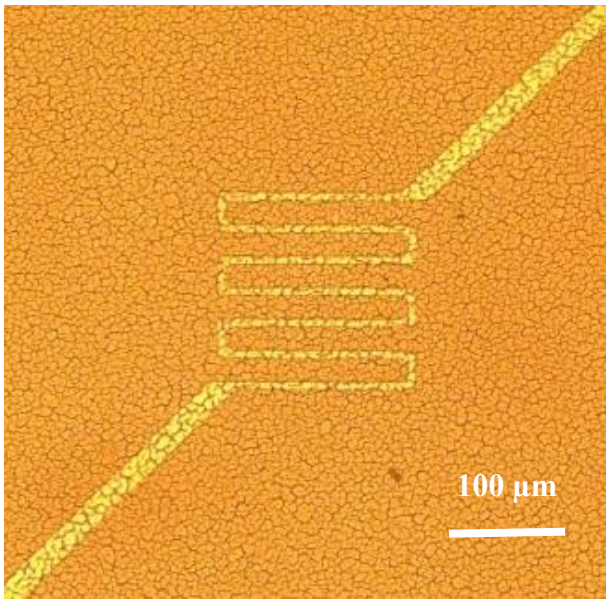

Figure 8.1 Optical image of the fabricated NiCr microheater on the thick film aerogel.

8.3 Results and discussion

8.3.1 Temperature measurement

In order to measure the temperature of the micro-heater versus applied power, the change in resistance of the heater was investigated at different applied powers, exploiting the following equation:

$$R = R_0(1 + \alpha(T - T_0)) \tag{8.1}$$

where R_0 is the initial resistance of the heater (3262.5 Ω) at the reference temperature T_0 (23°C). α is the temperature coefficient of resistivity (TCR) of NiCr heater. Before using equation 8.1, the exact value of α for the sputtered NiCr heater was determined by placing the wafer in the furnace and monitoring the resistance of the heater at different adjusted

temperatures. Figure 8.2 shows the apparatus used to measure the α. Figure 8.3 demonstrates the linearity of the resistance increase with the temperature. The TCR of NiCr was determined as $0.000188°C^{-1}$.

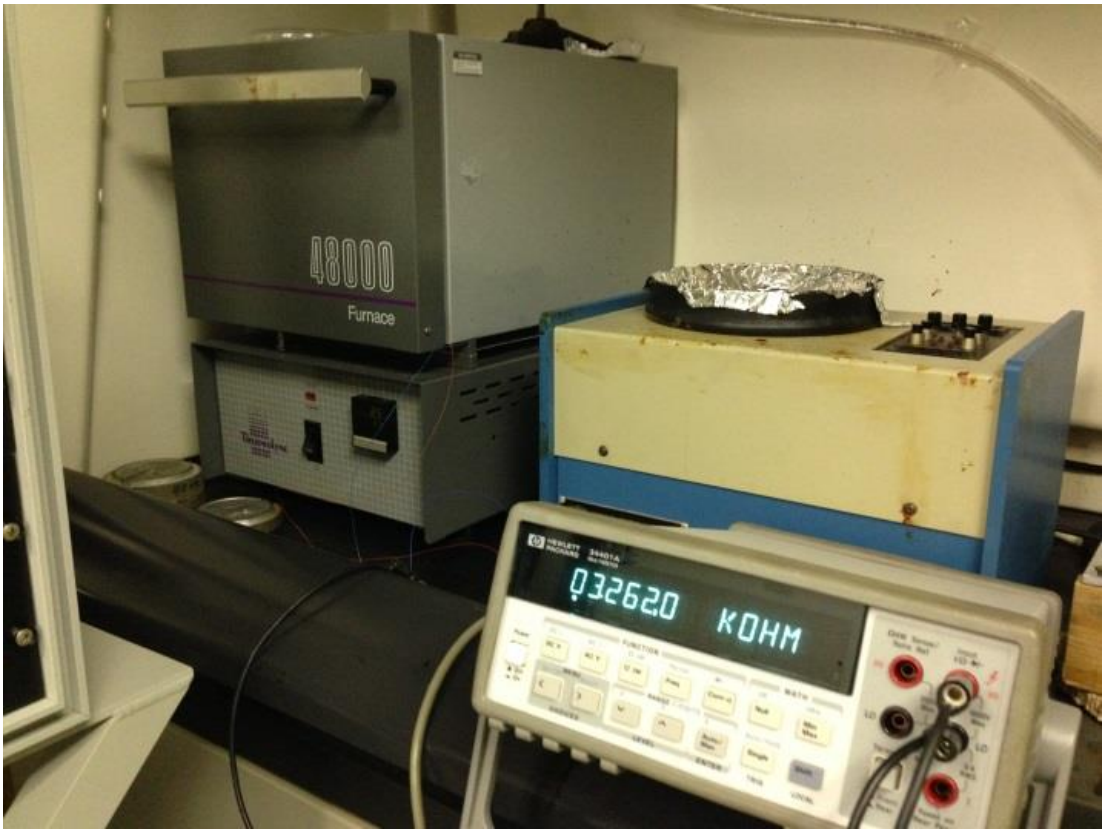

Figure 8.2 Measurement setup to determine TCR (α).

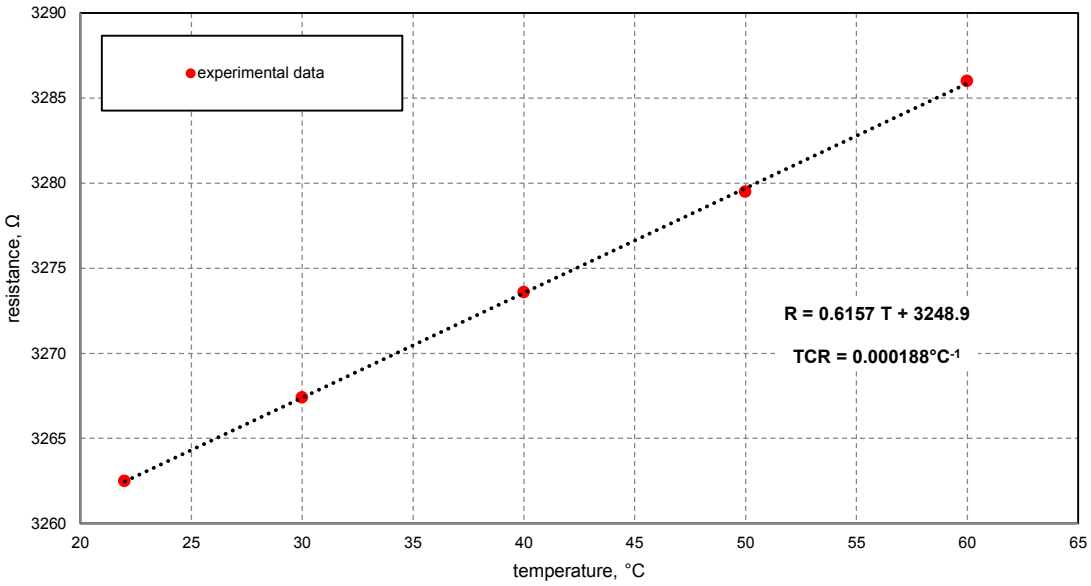

Figure 8.3 Linear relationship between the resistance and temperature for the NiCr microheater (TCR measurement).

8.3.2 Temperature versus power

The heater was powered up incrementally by applying constant currents through the heater using a semiconductor parametric analyzer (HP-4156) and measuring the voltages across it. The resistance and the temperature of the heater were calculated for each applied power. Figure 8.4 shows the measured temperature and resistance of the micro-heater at different applied powers.

The whole structure was also simulated by COMSOL multiphysics to validate the experimental measurements using aerogel physical parameters and the measured TCR (α) of sputtered NiCr. As shown in the figure, the simulation and experimental results are in very good agreement.

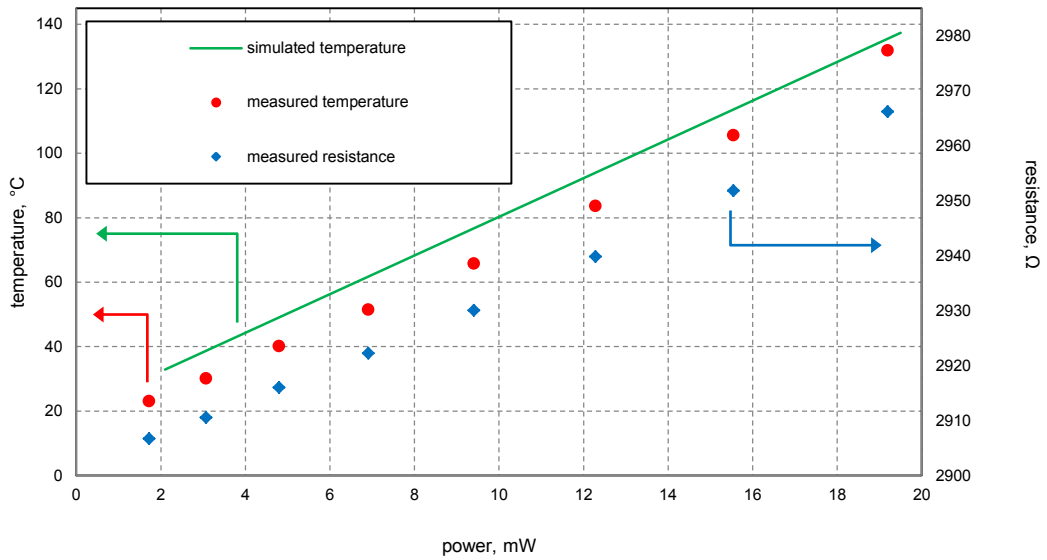

Figure 8.4 Variation of the temperature and resistance of the microheater with the applied power.

8.3.3 Temperature distribution

Figure 8.5 illustrates the FEA simulation results for our fabricated microheater on thick film aerogel. A uniform temperature distribution is clearly observed all over the heated area verifying the excellent thermal insulation capability of the aerogel film. It is noticeable that this temperature distribution uniformity obtained with only 5 µm thickness of the silica aerogel, whereas in the case of conventional microheaters the insulation thickness is over 100 µm that is created by micromachining the silicon substrate.

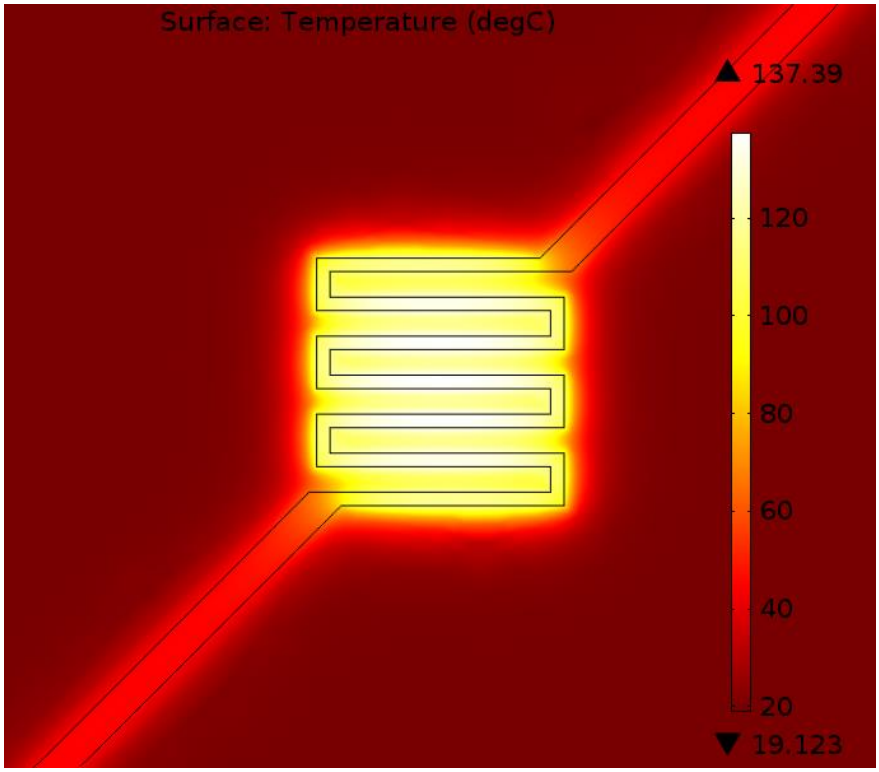

Figure 8.5 Simulation showing uniform temperature distribution for the microheater fabricated on the thick film silica aerogel (at 19mW).

8.3.4 Transient analysis

We have also investigated the thermal transient behavior of the microheater to see how fast it reaches to the high temperature by applying the power and how quick it cools down after switching off the power source. Figure 8.6 depicts the transient response of the microheater both with measurement and simulation. It indicates that the microheater has a faster response in measurement than simulation. For instance, the rise time is approximately 3 ms in simulation compared to 1.2 ms in measurement. The difference is due to the fact that in simulation, the actual temperature is determined by finite element analysis whereas in case of measurement, the temperature is calculated based on the changes in resistance according to changes in voltage. In other words, the heat capacitances of the layers are not taken into

account in case of measurement. Therefore, it shows a quicker rise and fall time than simulation.

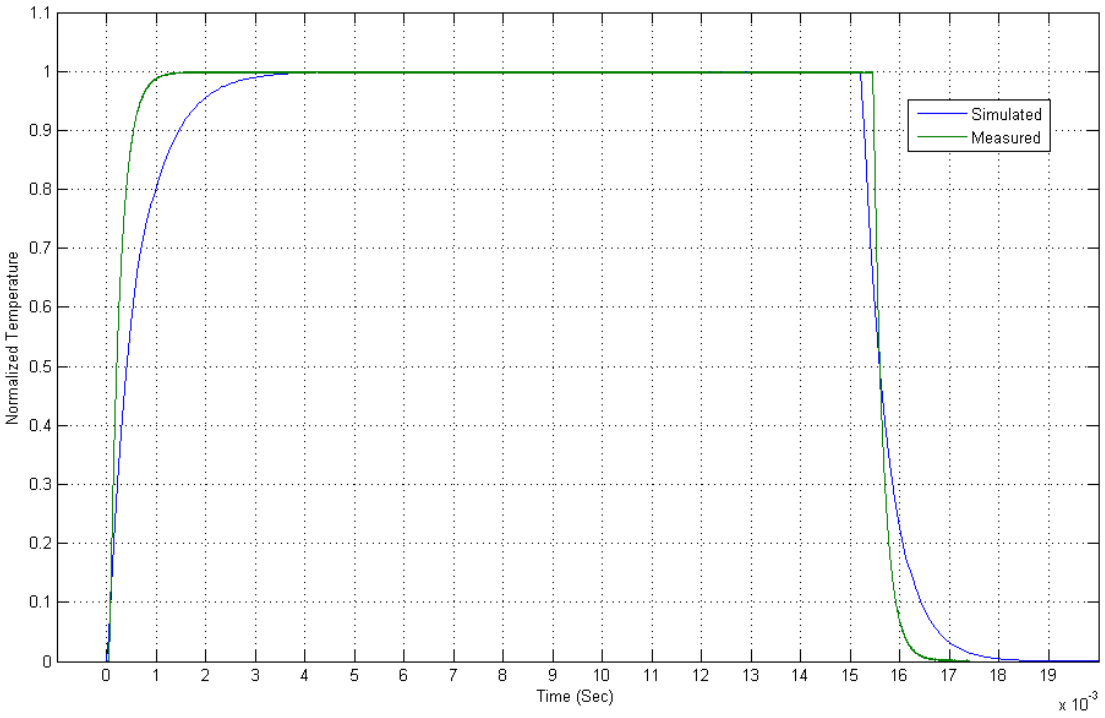

Figure 8.6 Transient response time of the microheater.

8.3.5 Comparison with related works

Table 8.1 in the next page represents the same reports presented in chapter 1. Here we include our own microheater built on our novel silica aerogel thick film. It is noticeable that in our design, all the occupied chip area is efficiently used as the heated area, meaning that the ratio of μheater to sacrificed area is 100%, whereas in other studies it never reaches 45%. The other remarkable point is that all other works are using either front-side or back-side micromachining, having at least 100 μm insulation thickness, while we only have 5μm silica aerogel insulation thickness. We have simulated our structure to investigate the power

consumption at different thicknesses of silica aerogel to maintain 400°C. As depicted in Figure 8.7, there is no significant power saving for more than 10 µm thickness of aerogel.

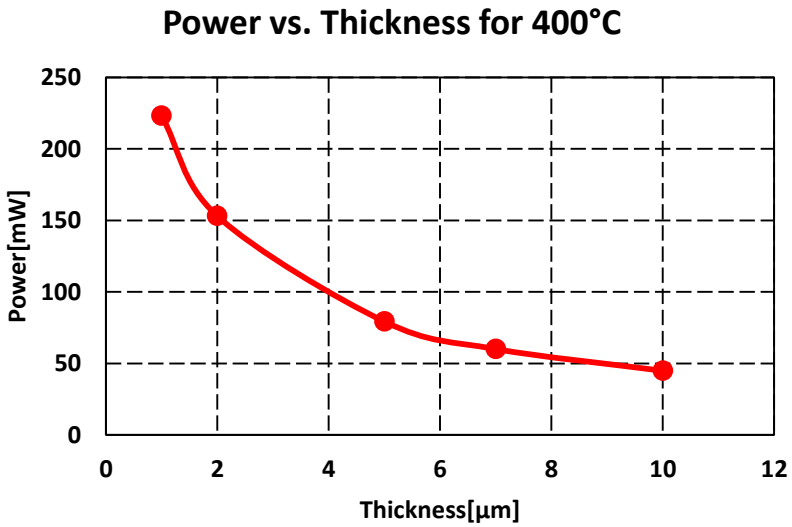

Figure 8.7 Microheater power consumption versus thickness of silica aerogel.

Table 8.1 Comparison between our µHeater and related arts.

Ref. / Year	µHeater Area (μm^2)	Sacrificed Chip Area (μm^2)	Temp. (°C)	Power (mW)	Power per Heated Area ($\mu W/\mu m^2$)	Insulation Thickness (µm)	µHA/SCA (%)
[14]/2015	1200	202500	430	15	12.5	> 100	0.6
[15]/2012	585000	1610000	200	140	0.24	> 100	36.3
[16]/2012	90000	640000	500	170	0.78	> 100	14.1
[17]/2011	6400	40000	550	25	3.9	> 100	16.0
[18]/2011	14700	122500	400	18	1.2	> 100	12.0
[19]/2011	1000000	2250000	250	250	0.25	> 100	44.4
[20]/2009	17670	246300	300	16	0.90	> 100	7.2
[21]/2009	36100	90000	300	23	0.64	> 100	40.1
[22]/2008	108900	3062500	500	58	0.53	> 100	3.6
[23]/2008	562500	2250000	325	66	0.12	> 100	25.0
[9]/Kebaili	62500	250000	425	68	1.1	> 100	25.0
Our µHP	**27225**	**27225**	**325**	**52**	**1.91**	**5**	**100**
Our µHP	**27225**	**27225**	**325**	**45**	**1.65**	**10**	**100**

8.3.6 Cost analysis

For the economical assessment of our proposed idea of substituting silica aerogel to micromachining, we need to know the current fabrication cost of micromachining and/or MEMS-based products. Lawes et al. [99] have reported the manufacturing costs for microsystems/MEMS using high aspect ratio microfabrication techniques. Figure 8.8 demonstrates their report on the fabrication cost per wafer layer versus annual substrate production. As an example, for the production of 1000 wafers per year each having 5 layers processing, the cost will be around $30 per wafer layer. This means eliminating each layer will result in the cost saving of around $30,000 per year. However, since micromachining is more time-consuming than the other layers processing, the savings would be even more. For instance, it can be double if micromachining process time is twice the other layers on average, which is a reasonable assumption.

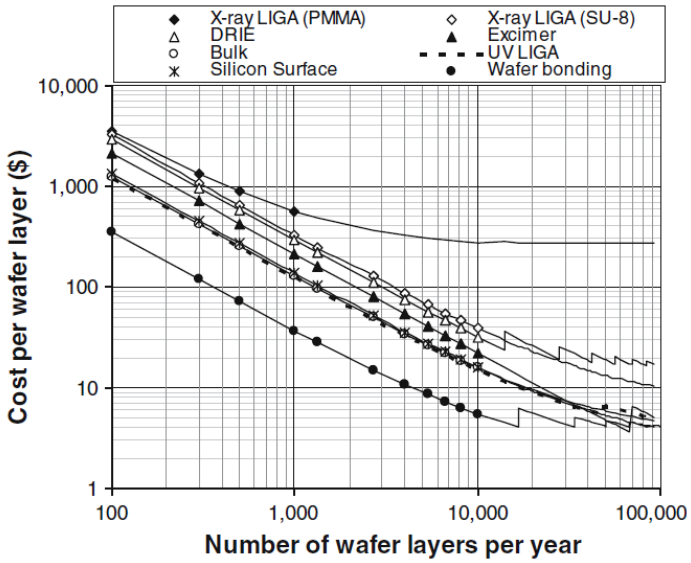

Figure 8.8 Fabrication cost ($) per wafer layer versus annual substrate production [99].

8.4 Conclusion

Silica aerogel film of 5 µm thickness was successfully fabricated on top of silicon wafers with good uniformity, low roughness, and no crack, using our unique patent-pending method. A low power micro-heater (built on the aerogel film) with uniform temperature distribution confirmed the outstanding competency of thick film aerogel for thermal insulation. The thermal transient response of the microheater was also investigated. Such insulation can be exploited as an alternative to conventional micromachined air pit in MOX gas sensor to isolate the heat sink from the µHP to the silicon substrate. Simulations are also in good agreement with the practical results.

9. CONCLUSION AND FUTURE WORK

Thin and thick films of silica aerogel have been proposed to be used as the thermal insulator, replacing the conventional micromachined air cavity in the fabrication of microhotplates.

First, the simulation study of recessed silica aerogel in the silicon substrate was conducted. The air cavity filled with aerogel was simulated to investigate the thermal insulation property of aerogel under the microheaters where it showed a high chip area saving (ten times less than air cavity) as well as ultra-low power consumption. It has also been found that by using recessed silica aerogel the problem of step coverage, which reduces the yield of micro sensors fabrication when the MOX sensors are integrated in an IC chip, can be wiped out.

A multilayer aerogel processing approach was introduced to overcome the limitation of making thick film aerogel. The aerogel layers were interleaved with sputtered SiO_2 to cap their porosity making them capable of building up thickness without liquid penetration during coating. A smooth two-layer aerogel with 85% porosity was successfully processed. The simulation was carried out to study the steady state temperature and the transient response of the microheaters in both cases of multilayer and single thick layer aerogel. The multilayer interleaved aerogel did not compromise either the maximum steady state temperature or the transient response time.

Next, a thin layer silica aerogel has been developed successfully through ambient pressure sol-gel processing. A low refractive index of 1.133 confirmed the high porosity of 70.8%, representing the dielectric constant as low as 1.49. Also, the FTIR spectrum verified the presence of Si-O-Si and $–CH_3$ bonds.

Later, a thin film of silica aerogel has been successfully developed on the silicon wafer via supercritical drying. The film was crack-free, uniform, and smooth. The temperature of 140°C was measured at the low power of 1.6 μW/μm^2. Simulations were also in very good agreement with the experimental results.

A novel sol-gel processing (patent pending) was then introduced for the preparation of silica aerogel avoiding the conventional supercritical drying and/or solvent exchange processes typically involved in producing aerogels. Impregnation of ethanol with functional colloidal alcogel particles was implemented to prepare a "special sauce" capable of being spin coated multiple times on the silicon substrate to provide thick, crack-free, uniform, smooth, and porous films. Different parameters were investigated to get the highest quality films, among which molar ratio of acid to base was found to be crucial. Our innovative sol-gel processing can be particularly employed for many coating applications where thermal insulation coating is needed.

Finally, a thick silica aerogel film of 5 μm was successfully fabricated on top of silicon wafers, for the first time, utilizing our novel method. The microheaters were performing at low power with uniform temperature distribution, verifying the super thermal insulation capability of the thick film aerogel. The thermal transient response of the microheaters illustrated a fast temperature rise time of 3 ms which closely matched the simulation results. The thick film silica aerogel can be an excellent substitute for the micromachined air cavity in MOX gas sensor to isolate the heat sink from the μHP to the silicon substrate.

Although we have demonstrated the advantages of using silica aerogel as heat insulator, it would be of great interest to fabricate the whole gas sensor device with built-in

aerogel and investigate the performance of such gas sensors as far as reliability over a relatively long period of time and mechanical stability. Another research area in this field would be using tin oxide (or other metal oxide) aerogels as sensing material and combining it with silica aerogel as heat insulator to increase the sensitivity while maintaining the low power consumption.

BIBLIOGRAPHY

[1] X. Xu, H. Fan, Y. Liu, L. Wang, T. Zhang, Au-loaded In_2O_3 nanofibers-based ethanol micro gas sensor with low power consumption, Sens. Actuators B 160 (2011) 713-719.

[2] J. Wang, P. Zhang, J.Q. Qi, P.J. Yao, Silicon-based micro-gas sensors for detecting formaldehyde, Sens. Actuators B 136 (2009) 399-404.

[3] M. Trincavelli, S. Coradeschi, A. Loutfi, Online classification of gases for environmental exploration, In Proceedings of the IEEE/RSJ International Conference on Intelligent Robots and Systems (IROS), St. Louis, MO, USA, 11-15 October 2009, pp. 3311-3316.

[4] M. Trincavelli, M. Reggente, S. Coradeschi, H. Ishida, A. Loutfi, A.J. Lilienthal, Towards environmental monitoring with mobile robots, in: Proceedings of the IEEE/RSJ International Conference on Intelligent Robots and Systems (IROS), Nice, France, 22-26 September 2008, pp. 2210-2215.

[5] N.E. Barbri, J. Mirhisse, R. Ionescu, N.E. Bari, X. Correig, B. Bouchikhi, E. Llobet, An electronic nose system based on a micro-machined gas sensor array to assess the freshness of sardines, Sens. Actuators B 141 (2009) 538-543.

[6] J.G. Monroy, J.G. Jimenez, J.L. Blanco, Overcoming the slow recovery of MOX gas sensors through a system modeling approach, IEEE Sens. J. 12 (2012) 13664-13680.

[7] MEMS Industry Group, http://www.memsindustrygroup.org/news/217346/MIG-Announces-Finalists-for-MEMS--Sensors-Technology-Showcase-.htm.

[8] SGX Sensortech Ltd., http://www.osedirectory.com/1-7-586/sgx-sensortech-ltd-distributors.html.

[9] Kebaili Corporation, http://www.kebaili.com/pd_kmhp-100_mems_microhotplate.cfm.

[10] A. Helwig, G. Muller, G. Sberveglieri, M. Eickhoff, On the low-temperature response of semiconductor gas sensors, J. Sens., 2009, doi: 10.1155/2009/620720.

[11] G. Eranna , B.C. Joshi , D.P. Runthala, R.P. Gupta, Oxide materials for development of integrated gas sensors—a comprehensive review, Critical Reviews in Solid State and Materials Sciences, 29:3-4 (2004) 111-188.

[12] NIST, http://www.nist.gov/mml/bmd/bioprocess/chem_microsensors.cfm.

[13] J. Puigcorbe, D. Vogel, B. Michel, A. Vila, I. Gracia, C. Cane, J.R. Morante, Thermal and mechanical analysis of micromachined gas sensors, J. Micromech. Microeng. 13 (2003) 548-556.

[14] A. Harley-Trochimczyka, J. Chang, Q. Zhou, J. Dong, T. Pham, M.A. Worsley, R. Maboudian, A. Zettl, W. Mickelson, Catalytic hydrogen sensing using microheated platinum nanoparticle-loaded graphene aerogel, Sens. Actuators B 206 (2015) 399-406.

[15] S. Roy, C.K. Sarkar, P. Bhattacharyya, A highly sensitive methane sensor with nickel alloy microheater on micromachined Si substrate, Solid-State Electron. 76 (2012) 84-90.

[16] J.C. Chiou, C.Y. Lin, S.W. Tsai, W.C. Hong, Design and fabrication of micromachined LPD-based SnO_2 gas sensor integrated TaN with micro-hotplate, in: IEEE Sensors October 28-31, 2012, Taipei, pp. 1-4.

[17] L. Xu, T. Li, X. Gao, Y. Wang., R. Zheng, L. Xie, L. Lee, A low power catalytic combustion gas sensor based on a suspended membrane microhotplate, in: IEEE Conference on Nano/Micro Engineered and Molecular Systems, February 20-23, 2011, pp. 92-95.

[18] L. Xu, T. Li, X. Gao, Y. Wang, Development of a reliable micro-hotplate with low power consumption, IEEE Sens. J., 11-4 (2011) 913-919.

[19] J.W. Chen, S.P. Wu, Y.S. Huang, C.C. Lu, Design and fabrication of a nanoporous microhotplate for gas detection with low power and high sensitivity, in: IEEE Conference on Nano/Micro Engineered and Molecular Systems February 20-23, 2011, pp. 1044-1047.

[20] S.Z. Ali, S. Santra, I. Haneef, C. Schwandt, R.V. Kumar, W.I. Milne, F. Udrea, P.K. Guha, J.A. Covington, J.W. Gardner, Nanowire hydrogen gas sensor employing CMOS micro-hotplate, in: IEEE Sensors Conference, 2009, pp. 114-117.

[21] A. Beya Far, F. Flitti, B. Guo, A. Bermak, A bio-inspired pattern recognition system for tin-oxide gas sensor applications, IEEE Sens. J., 9, 6 (2009) 713-722.

[22] J.F. Creemer, J.F., D. Briand, H.W. Zandbergen, W. Vilst, C.R. Boer, N.F. Rooij, P.M. Sarro, Microhotplates with TiN heaters, Sens. Actuators A 148 (2008) 416-421.

[23] D. Briand, S. Colin, J. Courbat, S. Raible, J. Kappler, N.F. Rooij, Integration of MOX gas sensors on polyimide hotplates, Sens. Actuators B 130 (2008) 430-435.

[24] F. Lucklum, A. Schwaiger, B. Jakoby, Highly insulating, fully porous silicon substrates for high temperature micro-hotplates, Sens. Actuators A 213 (2014) 35-42.

[25] J. Laconte, D. Flandre, J. Raskin, Micromachined thin-film sensors for SOI-CMOS co-integration, Springer, Berlin, 2006.

[26] G. Korotcenkov, B.K. Cho, Engineering approaches to improvement of conductometric gas sensor parameters. Part 2: Decrease of dissipated (consumable) power and improvement stability and reliability, Sens. Actuators B 198 (2014) 316-341.

[27] D. Kim, H. Du, S. Bhandarkar, D.W. Johnson, Sol-gel processing of low dielectric constant nanoporous silica thin films, Mater. Res. Soc. Symp. Proc., 703 (2002) V3.21.1-V3.21.5.

[28] C.J. Brinker, G.W. Scherer, Sol-Gel Science, Academic Press, Boston, 1990.

[29] I. Smirnova, Synthesis of silica aerogels and their application as a drug delivery system, Ph.D. dissertation, Univ. Berlin, Berlin, 2002.

[30] S. Suttiruengwong, Silica aerogels and hyperbranched polymers as drug delivery systems, Ph.D. dissertation, Technischen Fakultät, Universität Erlangen-Nürnberg, Nürnberg, 2005.

[31] S. Sakka, Ed., Handbook of Sol-Gel Science and Technology, NY: Kluwer Academic Publishers, New York, 2005.

[32] S.S. Kistler, Coherent expanded aerogels and jellies, Nature 127 (1931) 741.

[33] Lawrence Livermore National Laboratory, https://str.llnl.gov/str/May05/Satcher.html.

[34] Wikipedia, http://en.wikipedia.org/wiki/Tetraethyl_orthosilicate.

[35] C.J. Brinker, K.D. Keefer, D.W. Schaefer, C.S. Achley, Sol-gel transition in simple silicates, J. Non-Cryst. Solids 48 (1982) 47-64.

[36] T.M. Tillotson, L.W. Hrubesh, Transparent ultralow-density silica aerogels prepared by a two-step sol-gel process, J. Non-Cryst. Solids 145 (1992) 44-50.

[37] K.C. Chen, T. Tsuchiya, J. D. Mackenzie, Sol-gel processing of silica: I. The role of the starting compounds, J. Non-Cryst. Solids 81 (1986) 227-237.

[38] P.B. Wagh, R. Begag, G.M. Pajonk, A.V. Rao, D. Haranath, Comparision of some physical properties of silica aerogels monoliths synthesized by different precursors, Mater. Chem. Phys. 57 (1999) 37.

[39] J.C. Pouxviel, J.P. Boilot, J.C. Beloeil, J.Y. Lallemand, NMR study of the sol-gel polymerization, J. Non-Cryst. Solids 89 1987) 345-360.

[40] R.A. Assink, B.D. Kay, Sol-gel kinetics I. Functional group kinetics, J. Non-Cryst. Solids 99 (1988) 359-370.

[41] L.C. Klein, Sol-gel processing of silicates, Ann. Rev. Mater. Sci. 15 (1985) 227-248.

[42] R. Aelion, A. Loebel, F. Eirich, Hydrolysis of ethyl silicate, J. Am. Chem. Soc. 72 (1950) 5705-5712.

[43] W. Cao, A.J. Hunt, Improving the visible transparency of silica aerogels, J. Non-Cryst. Solids, 176 (1994) 18-25.

[44] E.J.A. Pope, J.D. Mackenzie, Sol-gel processing of silica: II. The role of the catalyst, J. Non-Cryst. Solids 87 (1986) 185-198.

[45] M.A. Einarsrud, E. Nilsen, A. Rigacci, G.M. Pajonk, S. Buathier, D. Valette, M. Durant, B. Chevalier, P. Nitz, F. Ehrburger-Dolle, Strengthening of silica gels and aerogels by washing and aging processes, J. Non-Cryst. Solids 285 (2001) 1-7.

[46] S. Dai, Y.H. Ju, H.J. Gao, J.S. Lin, S.J. Pennycook, C.E. Barnes, Preparation of silica aerogel using ionic liquids as solvents, Chem. Commun. 3 (2000) 243-248.

[47] S.S. Kistler, Coherent expanded-aerogels, J. Phys. Chem. 36 (1932) 52-64.

[48] P.B. Sarawade, J.K. Kim, H.K. Kim, H.T. Kim, High specific surface area TEOS-based aerogels with large pore volume prepared at an ambient pressure, Appl. Surf. Sci. 254 (2007) 574-579.

[49] F. Schwertfeger, D. Frank, M. Schmidt, Hydrophobic waterglass based aerogels without solvent exchange or supercritical drying, J. Non-Cryst. Solids 225 (1998) 24-29.

[50] L.W. Hrubesh, Aerogel applications, J. Non-Cryst. Solids 225 (1998) 335-342.

[51] M.D. Grogan, S.G. Leon-Saval, R. Williams, R. England, T.A. Birks, Optical fibre with an aerogel-filled core, Conf. 2009 Quantum Electron. Laser Sci. 2009, pp. 1-2.

[52] L.W. Hrubesh, J.F. Poco, Thin aerogel films for optical, thermal, acoustic, and electronic applications, J. Non-Cryst. Solids 188 (1995) 46-53.

[53] N. Kawakami, Y. Fukumoto, T. Kinoshita, K. Suzuki, K. Inoue, A super low-k (k=1.1) silica aerogel film using supercritical drying technique, in: Proceedings of IEEE 2000 International Conference of Interconnect Technology, 2000, pp. 143-145.

[54] B.N. Joshi, A.M. Mahajan, Porous SiO_2 thin films for ULSI applications, in: International Workshop on Physics of Semiconductor Devices, 2007, pp. 261-263.

[55] L. Li., L. Zhang, X. Yao, Preparation and characterization of thick porous SiO_2 film for multilayer pyroelectric thin film IR detector, Ceram. Int. 30 (2004) 1843-1846.

[56] Y. Ishii, H. Kawai, H. Kishimoto, H. Nakayama, M. Tabata, Y. Tajima, H. Yokogawa, H. Yoshida, Performance evaluation of silica aerogel cherenkov counters with n >> 1.08, Nucl. Sci. Symp. Conf. Rec. 1 (2007) 663.

[57] A.Y. Barnyakov, M.Y. Barnyakov, J. Bahr, T. Bellunato, K.I. Beloborodov, V.S. Bobrovnikov, A.R. Buzykaev, M. Calvi, A.F. Danilyuk, V. Djordjadze, V.B. Golubev, S.A. Kononov, E.A. Kravchenko, D. Lipka, C. Matteuzzi, M. Musy, A.P. Onuchin, D. Perego, V.A. Rodiakin, G.A. Savinov, S.I. Serednyakov, A.G. Shamov, F. Stephan, V.A. Tayursky, A.I. Vorobiov, Development of aerogel Cherenkov counters at Novosibirsk, Radiat. Phys. Chem. 75 (2006) 862-867.

[58] Jet Propulsion Laboratory, NASA's Comet Sample Return Mission, Available: http://stardust.jpl.nasa.gov.

[59] B.C. Dunn, P. Cole, D. Covington, M.C. Webster, R.J. Pugmire, R.D. Ernst, E.M. Eyring, N. Shah, G.P. Huffman, Silica aerogel supported catalysts for Fischer-Tropsch synthesis, Appl. Catal. A 278 (2005) 233-238.

[60] A. Hilonga, J. Kim, P.B. Sarawade, H.T. Kim, Low-density TEOS-based silica aerogels prepared at ambient pressure using isopropanol as the preparative solvent, J. Alloys Compd. 487 (2009) 744-750.

[61] J. Shen, Z. Zhang, G. Wu, B. Zhou, X. Ni, J. Wang, Preparation and characterization of silica aerogels derived from ambient pressure, J. Mater. Sci. Technol. 22 (2006) 798-802.

[62] Y. Liu, L. Zhang, X. Yao, C. Xu, Development of porous silica thick films by a new base-catalyzed sol–gel route, Mater. Lett. 49 (2001) 102-107.

[63] M. Madani, D.R. Lankireddy, N.F. Tzeng, Gaseous sensor arrays with area- and energy-efficient microhotplates through silicon aerogel for heat insulation, in: IEEE Proceedings of International Conference on Microelectronics (ICM), 2009, pp. 402-405.

[64] S. Fan, C. Kim, J. Paik, B. Dunn, P. Patterson, M. Wu, MEMS with thin-film aerogel, in: IEEE 14th International Conference on Micro Electro Mechanical Systems, 2001, pp. 122-125.

[65] H. Bargozin, L. Amirkhani, J. Moghaddas, M. Ahadian, Synthesis and application of silica aerogel-MWCNT nanocomposites for adsorption of organic pollutants, Sci. Iran 17 (2010) 122-132.

[66] J. Farmer, D. Fix, G. Mack, R. Pekala, J. Poco, Capacitive deionization of NaCl and $NaNO_3$ solutions with carbon aerogel electrodes, J. Electrochem. Soc. 143 (1996) 159-169.

[67] L. Aranda, Silica aerogel, IEEE Potentials 20 (2001) 12-15.

[68] S. Kim, S. Hwang, S. Hyun, Preparation of carbon aerogel electrodes for supercapacitor and their electrochemical characteristics, J. Mater. Sci. 40 (2005) 725-731.

[69] J. Arenas, M. Crocker, Recent trends in porous sound-absorbing materials, J. Sound Vib. 44-7 (2010) 12-18.

[70] K. Oh, D. Kim, S. Kim, Ultra-porous flexible PET/aerogel blanket for sound absorption and thermal insulation, Fibers Polym. 10-5 (2009) 731-737.

[71] X. Lu, R. Caps, J. Fricke, C. Alviso, R. Pekala, Correlation between structure and thermal conductivity of organic aerogels, J. Non-Cryst. Solids 188-3 (1995) 226-234.

[72] S. Prakash, C. Brinker, A. Hurd, Silica aerogel films at ambient pressure, J. Non-Cryst. Solids 190-3 (1995) 264-275.

[73] A. Rao, G. Pajonk, S. Bhagat, P. Barboux, Comparative studies on the surface chemical modification of silica aerogels based on various organosilane compounds of the type R_nSiX_{4-n}, J. Non-Cryst. Solids 350 (2004) 216-223.

[74] A. Katti, N. Shimpi, S. Roy, H. Lu, E. Fabrizio, A. Dass, L. Capadona, N. Leventis, Chemical, physical, and mechanical characterization of isocyanate cross-linked amine-modified silica aerogels, Chem. Mater. 18-2 (2006) 285-296.

[75] M. Jo, J. Hong, H. Park, J. Kim, S. Hyun, Evaluation of SiO_2 aerogel thin film with ultra low dielectric constant as an intermetal dielectric, Microelectron. Eng 33-1 (1997) 343-348.

[76] I. Elmi, S. Zampolli, E. Cozzani, M. Passini, G. Cardinali, M. Severi, Development of ultra low power consumption hotplates for gas sensing applications, in: IEEE Conference on Sensors, 2006, pp. 243-246.

[77] I. Elmi, S. Zampolli, E. Cozzani, M. Passini, G. Pizzochero, G. Cardinali, M. Severi, Ultra low power MOX sensors with ppb-level VOC detection capabilities, in: IEEE Conference on Sensors, 2007, pp. 170-173.

[78] S. Fung, Z. Tang, P. Chan, J. Sin, P. Cheung, Thermal analysis and design of a micro-hotplate for integrated gas-sensor applications, Sens. Actuators A 54 (1996) 482-487.

[79] D. Briand, S. Colin, A. Gangadharaiah, E. Vela, P. Dubois, L. Thiery, N.D. Rooij, Micro-hotplates on polyimide for sensors and actuators, Sens. Actuators A 132 (2006) 317-324.

[80] M. Graf, D. Barrettino, H. Baltes, A. Hierlemann, CMOS hotplate chemical microsensors, Springer, 2007.

[81] M. Bauer, C. Bauer, M. Fish, R. Matthews, G. Garner, A. Litchenberger, P. Norris, Thin-film aerogel thermal conductivity measurements via ω3, J. Non-Cryst. Solids 357 (2011) 2960-2965.

[82] C. Wang, C. Wu, Electrical sensing properties of silica aerogel thin films to humidity, Thin Solid Films 496 (2006) 658-664.

[83] S. Ghandhi, VLSI Fabrication Principles: Silicon and Gallium Arsenide, John Wiley & Sons, 2008.

[84] Z.W. He, X.Q. Liu, D.Y. Xu, Y.Y. Wang, Effect of annealing on the properties of low-k nanoporous SiO_2 films prepared by sol-gel method with catalyst HF, Microelectron. Rel. 46 (2006) 2062-2066.

[85] T.E. Gómez, E. Rodríguez, A. Roig, E. Molins, F.M. Espinosa, Fabrication and characterization of silica aerogel films for aircoupled piezoelectric transducers in the megahertz range, in: IEEE Proceedings on Ultrasonics Symposium, 2002, pp. 1107-1110.

[86] S.V. Nitta, V. Pisupatti, A. Jain, P.C. Wayner, W.N. Gill, J.L. Plawsky, Surface modified spin-on xerogel films as interlayer dielectrics, J. Vac. Sci. Technol. B 17 (1999) 205-212.

[87] Z.W. He, X.Q. Liu, Q. Su, Y.Y. Wang, Improvement of electrical properties of low dielectric constant nanoporous silica films prepared using sol-gel method with catalyst HF, Appl. Phys. A 82 (2006) 349-355.

[88] A. Matsuda, Y. Matsuno, M. Tatsumisago, T. Minami, Porosity and amounts of adsorbed water in sol-gel derived porous silica films with heat treatment, J. Sol-Gel Sci. Technol. 20 (2001) 129-134.

[89] F. Shi, L. Wang, J. Liu, M. Zeng, Effect of heat treatment on silica aerogels prepared via ambient drying, J. Mater. Sci. Technol. 23 (2007) 402-406.

[90] J.L. Gurav, A.V. Rao, U.K.H. Bangi, Hydrophobic and low density silica aerogels dried at ambient pressure using TEOS precursor, J. Alloys Compd. 471 (2009) 296-302.

[91] R. Al-Oweini, H. El-Rassy, Synthesis and characterization by FTIR spectroscopy of silica aerogels prepared using several $Si(OR)_4$ and $R''Si(OR')_3$ precursors, J. Mol. Struct. 919 (2009) 140-145.

[92] S.B. Jung, H.H. Park, Control of surface residual –OH polar bonds in SiO_2 aerogel film by silylation, Thin Solid Films 420-421 (2002) 503-507.

[93] P. Mezza, J. Phalippou, R. Sempere, Sol-gel derived porous silica films, J. Non-Cryst. Solids 243 (1999) 75-79.

[94] G.S. Chung, J.M. Jeong, Fabrication of micro heaters on polycrystalline 3C-SiC suspended membranes for gas sensors and their characteristics, Microelectron. Eng. 87 (2010) 2348-2352.

[95] M.S. Jalali, S. Kumar, M. Madani, N. Tzeng, Microhotplates for low power, and ultra dense gaseous sensor arrays using recessed silica aerogel for heat insulation, in: IEEE Sensors Applications Symposium, Galveston, TX, February 2013, pp. 133-136.

[96] P. He, X.D. Gao, X.M. Li, Z.W. Jiang, Z.H. Yang, C.L. Wang, Z.Y. Gu, Highly transparent silica aerogel thick films with hierarchical porosity from water glass via ambient pressure drying, Mater. Chem. Phys. 147 (2014) 65-74.

[97] M. Seyedjalali, S. Kumar, M. Madani, Ultra-dense and ultra-low power microhotplates using silica aerogel, Electron. Lett. 49 (2013) 1168-1170.

[98] R. Yokokawa, J.A. Paik, B. Dunn, N. Kitazawa, H. Kotera, C.J. Kim, Mechanical properties of aerogel-like thin films used for MEMS, J. Micromech. Microeng. 14 (2004) 681-686.

[99] R. A. Lawes, Manufacturing costs for microsystems/MEMS using high aspect ratio microfabrication techniques, Microsyst. Technol. 13 (2007) 85-95.

APPENDIX: SUPERCRITICAL DRYING

A. Apparatus

In order to do supercritical drying the alcogel-coated 4-inch wafers, we have designed a chamber of 5 inch inner diameter to place the wafer in. It is equipped with a window plug to be able to monitor the wafer while drying. The chamber has an outlet at the bottom for drainage. The pressure and the temperature are monitored by the barometer and the thermometer gauges, connected onto stainless steel cap which is tightened to the pressure vessel by 8 screws. Figure A.1 shows the photo of the apparatus with all the components.

Figure A.1 Photograph of the supercritical drying apparatus.

B. Loading the wafer

After spin-coating the solution on the silicon substrate, the film needs to be aged in ethanol for some time (depends on the film thickness) to strengthen its network before performing supercritical drying. Once the coated wafer got ready, with the drain valve closed, it is placed in the vessel that is already having a level of ethanol (2 mm) to avoid unwanted evaporation of the film causing cracks (Figure A.2). Then the cap is closed very tight with 8 screws. Since the supercritical drying is done by liquid CO_2 having it in the form of liquid is necessary. Otherwise, it is not exchanged with the ethanol in the film. In order to have CO_2 in the form of liquid, the temperature of the chamber should be around 5 to 15°C. In fact, CO_2 will be directed from the tank to the chamber by siphon action once the CO_2 intake valve opens. So we filled the wooden box with ice and water to cool down the vessel before opening the CO_2 intake valve.

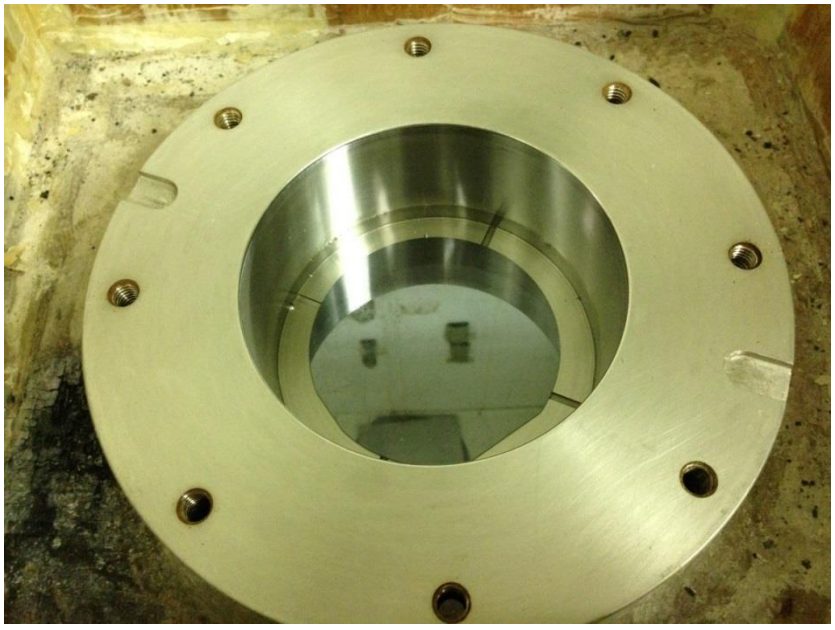

Figure A.2 Pressure vessel with a level of ethanol before loading the wafer.

C. CO_2 intake and exchange

Now we open the CO_2 valve and slowly open the intake valve on the cap. The liquid CO_2 will start to fill in the chamber. The pressure will increase to between 650 to 850 psi, depending on the tank pressure and its temperature. We let the CO_2 in about the same amount that we pore ethanol in. Later, we close the intake valve and wait for 10 minutes to let the CO_2 mix with the ethanol. After that, the mixture is vented out from the valve at the bottom of the vessel (Figure A.3).

Figure A.3 Depressurizing or venting valve.

Not all the ethanol will be collected at the first venting attempt since it has not mixed completely with the CO_2. Hence, the chamber will be filled with CO_2 again and let mix with ethanol for another 30 minutes before collecting. This will be repeated a few times to make

sure at least 90% of the initial ethanol is collected. The film on the wafer will then be under pure CO_2 liquid to exchange all its solvents inside with CO_2 over a few aging periods of 30 minutes each. It should be noticed that the temperature inside the vessel should be kept between 5 to 15°C during all CO_2 intakes to have the liquid CO_2 and not the gas.

D. Supercritical drying

After soaking the film long enough in the CO_2, it is time to dry the gel supercritically. All the valves are closed including the gas tank. The wooden box is emptied of ice and water. The body of the vessel is being heated using a heat gun (Figure A.4). The temperature and the pressure are monitored carefully to reach approximately 40°C and 1200 psi that is slightly above the critical condition of CO_2 (31.1°C and 1071 psi). The chamber is kept at this supercritical condition for 60 minutes.

Figure A.4 Heating the vessel with a heat gun.

E. Depressurizing the vessel

After aging the sample at supercritical condition for about an hour, the vessel is heated up to reach 1400 psi. It is maintained at this condition for 20 minutes to stabilize. Then the chamber is depressurized by crack opening the needle valve to lose 300 psi over the course of 15 minutes. In fact, we are making sure that the temperature is not reduced suddenly by depressurizing the vessel to avoid cracking the film. Next, the needle valve is closed and the vessel is again heated up to reach 1400 psi. This heating up and depressurizing is repeated until the pressure doesn't build up with heating or until the temperature reaches 60°C. Now the needle valve is crack opened and the vessel is allowed to depressurize down to 500 psi. Later, we can open the valve little more to reach the near ambient pressure faster. Finally, the needle valve is completely opened to make sure the ambient pressure is satisfied. At this time, the chamber can be opened and the aerogel coated wafer is ready (Figure A.5).

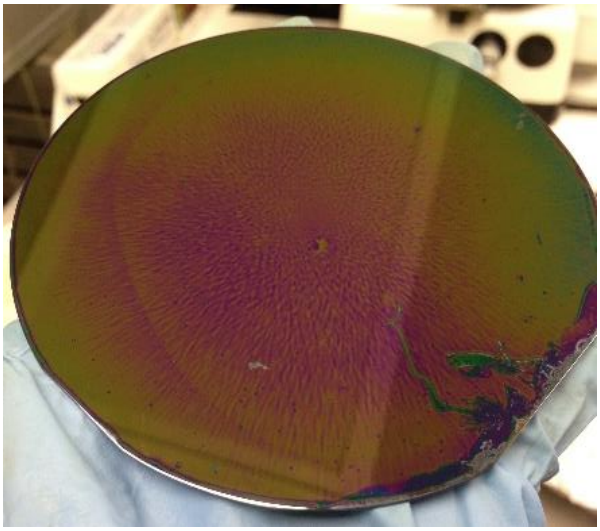

Figure A.5 Supercritically dried silica aerogel thin film.

Seyed Jalali Aghdam, Seyed Mohammad. Bachelor of Science, University of Tehran, Spring 2004; Master of Science, University of Louisiana at Lafayette, Spring 2011; Doctor of Philosophy, University of Louisiana at Lafayette, Spring 2015
Major: Computer Engineering
Title of Dissertation: Silica Aerogel, an Alternative to Micromachined Air Gap for Thermal Insulation of Microheaters
Dissertation Director: Dr. Mohammad Madani
Pages in Dissertation: 128; Words in Abstract: 201

ABSTRACT

Metal oxide semiconductor (MOX) gas sensors are one of the most popular types of electronic noses due to their high sensitivity and affordability. MOX sensors detect gases by sensing the change in resistance of the sensing material, while being exposed to gases at elevated temperatures between 300ºC to 500ºC, which is achieved by applying electrical power to a microhotplate (μHP) that should be thermally insulated from the substrate to provide low power consumption as well as quick response time. The conventional method to deliver insulation is to micromachine the silicon wafer to suspend the μHP in air. That has some disadvantages, such as the low mechanical stability of the thin suspended membranes, the large sacrificed chip area to create the air gap for a single μHP, and the impossibility of lithographic processing of sensing material on top of the suspended layers. In this dissertation, a novel idea is proposed to use silica aerogel films as heat insulator rather than creating air gaps. The proposed idea is implemented practically and is demonstrated to offer power-efficient and area-efficient μHPs. Moreover, our state-of-the-art sol-gel processing (patent pending) suggests an easy method to prepare aerogel films avoiding the conventional supercritical drying and/or solvent exchange steps.

BIOGRAPHICAL SKETCH

Seyed Mohammad Seyed Jalali Aghdam was born in Tehran, Iran on September 19, 1981. He graduated from the University of Tehran, Iran in Spring 2004 with a Bachelor degree in Chemical Engineering. In fall 2008, he joined the Telecommunications program at the University of Louisiana at Lafayette and received his master's degree in spring 2011.

Then he joined the Center for Advanced Computer Studies (CACS) at the University of Louisiana at Lafayette in fall 2011 to pursue his PhD degree in Computer Engineering. With his background in Chemical Engineering, he conducted a multidisciplinary research to develop and use silica aerogel films to eliminate micromachining for thermal insulation of microhotplates, which led to two U.S. patents. He earned his Doctor of Philosophy in Computer Engineering in Spring 2015.